WLOL
NASA
CR
72557
c.1
TECH LIBRARY KAFB, NM
0062497

NASA CR 72557
Report MDC H296

Radiation Cooled MPD Arc Thruster

by

D.W. Esker,

J.C. Kroutil,

R.J. Checkley

Prepared for
National Aeronautics and Space Administration
NASA Lewis Research Center
Contract NAS3-11518

MCDONNELL RESEARCH LABORATORIES
ST. LOUIS, MISSOURI

MCDONNELL DOUGLAS
CORPORATION

This report was prepared as an account of Government sponsored work. Neither the United States, nor the National Aeronautics and Space Administration (NASA), nor any person acting on behalf of NASA:

A.) Makes any warranty or representation, expressed or implied, with respect to the accuracy, completeness, or usefulness of the information contained in this report, or that the use of any information, apparatus, method, or process disclosed in this report may not infringe privately owned rights; or

B.) Assumes any liabilities with respect to the use of, or for damages resulting from the use of any information, apparatus, method or process disclosed in this report.

As used above, "person acting on behalf of NASA" includes any employee or contractor of NASA, or employee of such contractor, to the extent that such employee or contractor of NASA, or employee of such contractor prepares, disseminates, or provides access to, any information pursuant to his employment or contract with NASA, or his employment with such contractor.

Requests for copies of this report should be referred to:

National Aeronautics and Space Administration
Scientific and Technical Information Facility
P.O. Box 33
College Park, Maryland 20740
Attn: NASA Representative RQT-2448

TECH LIBRARY KAFB, NM

0062497

Report MDC H296
Copy No. 30

Radiation Cooled MPD Arc Thruster

by D.W. Esker, J.C. Kroutil, R.J. Checkley

McDonnell Research Laboratories
McDonnell Douglas Corporation
St. Louis, Missouri 63166

Prepared for
National Aeronautics
and Space Administration
July 1969
Contract NAS3-11518

Technical Management
NASA Lewis Research Center
Cleveland, Ohio 44135
Electromagnetic Propulsion Division
D. J. Connolly

MCDONNELL DOUGLAS CORPORATION

Foreword

The work described in this report was performed by McDonnell Douglas Corporation under Contract NAS 3–11518 for the Lewis Research Center of the National Aeronautics and Space Administration. The contract period was 2 May 1968 through 1 May 1969. Mr. D.J. Connolly of NASA was Project Manager for the program.

The principal investigator was D.W. Esker and Messrs. J.C. Kroutil and R.J. Checkley were co-investigators. The work was accomplished in the Plasma Physics Laboratory under the direction of Dr. William M. Van Camp.

Other personnel who contributed to the program were A.V. Sedrick, W.C. Good, R.C. Pettitt, D.D. Hilleman and R.T. Turnbull.

Abstract

A radiation cooled MPD arc thruster was designed and tested in a power range of 14 to 41 kilowatts and specific impulses between 800 and 3200 seconds, using ammonia as the propellant. Thrust performance was obtained for throat diameters from 1.524 to 2.286 cm, magnetic fields from 0.1 to 0.18 tesla, arc currents from 300 to 700 amps and mass flow rates from 0.020 to 0.040 g/sec. An uninterrupted lifetest was conducted for 508 hours at a nominal power of 32 kW, thrust 57g (0.126 lb), and a specific impulse level of 1900 seconds.

Contents

Page

Summary iv

1. Introduction 1

2. Design study 3

2.1 Heat transfer study 5

2.2 X–7 Thruster design 9

3. Experimental results and discussion of results 17

3.1 Experimental apparatus 17

3.2 X–7 parametric testing 18

3.3 Parametric test conclusions 27

3.4 500-hour lifetest 30

4. Conclusions 47

5. Recommendations for future work 49

6. Appendices 51

Appendix A – X–4A radiation cooled thruster 51

Appendix B – Design study guidelines 55

Appendix C – Radiation cooled magnet study 59

Appendix D – 500-hour lifetest data 79

7. References 91

8. Distribution list 93

Summary

This report describes the design work, performance and duration testing of a lightweight radiation-cooled MPD arc thruster. The design phase of the work consisted of a heat transfer analysis and a radiation-cooled magnet study which in conjunction with some experimental thruster results established a preliminary thruster design (X–7) for testing evaluation.

Design study

The thruster incorporated a composite anode assembly with a cylindrical tungsten inner core surrounded by a graphite radiation flange with the electromagnet located to the rear of the unit. The electromagnet was designed to simulate an annular permanent magnet. Radiation shields were placed between the magnet and anode assembly to reduce heat to the magnet.

The heat transfer study utilized a computer solution of the heat balance equations applied to the thruster assembly under the assumption that the anode heat load was incident at the nozzle throat of the device. The solutions provided temperature distributions throughout the thruster assembly and allowed an evaluation of various geometrical changes. The calculated temperatures agreed with the experimental thruster measurements.

The results of the mass optimization study provide the geometry of a minimum mass magnet when the required field, internal radius, and distance between magnet face and cathode tip are specified. These results were obtained under the assumption of constant magnetization throughout the magnet volume. Experimental measurements on Alnico-5 and Columax-9 magnets showed this assumption to be in error. A semi-empirical investigation of the effects of flux leakage on the field distribution of annular permanent magnets was then conducted and yielded fair agreement between predicted and measured centerline field distribution for thirteen (13) Alnico-5 magnets provided an empirical B/H curve was used. Application of this technique to several Columax-9 magnets did not produce good agreement.

Thruster tests

Parametric testing of the X–7 thruster was carried out for nozzle throat diameters of 1.524, 1.780, 2.032, and 2.286 cm. Arc current levels up to 700 amps, bias magnetic fields between 0.1 and 0.18 tesla, and ammonia propellant flow rates between 0.020 and 0.040 g/sec were conditions covered in the parametric tests. Arc powers tested ranged between 14.4 and 41.3 kW. The results of these tests showed that MPD thrust efficiency is a linear function of specific impulse between the range of 800 and 3200 seconds with a slope proportional to mass flow rate. The average thrust to power ratios at mass flow rates of 0.040, 0.030 and 0.020 g/sec were 2.2, 1.95 and 1.7 g/kW, respectively.

A 508 hour uninterrupted lifetest of the X–7 thruster was conducted after a modification to the initial cathode electrode geometry was made. Upon inspection of the thruster an additional 46 hours of test time was logged on this unit. Duration testing of the X–7 thruster

produced a transfer from low voltage to a high voltage mode of operation after some 4 hours of test duration and a gradual increase in arc voltage from 50 to 64 volts was recorded over the length of the lifetest. The nominal power level during the lifetest was 32 kW with a specific impulse of 1900 seconds, thrust efficiency without magnet power of 15.6% and with the magnet power an efficiency of 14.5%.

Erosion of the tungsten graphite anode, cathode and boron nitride electrical insulator was 2.2% of their combined original weight with the electrical insulator undergoing the greatest erosion percentage of 41.4%. Motion pictures of the cathode-anode region taken during the lifetest revealed several modes of cathode spot attachment which correlated closely with arc voltage.

Hardware delivery

Delivery of two (2) McDonnell X–4A and eight (8) X–7 radiation-cooled thrusters was made during the contract period. Tests of an X–4A and an X–7 thruster in the NASA Lewis 15-foot diameter facility were in good agreement with the data obtained in this laboratory.

SUMMARY

1 Introduction

Background

The magnetoplasmadynamic (MPD) arc thruster is a low voltage (approximately 50 volts) device which consists of an arc discharge located between a central cathode and a coaxial anode with an applied axial magnetic field. Acceleration of the propellant is accomplished via the electromagnetic body forces that result from the interaction of the magnetic fields and the currents in the ionized propellant. The MPD arc thruster is considered a primary propulsion system candidate due to its relatively high thrust density, simplicity, favorable current-voltage characteristics, and high power capability. Recognition of the potential advantages of MPD arc thrusters has been based upon investigations carried out during the last several years with a variety of propellants and thruster geometries. Specific impulse levels up to 10,000 seconds, input powers between 3 and 300 kW and thrust efficiency up to 40% have been reported in the literature.[1–6] The majority of the investigations have been carried out on water cooled devices. The eventual usefulness of the MPD arc thruster depends upon the success achieved in duplicating or improving water-cooled thruster performance in a radiation-cooled configuration.

Radiation-cooled thruster performance has been reported by Bennett, et al[1] on an ammonia thruster and by Cann and Nelson[2] on a lithium fueled unit. The results of these studies showed that radiation-cooled thrusters gave performance levels comparable to the water-cooled design although some differences in thruster electrical characteristics were noted.

Objectives

The work conducted under this study was directed towards two major objectives: (1) establishment of a minimum weight thruster design with a radiation-cooled magnet, and (2) determination of the reliability of a radiation-cooled thruster by means of a 500 hour life-test. The specific goals of the work were as follows:

(a) Design – A radiation-cooled MPD thruster including electrode system (anode, cathode), electrical insulators, thermal insulators, and radiation-cooled magnet system shall be designed to meet the following requirements:

Power input – 25 kW

Propellant – NH_3

Efficiency – 40% at a given specific impulse between 2000 and 3500 seconds

Maximum heat transfer to the magnet coils of 100 watts

Maximum electrode erosion of 1% by weight per 500 hours at design performance

Minimum weight consistent with reliable performance and minimum electrode erosion

Capability to start and stop ten (10) times without failure to restart.

(b) Testing – The designed radiation-cooled anode-cathode insulator assembly and a

water-cooled version of the magnet system will be fabricated and tested under the following requirements.

> Thruster performance shall be parametrically mapped in the vicinity of the design operating point. This mapping shall be done by varying the input power, mass flow, and magnetic field by ± 10% of the design power.
>
> A 500 hour lifetest shall be conducted to demonstrate that the design requirements have been met. The lifetest shall be conducted in a vacuum facility with a background pressure of 0.1 torr or less.

(c) Delivery of Hardware – Two (2) thrusters of the McDonnell Douglas X–4A (see Appendix A) design will be delivered to the NASA Lewis Research Center within the first two months of the contract. These thrusters will be operated by NASA so that thrust performance obtained in the NASA facility may be compared with that obtained in the McDonnell Douglas facility. After the design study has been completed and within the first five months of the contract, two (2) anode-cathode insulator assemblies and one (1) magnet assembly conforming to the configuration approved under the design phase shall be delivered to NASA. Upon completion of the 500 hour lifetest and within the twelfth month of the contract, six (6) anode-cathode insulator assemblies and two (2) magnet assemblies of a configuration which passed the 500 hour lifetest shall be delivered to NASA/Lewis.

2 Design study

The objective of this phase of the work was the establishment of a thruster configuration capable of radiation-cooled operation at the conditions specified in the contract goals (see Introduction, Section 1). The quantities to be determined were the thruster independent operating parameters (i.e., mass flow rate, arc current and applied magnetic field) and the physical dimensions of the unit.

A number of design guidelines and considerations were set forth which further delineated the design problem. These conditions are given below and the rationale pertinent to their selection is given in Appendix B.

Operating parameters

- Propellant mass flow rate – 17 to 52 mg/sec
- Arc current – 400 to 750 amps
- Power radiated from anode assembly – 12.5 kW
- External magnetic field at cathode tip – 0.05 to 0.2 tesla

Thruster geometry

- The diameter of the cathode rod or support exterior to the thruster should be minimized so that the inner radius of the magnet may be as small as possible.
- The distance between the cathode tip and the downstream face of the magnet should be minimized.
- Provisions should be incorporated for changing the electrode gap and nozzle throat diameter so the thruster performance may be optimized with respect to these two dimensions.
- A composite anode assembly consisting of a tungsten inner core and a graphite radiation flange should be utilized to provide a low thruster weight.
- Thermal conduction paths between the magnet and rear surface of the anode should be minimized.
- Propellant should be introduced through the cathode. The high current operation required that the limited regenerative-cooling capability of ammonia be utilized in the cathode region to reduce erosion.

Using the above guidelines a preliminary thruster geometry was set and is shown in Fig. 2.1. This configuration (designated X–6) is similar in design to the X–4A thruster (Appendix A) which had been tested at McDonnell Research Laboratories. The anode structure consists of an inner tungsten annulus and two graphite flanges lap fitted and bolted to the tungsten annulus. The tungsten core forms the nozzle throat and housing which supports and seals the cathode and electrical insulator assembly. The graphite flanges provide a large surface area of high emissivity for radiation of the anode heat load with relatively low mass. The

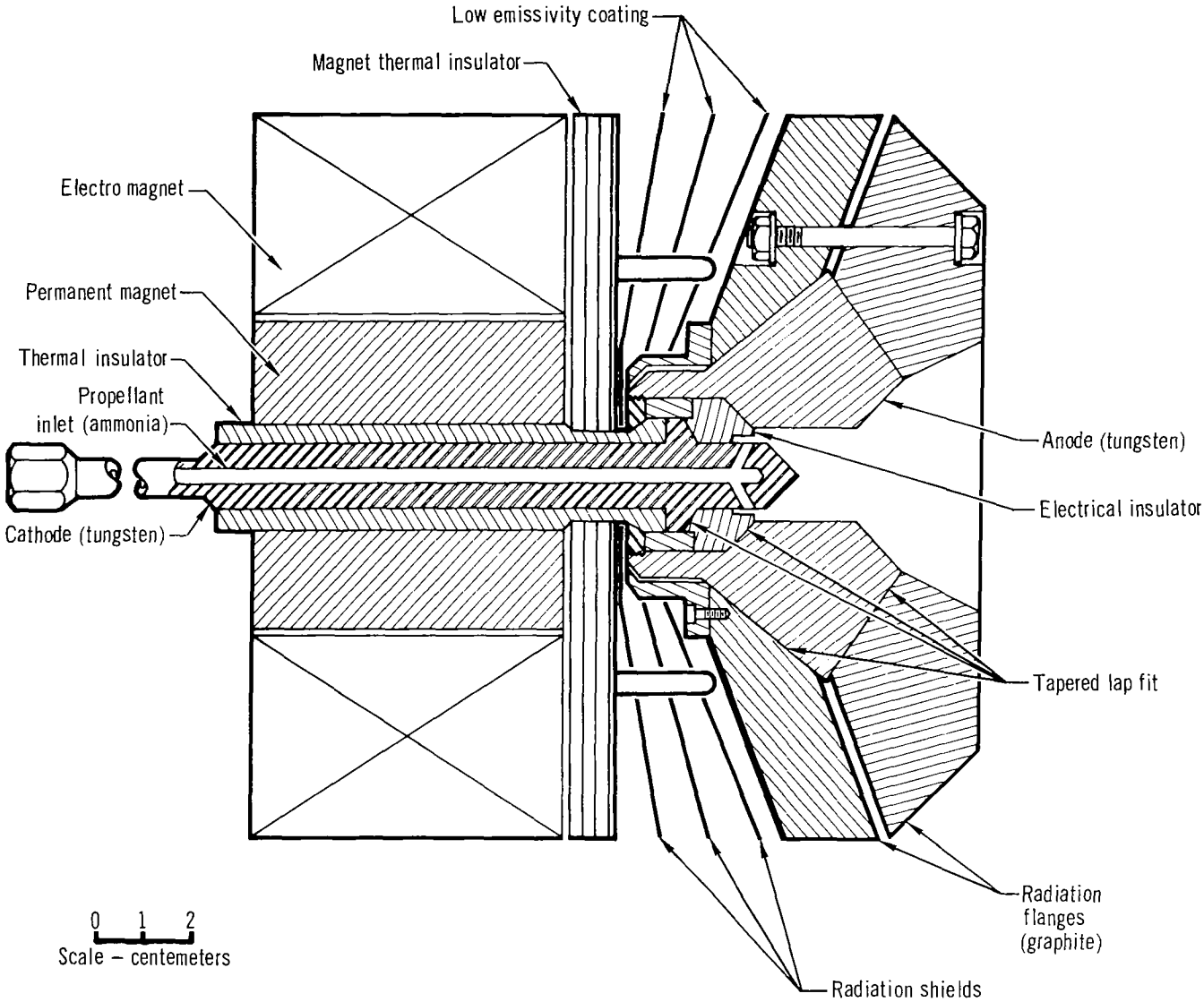

Fig. 2.1 X–6 MPD thruster configuration

cathode consists of a pointed rod with a hole bored along the axis for propellant supply. The propellant is injected through ports drilled into the cathode behind the tip. The cathode has a tapered flange lap-fitted to a boron nitride insulator which in turn is lap-fitted to the anode to form a gas tight seal. Located between the rear graphite flange and the face of the magnet are a series of radiation shields which reduce rearward radiation heat transfer.

With the X–6 thruster geometry set up as a preliminary model the design study was subdivided into two areas; 1) a heat transfer study (described below) to determine the temperature distribution in the thruster and evaluate the effects of geometry changes on the temperature distributions, and 2) a radiation-cooled magnet study (see Appendix C) which for a given magnetic field and separation from the cathode would provide the geometry of the minimum mass magnet.

2.1 Heat transfer study

Heat transfer calculations for the MPD thruster geometry were made by subdividing the assembly into a number of volume elements or nodes and simultaneously solving the heat flux balance equations for each node by means of a computer. The computer program uses the method of finite differences with the heat balance equations solved in the implicit or backward difference method. An initial temperature distribution is estimated, and the program iterates to the correct solution.

Two computer programs were used in the heat transfer calculations. The first program was limited to approximately 144 nodes. The initial calculations were made in the anode region using this program. The second program became available during the study and had a capacity for at least 250 nodes. This program was set up on a high speed digital computer and resulted in shorter computation times.

Assumptions and approximations

The assumptions made for the calculations include the following:

(1) heat into the anode was at the arc attachment region,

(2) arc attachment on the anode takes place in the last 0.508 cm length of the throat, and

(3) no heating or cooling by the propellant.

In addition to assigning values to the different coefficients such as conductivity and emissivity, other approximations perhaps less accurate were required. These quantities include several interface resistances and the convective heat transfer coefficient in the water-cooled magnet.

The interface resistance was approximated by first analyzing the surface contact. A point contact may exist with almost zero transfer area which may appear as follows:

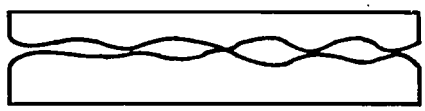

or an exact surface contact could be assumed such that 100% of the area would transfer heat by conduction. These surfaces may appear as follows:

However, if these two surfaces were only slightly mismatched as follows:

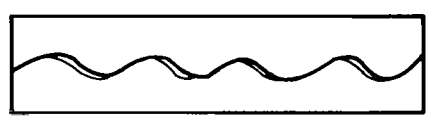

then about 50% of total contact exists. The probability of this condition is small because the grooves on the two surfaces will seldom be alike.

One would conclude that the point contact condition would represent the actual interface without any force applied to cause deformation of the peaks. All interface surfaces of the thruster were under load. Therefore, the contact area was actually increased. A value of 0.25 of the total interface area was chosen to represent the heat transfer area by conduction.

A comparison of conduction over 0.25 of the area and radiation over the remaining 0.75 showed that conduction far exceeds radiation as the mode of heat transfer across the interface.

The interface conductance was chosen to be 0.25 of the average quotient of the thermal conductivity of the two materials divided by the total height of surface roughness. If the interface was a lapped joint, then a value of 0.5 of the total area was used to describe the heat conduction area.

An estimation of the convection coefficient was made using an empirical expression recommended by Wiegand[7] for a fluid in a flat or annular passage. This expression is valid for Reynolds numbers greater than 5000.

$$\frac{h\,D_e}{k} = 0.023\,(R_e)^{0.8}\,(P_r)^{1/3} \qquad (2.1)$$

where h = convective heat transfer coefficient,
k = thermal conductivity of fluid,
D_e = equivalent diameter of passage,
R_e = Reynolds number at film temperature,
P_r = Prandtl number at film temperature.

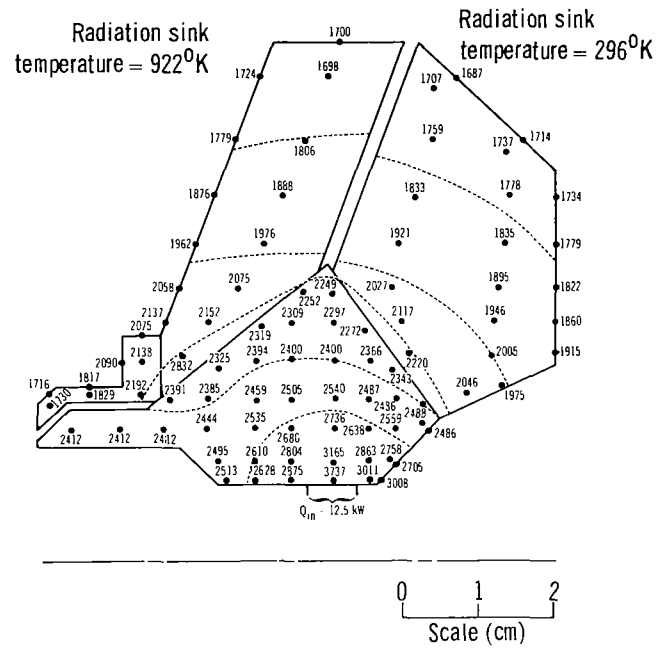

Fig. 2.2 Calculated temperature distribution in X–6 thruster for Q_{in}= 12.5 kW

Calculations

In the initial phase of the MPD heat transfer analysis only the anode assembly was considered, since in this region the highest temperatures occur and a relatively simple thermal model was desired for initial checkout procedures and program debugging.

A radiation sink temperature of 296°K was assumed for the surfaces viewing the vacuum facility. Thermal conductivity and emissivity of the tungsten and graphite were considered as functions of temperature. The tungsten-graphite interface conductance was neglected in the initial phase of the calculations. Figure 2.2 shows the initial temperature distribution calculated for the X–6 anode assembly. The heat input was 12.5 kW and the throat diameter was 1.524 cm. As indicated, the temperature of the throat region of the anode is slightly above the melting point of tungsten (3683°K).

The first geometry change was adjusting the graphite expansion angle so that it was equal to the tungsten expansion angle. Figure 2.3 shows the temperature

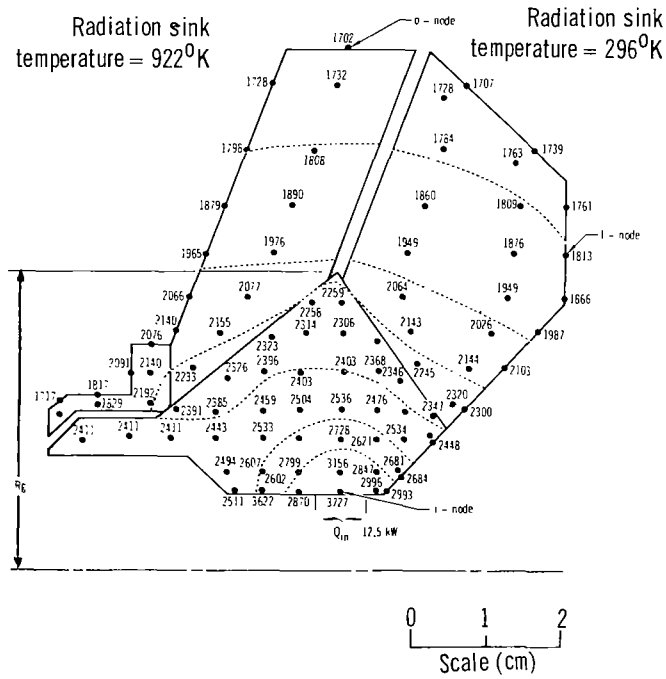

Fig. 2.3 Calculated temperature distribution in X–6 thruster for Q_{in}= 12.5 kW

distribution for this case and comparison with Fig. 2.2 shows a slight reduction which in conjunction with the reduced mass of the graphite makes this feature desirable.

The next step in the heat transfer analysis was a systematic variation of the anode geometry to determine which configuration gives the lowest temperature at the throat and rearward heat transfer to the magnet consistent with reasonable thruster weight. The parameters that were varied are:

(a) throat heat flux, total power to anode ranged from 12.5 to 6 kW,

(b) throat diameter, 1.52 to 2.03 cm,

(c) graphite radiation flanges, outside diameter and internal expansion angle,

(d) tungsten anode geometry, external ramp angle was changed,

(e) rearward radiation shields, materials and number of shields.

The total power to the anode was supplied in 8 steps ranging from 12.5 kW to 6 kW. The temperature distributions were calculated for each power step and for throat diameters of 1.524, 1.778, and 2.032 cm. For these three diameters the maximum throat temperatures were 3617, 3675 and 3740°K respectively, for 12.5 kW power to the anode. An increase in throat temperature with throat diameter occurs because the effects of the lower incident heat flux are outweighed by the reduced radiation surface area. Enlarging the throat diameter is one method of increasing the power capability of the thruster since it is usually accompanied by an increase in arc voltage.

For the purpose of discussion, three characteristic nodes are shown in Fig. 2.3. These are the "i node" which is the maximum throat temperature and the incident heat flux location, the "f node" which is the front surface location, and the "o node" which is on the outer diameter surface of the graphite radiation flange.

Table 2.1 presents the temperatures for the characteristic nodes for the X–6 thruster where the outer radius of the graphite radiation flanges was varied between 14 and 20.3 cm and the heat into the anode was varied between 6.0 and 12.5 kW. A significant reduction in the throat temperature can be obtained by increasing the outer diameter of the radiation flanges. Increasing the radiation flange diameter thus allows a scaleup in the power capability of the thruster.

Table 2.1 Calculated X–6 characteristic node temperatures as a function of radiation flange radius and incident heat load

Radiation flange outer radius (cm)	Heat load (kW)	Node temperatures (^{o}K)		
		T_i	T_f	T_o
14	12.5	3727	1813	1702
14	12.0	3621	1795	1687
14	11.0	3414	1757	1656
14	10.0	3205	1716	1622
14	9.0	2994	1671	1586
14	8.0	2783	1622	1545
14	7.0	2572	1569	1500
14	6.0	2354	1508	1449
16.5	12.5	3582	1664	1489
16.5	12.0	3474	1646	1476
16.5	11.0	3270	1608	1450
16.5	10.0	3056	1567	1420
16.5	9.0	2845	1523	1389
16.5	8.0	2633	1475	1353
16.5	7.0	2423	1424	1315
16.5	6.0	2207	1366	1271
20.3	12.5	3367	1517	1198
20.3	12.0	3262	1499	1188
20.3	11.0	3057	1460	1169
20.3	10.0	2851	1419	1148
20.3	9.0	2644	1375	1124
20.3	8.0	2436	1327	1098
20.3	7.0	2231	1277	1069
20.3	6.0	2019	1220	1036

Figure 2.4 illustrates the effect of thruster mass on throat temperature when the outer radiation flange diameter is increased. A throat temperature decrease of approximately 310°K per kg of mass can be expected by increasing the radiation flange diameter.

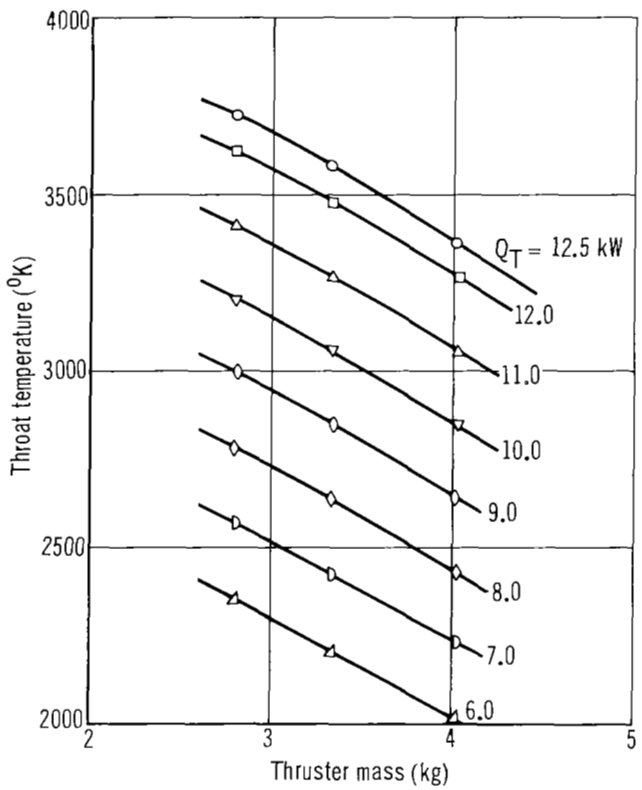

Fig. 2.4 X–6 throat temperature vs thruster mass for various heat inputs

The effect of changing the tungsten geometry on the temperature distribution was also investigated. The maximum radius R_g (see Fig. 2.3) of the tungsten anode was varied from 2.54 to 5.72 cm. In changing this diameter, both ramp angles were varied and the axial location of the apex of the angles was maintained so that the apex remained in the middle of the slot between the radiation flanges. Table 2.2 shows the characteristic node temperatures for the three cases considered.

Table 2.2 Calculated X–6 characteristic node temperatures as a function of maximum tungsten anode radius

Tungsten anode maximum radius (cm)	Heat load (kW)	Node temperatures (°F)		
		T_i	T_f	T_o
5.72	12.5	3506	1761	1672
5.72	12.0	3410	1744	1677
5.72	11.0	3222	1708	1646
5.72	10.0	3033	1669	1612
5.72	9.0	2842	1627	1575
5.72	8.0	2648	1580	1534
5.72	7.0	2454	1530	1489
5.72	6.0	2253	1474	1438
3.18	12.5	3701	1800	1730
3.18	12.0	3595	1783	1715
3.18	11.0	3389	1745	1683
3.18	10.0	3181	1704	1647
3.18	9.0	2973	1661	1608
3.18	8.0	2763	1612	1566
3.18	7.0	2554	1560	1520
3.18	6.0	2339	1501	1466
2.54	12.5	3761	1831	1684
2.54	12.0	3650	1813	1669
2.54	11.0	3437	1774	1639
2.54	10.0	3221	1732	1606
2.54	9.0	3007	1687	1571
2.54	8.0	2792	1637	1530
2.54	7.0	2578	1582	1486
2.54	6.0	2358	1521	1436

Figure 2.5 shows that a throat temperature decrease of approximately 210°K per kg of mass can be realized by increasing the tungsten outside diameter. Therefore, for a given heat load into the anode a reduction in the throat temperature is best accomplished by enlarging the radiation graphite flanges rather than the tungsten anode section.

A limited amount of work was done on the rearward radiation shields up to this point due to the node limitation of the program.

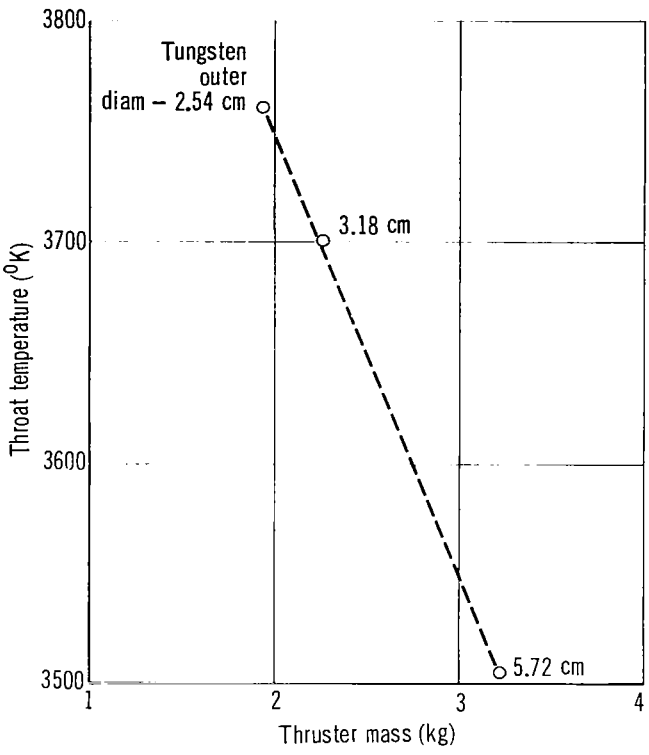

Fig. 2.5 Effect of increasing mass of tungsten in X-6 thruster, Q = 12.5 kW

2.2 *X-7 thruster design*

At this stage in the design study and after three months into the contract period, the contract work schedule called for the definition of an initial thruster design. The heat transfer and radiation-cooled magnet design studies were being carried out concurrently with continued experimental tests on the X–4A thruster. The results of these tests and the design work were used to establish the X–7 thruster configuration shown in Fig. 2.6.

The basic features of the X–4A thruster geometry were included in the X–7 design. The design aspects which were considered to be basically proven were as follows:

(a) a composite anode comprised of an inner 2% thoriated tungsten surrounded by a graphite radiation flange and in contact with the tungsten annulus by means of a lapped taper joint;

(b) a central rod cathode incorporating propellant feed through the rod; thereby, providing regenerative-cooling to the cathode;

(c) a magnet located to the rear of and concentric with the anode assembly, with radiation shields interposed between the magnet and anode to reduce rearward heat transfer to the magnet.

Continued operation of the X–4A served to point out several design aspects which appeared marginal for long duration tests. These critical areas were as follows:

(a) The bolts securing the graphite radiation flanges to the tungsten annulus loosened with continued operation. The loosening became aggravated as the test continued indicating a stretching and expansion of the bolts under the high temperatures encountered.

(b) The screws holding the cathode holder and insulator in compression within the tungsten annulus also loosened with continued operation; thereby allowing some propellant leakage at the rear of the thruster.

(c) The internal expansion surface of the downstream radiation flange suffered some erosion near the downstream edge of the tungsten annulus. This erosion is thought to be caused by either friction with the high temperature plasma flow or some arc current attachment in the location of the erosion.

(d) The forward edge of the boron nitride insulator which viewed the arc discharge and was in contact with tungsten annulus at its outer edge suffered some erosion.

(e) The internal surface of the boron nitride insulator immediately surrounding the propellant inlet holes in the cathode suffered erosion. This erosion was due to the impingement of the propellant on the insulator surface and was clearly defined near the three propellant inlets.

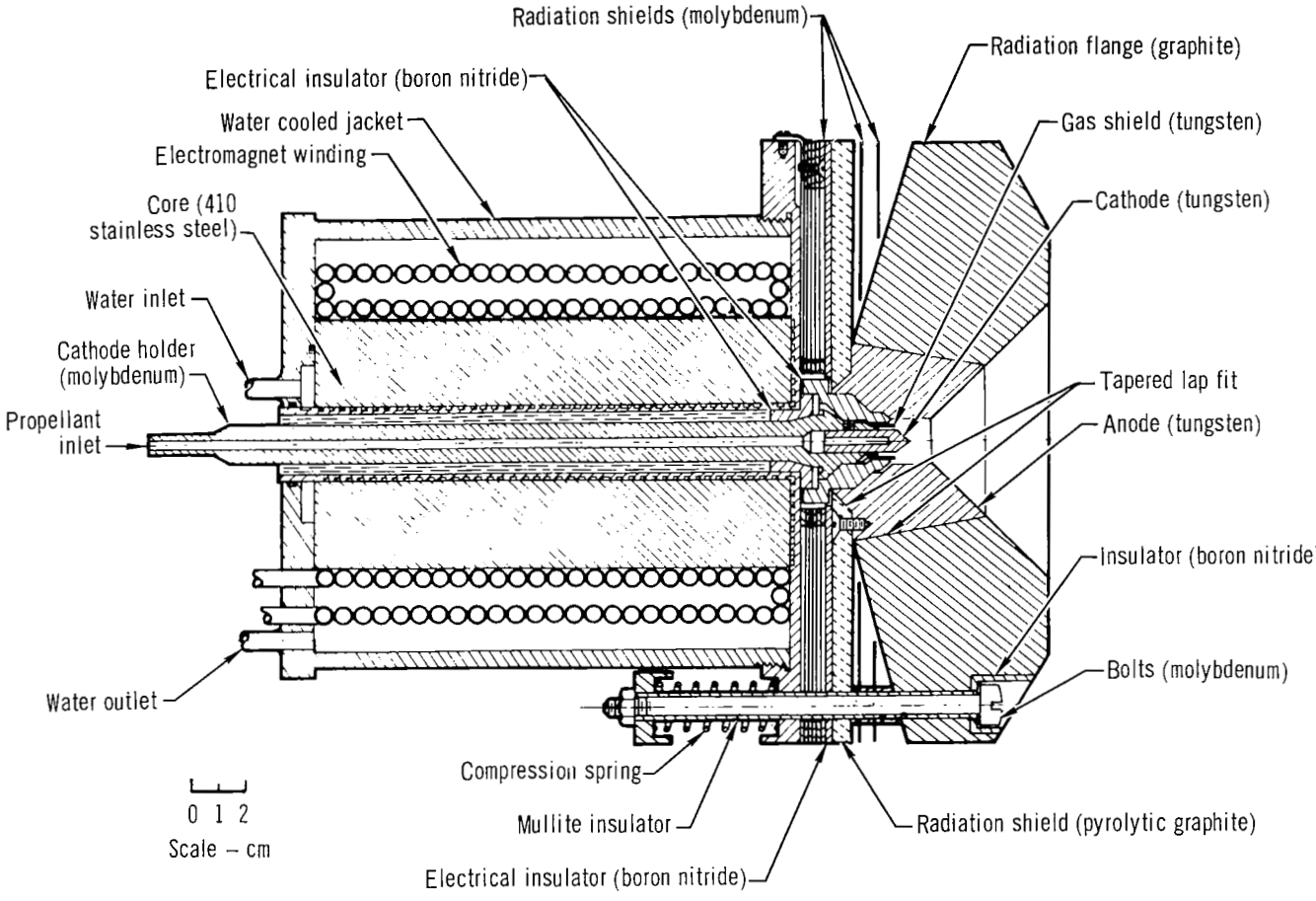

Fig. 2.6 X–7 Radiation cooled MPD thruster

The X–7 design was aimed at circumventing the above problem areas and the especial aspects of the design are enumerated below.

(a) The anode-cathode insulator assembly is held in compression with the magnet by means of four compression springs. This arrangement allows for thermal expansion of the unit during warm-up while still maintaining a compressive load for gas sealing.

(b) The dual radiation flange geometry was replaced with a single flange.

This feature in combination with compression springs was designed to eliminate the problem associated with the bolts of the X–4A. The tungsten annulus came in contact with the radiation flange along a single surface rather than at the double ramp angle of the X–4A design. This feature served to reduce the applicability of the X–6 heat transfer calculations to the X–7 design; however, it was felt that the change in tungsten geometry was not so great as to invalidate the qualitative results obtained on the X–6 unit.

(c) The tungsten annulus of the X–7 design provided a greater surface area in the expansion region than the X–4A design. This feature coupled with the continued expansion of the graphite radiation flange along a 45° angle was aimed at reducing the erosion problem.

(l) The X–7 boron nitride cathode insulator was designed to move the loaded surface or gas seal surface upstream to a lower temperature region and also the forward end of the insulator was in direct contact with the tungsten anode. This change should decrease the erosion problem stated in (g).

(m) A tungsten gas shield was placed concentric to the cathode in the X–7 design. This shield floats electrically and eliminated the direct impingement of the propellant on the cathode insulator.

The X–7 unit had a tungsten maximum diameter of 6.35 cm and graphite radiation flange diameter of 20.3 cm. Based upon extrapolation of the X–6 heat transfer calculation it was estimated that this unit would be capable of steady operation in the range of 40 kW.

A water-cooled electromagnet was used in the X–7 configuration as a simulated permanent annular magnet. A design field of 0.1 tesla at a distance of 3.81 cm from the cathode tip was chosen as a condition which could be supplied by a radiation-cooled permanent annular magnet. The water-cooled magnet core dimensions were chosen to be the same as a minimum mass Columax–9 magnet. The magnet dimensions were R_o = 4.18 cm, R_i = 1.27 cm and L = 16.1 cm and were dictated by the results of the radiation-cooled magnet study.

A bar magnet would provide the lowest weight magnet; however, an annular magnet of internal radius of 1.27 cm requires an increase of only 1.77 kg over the bar magnet case. In view of the complexity of turning the cathode 90° to allow positioning of a bar magnet and the asymmetry thereby produced, it was concluded that the additional weight of the annular magnet was more than compensated for by design simplicity. Operation of an annular magnet on the B_z maximum was rejected because of the large weight required. This electromagnet incorporated a core of type 410 stainless steel and was wound with 80 turns of insulated 0.635 cm diameter copper tubing. Magnetic fields up to 0.18 tesla could be provided at the cathode tip.

Heat transfer to the magnet of the X–7 thruster was reduced below that of the X–4A unit (approximately 1 kW) by increasing the number of radiation shields to nine, seven adjacent to the thruster and two near the radiation flange. Located between the radiation shields and secured to the tungsten annulus was a pyrolytic graphite radiation plate 0.635 cm thick. This plate combined with a boron nitride shield, electrical insulation, and radiation shield was anticipated to reduce the heat transfer to the magnet to a range of several hundred watts.

X–7 heat transfer calculations

A heat transfer analysis of the X–7 radiation-cooled thruster was conducted to determine the steady state temperature distribution throughout the thruster assembly. This analysis was similar to that made on the X–6. The heat load was assumed incident at the anode in the throat region over an axial length of 0.508 cm. Calculations were set up to cover input heat loads between 8 and 20 kW.

The first node set up did not cover the entire thruster assembly because of the limited capacity of the computer program. The node size was next enlarged in the low temperature gradient regions to permit the performance of calculations over the entire thruster and water-cooled magnet. Although these calculations were qualitative they did yield several interesting results.

The heat transfer into the magnet was 1 kW with 16 kW as an input anode heat load. The maximum throat temperature was below the melting temperature of the tungsten with 16 kW applied to the anode. The temperature distribution in the pyrolytic graphite plate indicated that there was not a significant axial temperature gradient across it as was expected and that it was not serving as an effective thermal insulator.

The radial conduction path between the pyrolytic graphite and tungsten nozzle was broken by enlarging the tapered hole in the pyrolytic graphite. This in-

creased hole size made the pyrolytic graphite a more effective insulator; however, the maximum throat temperature also increased. Therefore, one can choose the direction of heat flow depending on whether it is desirable to decrease the heat flow back to the magnet.

The second heat transfer computer program with an increased nodal capacity became available at this period. This allowed a more refined analysis of the thruster. Areas that were refined included the forward end of the magnet where the cathode holder backing plate and insulator were undercut to reduce the conduction area. This modification resulted in about 35°K decrease in temperature at the magnet surface. Computations were extended to include the cathode holder resistive heating and the pyrolytic graphite plate nodes were subdivided.

Since the pyrolytic graphite plate in effect placed a high temperature surface between the radiation shields, a calculation was made wherein this plate was eliminated. The throat temperature increased 58°K, the graphite radiation flange surface temperature increased 16°K, and the magnet face temperatures were reduced by 1°K. Thus, simple elimination of the pyrolytic graphite does not produce an improvement in the temperature distribution.

For the next calculation a 0.025 cm thick sheet of molybdenum replaced the pyrolytic graphite. The surface temperature on the graphite flange and the maximum throat temperature were increased 1°K and 2°K, respectively, while the temperature on the radiation shield next to the magnet was reduced 50°K from the condition with the pyrolytic graphite.

Figure 2.7 shows a typical temperature distribution for the X–7 thruster with 16 kW applied to the anode and with water cooling supplied to the magnet housing.

To ascertain the operating temperature for a radiation-cooled permanent magnet thruster the water cooling was eliminated and the compression joint between the magnet and thruster assembly was moved to the upstream end of the magnet. In the water-cooled magnet calculation the pressure joint was at the downstream end. Figure 2.8 shows the complete temperature distribution for a radiation-cooled permanent magnet coated with lampblack on its outer surface ($\epsilon = 0.95$). As shown, the maximum temperature in the magnet is near 800°K, well below the Curie point of Columax–9. The total heat flow through the magnet at 16 kW into the anode was 0.41 kW.

The final calculations were made to investigate the use of more efficient insulators to replace the seven reflector shields. Three sheets of 0.254 cm thick zirconium felt were assumed. The calculated temperature on the thruster end magnet face at a radial position of 3.378 cm was 815°K with the zirconium felt and 730°K with the molybdenum reflector shields. It is therefore, still believed that the radiation shields are the preferred method to thermally insulate the magnet.

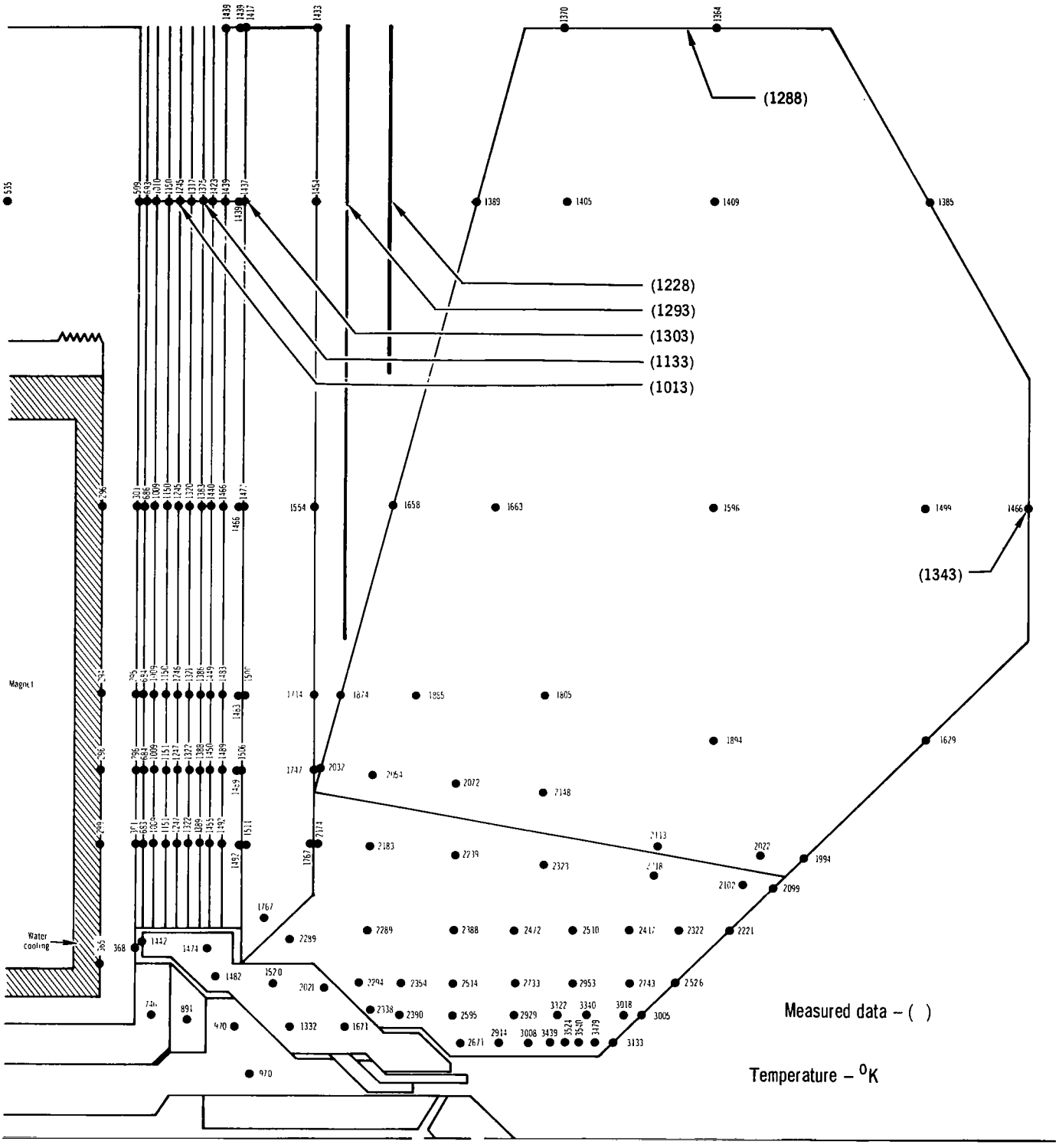

Fig. 2.7 Measured and calculated temperature distribution in X–7 thruster for Q_{in}= 16 kW

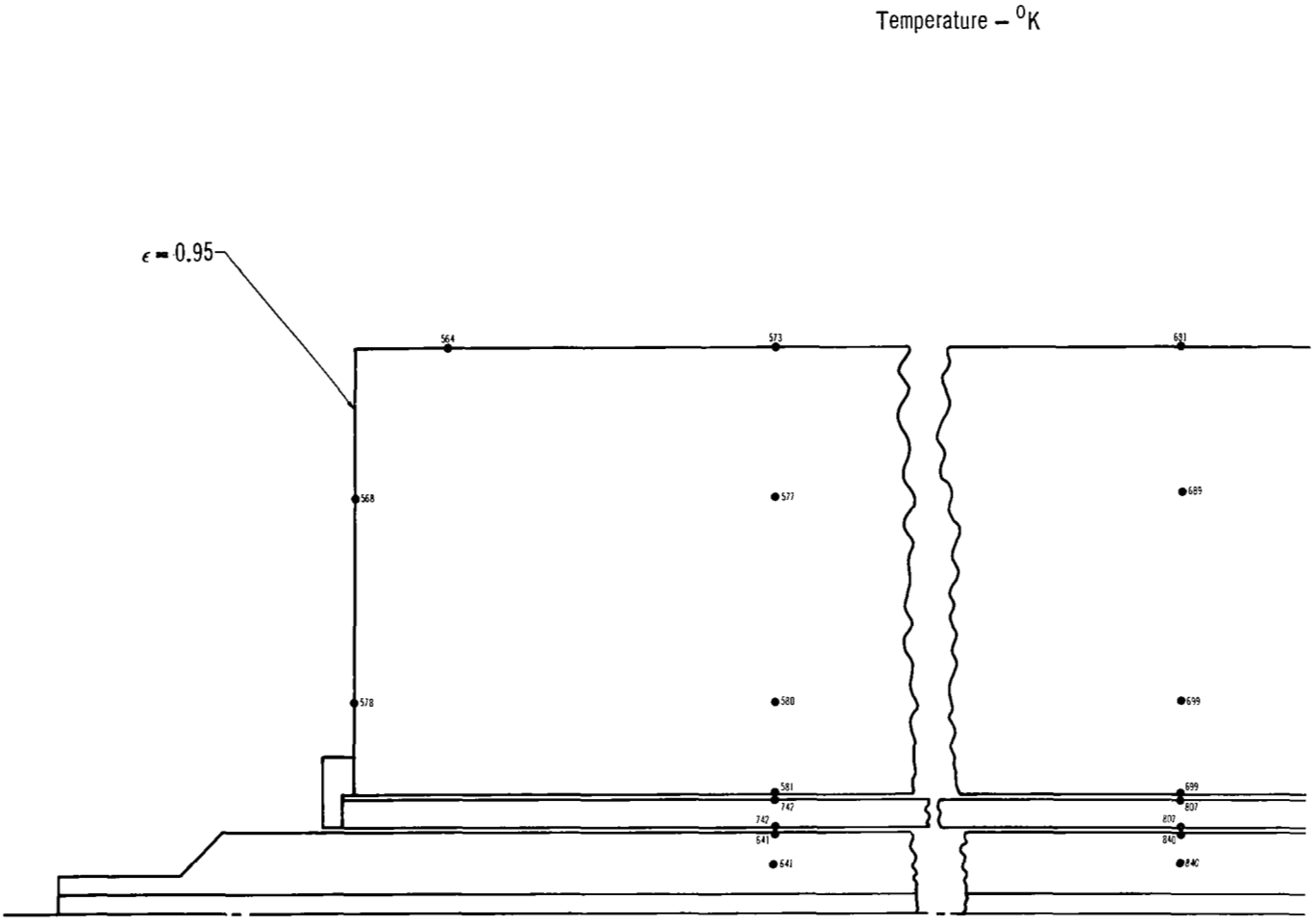

Fig. 2.8 Complete calculated temperature distribution for X–7 thruster Q_{in} = 16 kW

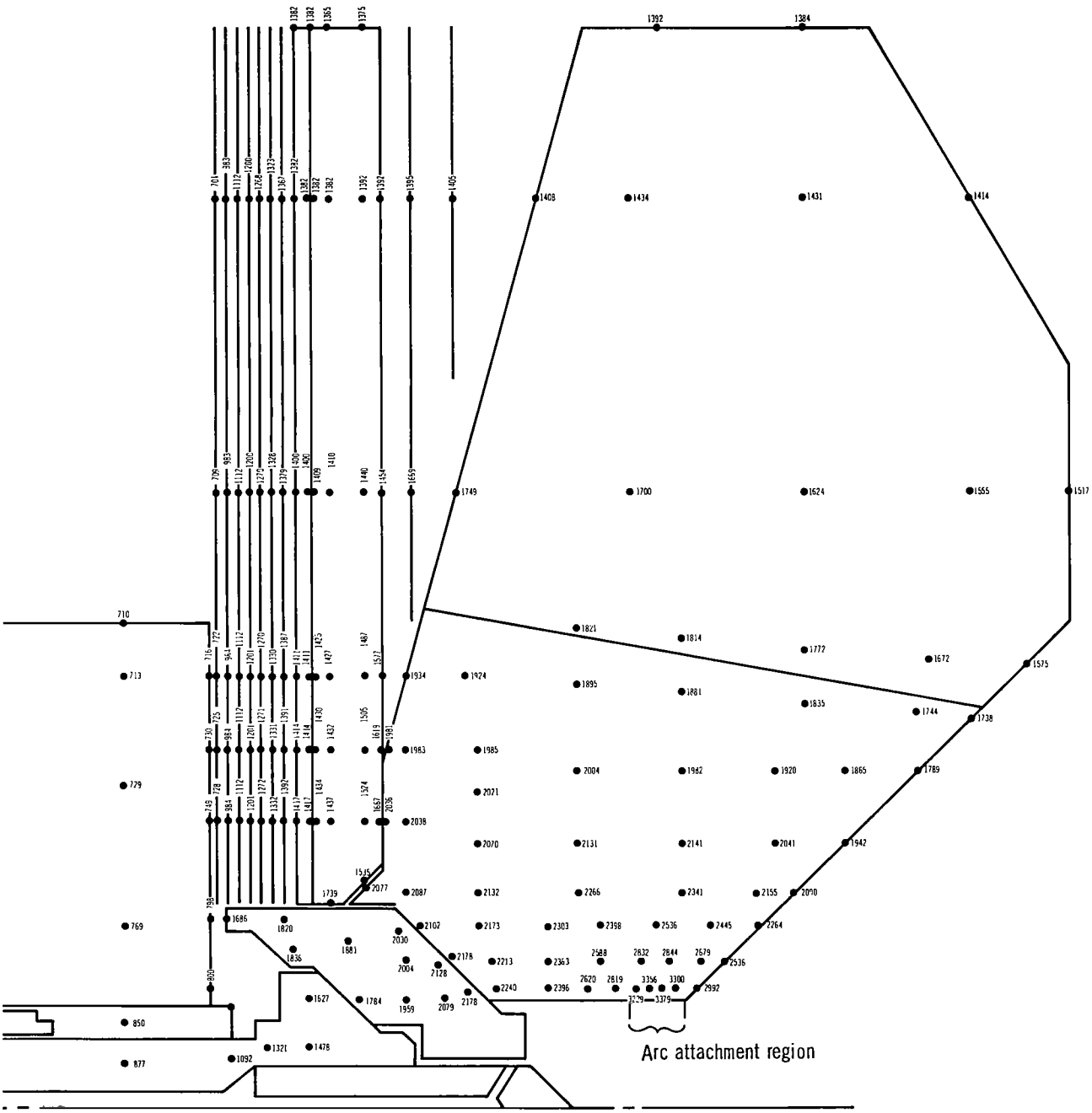

Fig. 2.8 Complete calculated temperature distribution for X–7 thruster Q_{in} = 16 kW (Continued)

3 Experimental results and discussion of results

In this section the experimental results of the X–7 parametric tests and the 500 hour lifetest are presented. Tests were conducted on the X–4A thruster during the design phase for comparison with tests conducted in NASA LeRC's high vacuum facility on a similar X–4A unit. The X–4A unit and the results of the tests are described in Appendix A.

3.1 *Experimental apparatus*

All the experiments were conducted using ammonia as the propellant and were performed in a 0.91 meter diameter, 4.0 meter long vacuum chamber. Background pressure was a function of mass throughput with a typical value of 10^{-2} Torr attainable with an ammonia flow rate of 0.040 g/sec, as measured with an alphatron vacuum gauge.

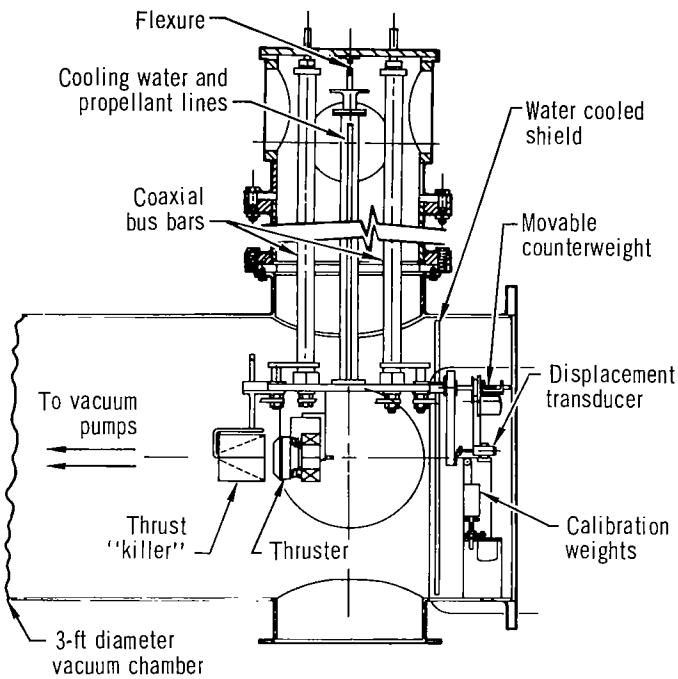

Fig. 3.1 Thrust stand

Thrust measurement – Thrust performance measurements were obtained by means of a single pendulum thrust stand. This stand, shown schematically in Fig. 3.1, has a pendulum 1.78 meters in length and is suspended by two thin stainless steel flexures. Cooling water and propellant lines are brought in through the top of the stand by means of rubber hoses. Electrical power for the thruster and magnet is connected to the stand by mercury pots and is brought to the thruster through coaxial buses. Power is supplied by four (4) 60 kW Miller welding rectifiers. The pendulum bar and mounting plate are water-cooled to reduce thermal drift. Deflection of the pendulum is determined by a linear displacement transducer with output indicated on a strip chart recorder. A calibration of thrust versus deflection is obtained by a pulley and known weight arrangement. A thrust "killer" or flow deflection bucket is attached to the stand and can be swung

in front of the thruster to turn the exhaust flow 90° to the thrust direction. Thrust was measured by blocking the exhaust with the "killer" for a period of 10 to 15 seconds and recording the change in deflection of the pendulum. Use of the "killer" technique has been previously reported[12] and is particularly useful for radiation-cooled thruster work where thermal drift of the stand is usually encountered.

Thruster measurements —Current and voltage to thruster and magnet were measured by standard dc current shunts and voltmeter. Ammonia mass flow rates were measured by use of sonic flow nozzles and water flow rates were recorded with standard rotometers. Cooling water temperatures were obtained with differential thermopiles located in the inlet and outlet cooling lines. Magnetic field measurements were determined using commercial Hall effect probes. Thruster operating temperatures were measured with 97 tungsten 3 rhenium versus 75 tungsten 25 rhenium thermocouples.

Experimental measurements of thrust, arc current, voltage and ammonia mass flow rate were used to determine the specific impulse and thrust efficiency from Eqs. (3.1) and (3.2):

$$I_{sp} = \frac{T}{\dot{m}\, g}, \tag{3.1}$$

$$\eta = \frac{T^2}{2\dot{m}\, P_a}, \tag{3.2}$$

where T = thrust,

$\dot{m}$ = mass flow rate,

P_a = arc power,

g = gravitational constant.

Thruster — The X–7 thruster was described in detail in Section 2. Figure 3.2 is a photograph of the component parts of the first X–7 thruster which was fabricated. Figure 3.3 is a photograph of the unit assembled with its water-cooled magnet. The axial and radial magnetic field distributions of this magnet at a magnet current of 400 amps is shown in Figs. 3.4 and 3.5

3.2 X-7 parametric testing

The program for this phase as originally outlined called for testing of nozzle throat diameters of 1.524, 1.780, 2.032 and 2.286 cm at mass flow rates of 0.040, 0.030 and 0.20 g/sec, magnetic fields of 0.1, 0.14 and 0.18 tesla and arc current levels of 300, 400, 500, 600 and 700 amps. Various difficulties which were encountered prevented testing at all of these points. The test data to be presented was generally taken during runs which lasted for periods of between 3 and 6 hours. The thruster was operated at each test point for approximately 0.5 hours before thrust data was recorded. A period of approximately 20 minutes was required before thermal equilibrium of the anode assembly was obtained.

1.524 cm throat diameter — Thrust performance of the X–7 thruster with a throat diameter of 1.524 cm was obtained for ammonia mass flow rates of 0.40 and 0.030 g/sec and for magnetic field values of 0.10, 0.14, and 0.18 tesla. Figure 3.6 shows the specific impulse and thrust efficiency characteristics obtained. The performance is similar to that recorded on the X–4A thruster in that the thrust-to-power ratio is mass flow dependent. The effect of increasing the magnetic field at constant mass flow rate serves only to increase the power of the device and not the thrust-to-power ratio. A summary of the data obtained on the 1.524 cm unit is shown in Table 3.1.

Testing at flow rates below 0.030 g/sec were scheduled; however, throat erosion was observed during a test at 700 amps. Subsequent checkout revealed an obstruction at the throat of the sonic flow nozzle used in controlling the mass flow rate, and consequently the erosion occurred due to reduced flow. Inspection of the thruster upon disassembly indicated

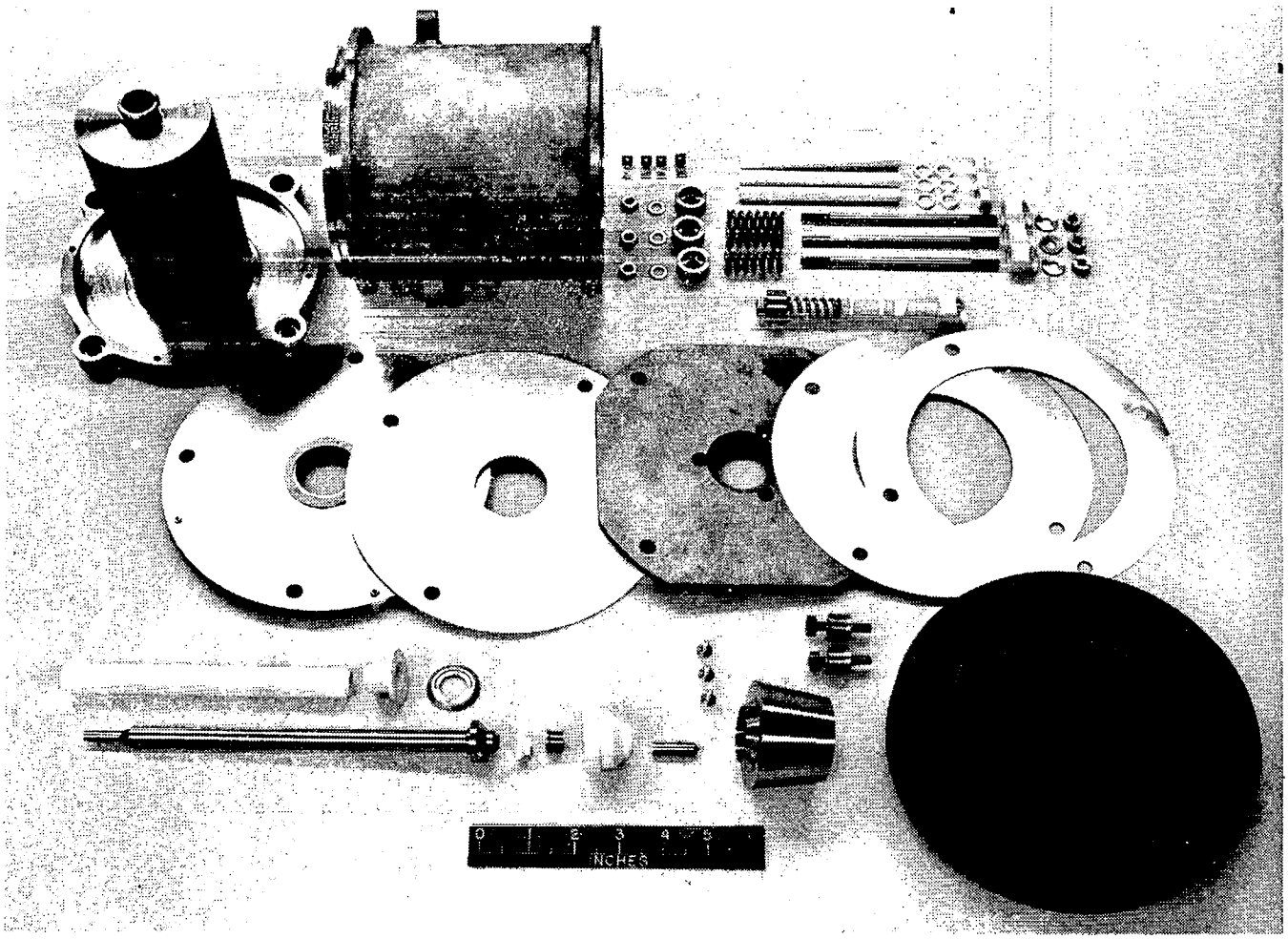

Fig. 3.2 X–7 Radiation cooled thruster components

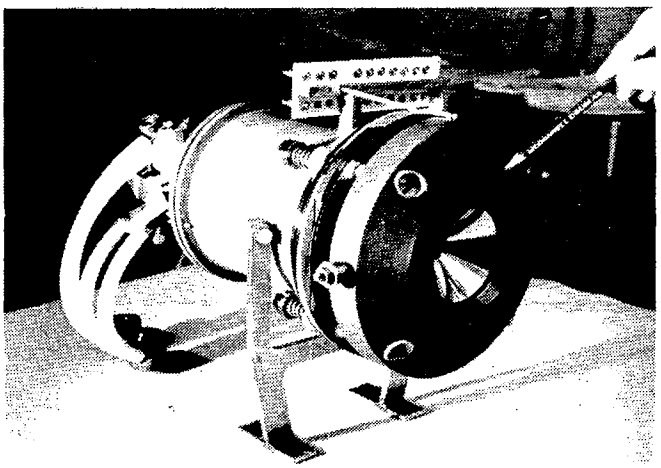

Fig. 3.3 X–7 thruster assembled

that the tungsten gas shield had loosened considerably due to a loss of the boron nitride sleeve which maintains the shield concentric to the cathode. Erosion was also observed on the downstream edge of the main cathode to anode insulator.

1.780 cm throat diameter – The throat of the tungsten nozzle was remachined to a diameter of 1.780 cm and the thruster was reassembled. A new anode-cathode insulator, gas shield, and gas shield sleeve insulator were used in this assembly. The anode-cathode insulator was machined from an improved grade of boron nitride (Union Carbide grade HD0092) rather than the previous hot pressed boron nitride.

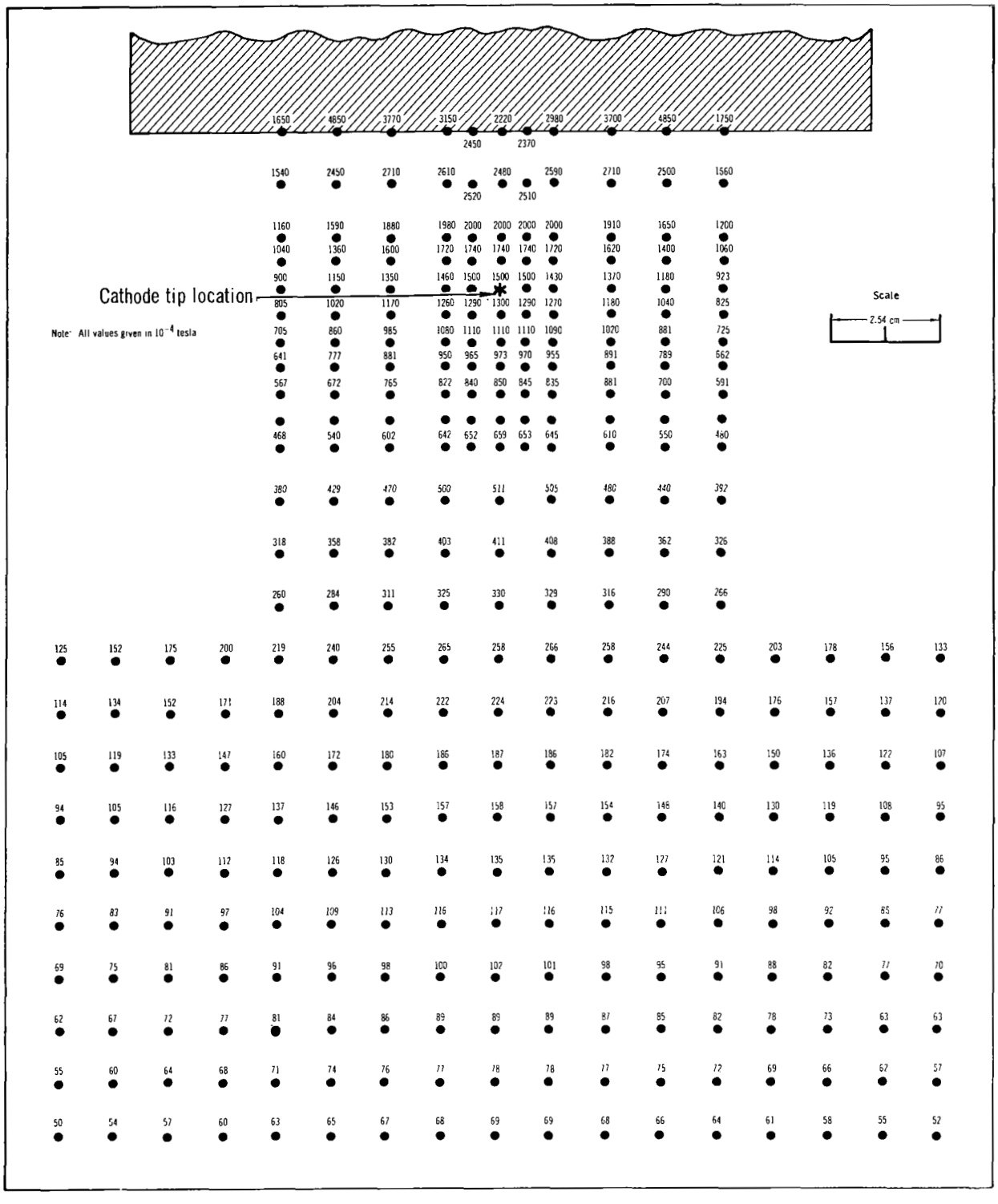

Fig. 3.4 Axial magnetic field of X–7 electromagnet (I_{mag} = 400 amperes)

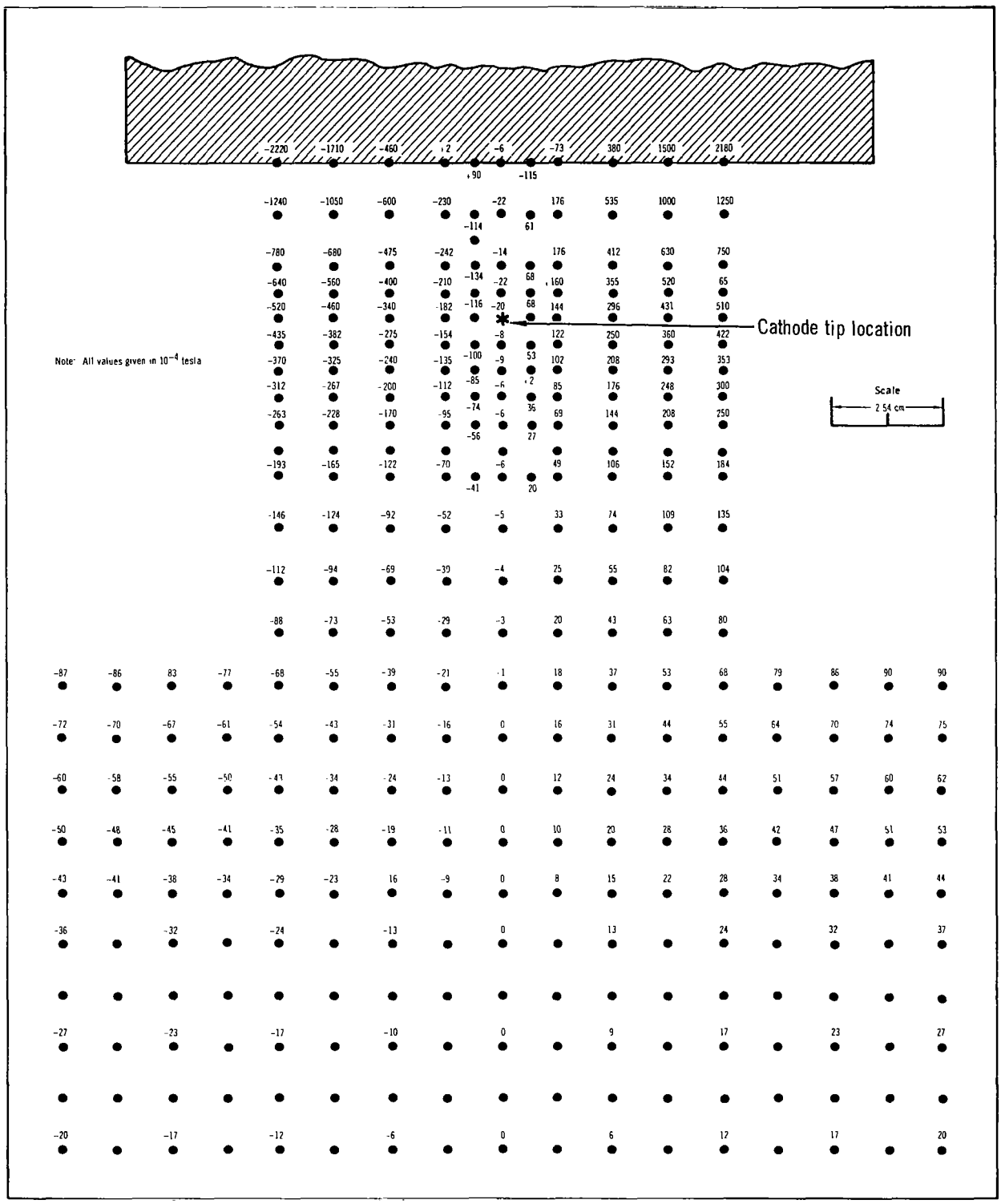

Fig. 3.5 Radial magnetic field of X–7 electromagnet (I_{mag} = 400 amperes)

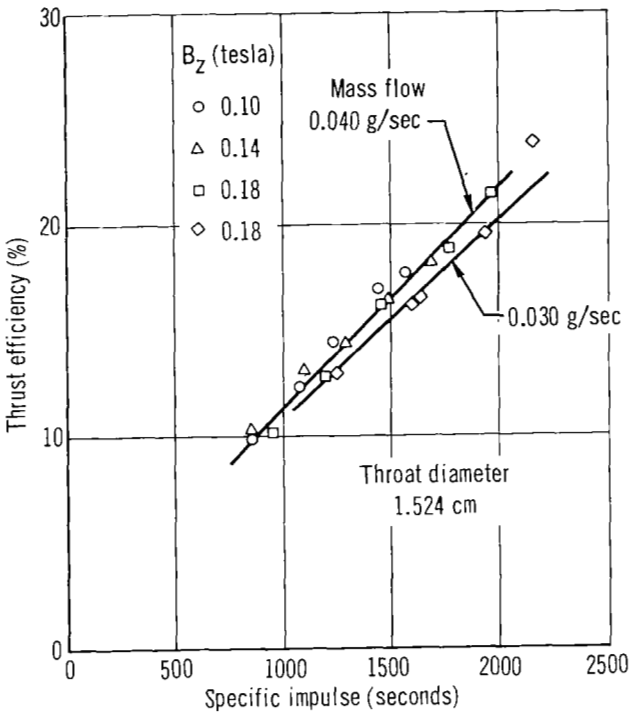

Fig. 3.6 X–7 Thrust performance

Performance data obtained on the 1.780 throat diameter X–7 thruster is shown in Fig. 3.7 for mass flow rates of 0.040, 0.030, and 0.020 g/sec and for a magnetic field of 0.14 tesla. Data at field values of 0.10 and 0.18 tesla were measured only at a flow rate of 0.040 g/sec. The 1.780 diameter performance data were slightly below (approximately 1 to 2%) those recorded on the 1.524 cm diameter engine. Testing of this unit was discontinued when a water leak was observed on the electromagnet. A maximum power of 37.9 kW was recorded during performance tests. A summary of the data obtained on the 1.780 cm throat is presented in Table 3.2.

The thruster was disassembled to repair the water leak and it was decided to rebore the nozzle throat to 2.032 cm at this time rather than obtain further data on the 1.780 cm diameter. It was felt that the time required to obtain additional 1.780 cm data would be better utilized investigating the higher input power range possible with larger throat diameters.

Inspection of the 1.780 cm thruster after testing showed the tungsten gas shield to be loosened as observed with the previous 1.524 cm diameter tests. The shield design was definitely marginal and required improvement. The HD0092 boron nitride anode-cathode insulator showed a marked improvement over the hot pressed BN material. The forward edge of the insulation suffered only a slight erosion of approximately 0.025 cm.

2.032 cm throat diameter – The tests conducted on the 2.032 cm throat configuration were made without the tungsten gas shield which surrounds the cathode since the previous tests at the small throat diameters revealed problems with the shield design. Table 3.3 summarizes the 2.032 cm test data. The arc voltage was generally lower than the data previously recorded on the 1.780 cm throat diameter engine at comparable operating conditions. An increase in arc voltage is normally observed with an increase in throat diameter. The reduction in voltage was attributed to the elimination of the gas shield which served to increase the gas pressure at the cathode tip. Observation of the arc discharge at the cathode tip revealed an intermittent wandering of the cathode spot off the cathode tip at the lowest flow rate tested, 0.020 g/sec. A change in exhaust flow luminosity was also associated with the wandering of the cathode spot. The tests of the 2.032 cm diameter unit were terminated when evidence of throat erosion was observed. Upon disassembly and inspection it was apparent that the arc discharge cathode attachment spot had transferred from the conical tip to a position on the cathode slightly upstream of the propellant injection ports. Evidence of this attachment mode was shown by eroded grooves located on the cathode diameter upstream of the injection ports and on the anode throat diameter. In view of the results of thruster tests with and without the cathode gas shield it appears that the shield is supplemental in providing a higher arc voltage and also in maintaining arc attachment at the cathode tip.

Table 3.1 Test data for X–7 MPD arc thruster

1.524 cm throat diameter				NH_3 – propellant			
Arc current (A)	Arc voltage (V)	Flow rate (g/sec)	Thrust (g)	Power (kW)	Specific impulse (sec)	Thrust efficiency (%)	Magnetic field (tesla)
300	50.0	40	34.9	15.0	876	9.76	0.10
400	45.0	40	42.8	18.0	1075	12.24	0.10
500	41.0	40	49.3	20.6	1238	14.26	0.10
600	39.0	40	57.4	23.5	1442	16.93	0.10
700	39.0	40	63.0	27.4	1582	17.49	0.10
700	43.0	40	67.1	30.2	1685	17.99	0.14
600	44.0	40	59.6	26.5	1491	16.15	0.14
500	45.0	40	51.7	22.6	1298	14.29	0.14
400	45.0	40	44.1	18.0	1108	12.99	0.14
300	48.0	40	35.0	14.4	879	10.23	0.14
300	57.5	40	38.2	17.3	959	10.17	0.18
400	54.0	40	47.8	21.7	1200	12.72	0.18
500	53.0	40	58.6	26.6	1472	15.59	0.18
600	54.0	40	70.7	32.5	1776	18.56	0.18
700	50.0	40	78.7	35.1	1977	21.29	0.18
500	56.0	30	58.2	28.1	1949	19.40	0.18
400	57.5	30	48.5	23.1	1624	16.40	0.18
300	59.0	30	37.6	17.7	1259	12.81	0.18
600	47.0	30	64.5	28.3	2160	23.66	0.18
400	57.5	30	48.0	23.1	1607	16.06	0.18

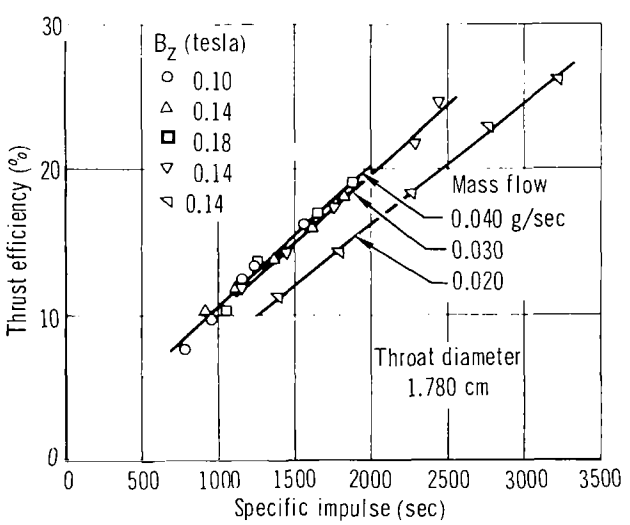

Fig. 3.7 X–7 Thrust performance

2.286 cm throat diameter – The X–7 tungsten nozzle was rebored to a diameter of 2.286 cm and the thruster was reassembled with a new anode-cathode insulator and gas shield of the initial design. Thrust measurements were obtained with this unit during a test which lasted a period of 260 minutes. Small variations in the arc voltage of the order of 1 to 4 volts were recorded during operation at constant arc current and at approximately 240 minutes into the test an abrupt decrease in arc voltage of approximately 14 volts was observed. Inspection of the throat region just after the reduction in voltage revealed that the cathode spot was located on the edge of the gas shield and at this time the test was stopped. Table 3.4 presents the thrust data obtained during this test. The last two data points in

Table 3.2 Test data for X–7 MPD arc thruster

1.780 cm throat diameter				NH_3 – propellant			
Arc current (A)	Arc voltage (V)	Flow rate (g/sec)	Thrust (g)	Power (kW)	Specific impulse (sec)	Thrust efficiency (%)	Magnetic field (tesla)
300	52.5	40	36.5	15.8	917	10.17	0.14
400	51.0	40	44.8	20.5	1125	11.83	0.14
500	50.0	40	53.4	25.1	1341	13.72	0.14
500	50.0	40	53.0	25.1	1331	13.51	0.14
600	51.0	40	63.9	30.7	1605	16.05	0.14
700	50.0	40	72.5	35.1	1821	18.06	0.14
700	42.0	40	62.8	29.5	1577	16.13	0.10
600	42.0	40	52.8	25.3	1326	13.30	0.10
500	40.0	40	45.2	20.0	1135	12.28	0.10
400	44.0	40	37.7	17.6	947	9.71	0.10
300	48.0	40	30.3	14.4	761	7.67	0.10
300	63.0	40	40.4	18.9	1015	10.38	0.18
400	64.0	40	53.3	25.7	1339	13.35	0.18
500	62.5	40	66.3	31.4	1665	16.92	0.18
600	60.0	40	75.2	36.1	1889	18.89	0.18
600	50.0	30	65.3	30.1	2187	22.80	0.14
500	50.0	30	52.2	25.1	1748	17.48	0.14
400	50.0	30	42.7	20.0	1430	14.62	0.14
300	51.0	30	34.2	15.3	1145	12.26	0.14
700	50.0	30	73.0	35.1	2445	24.42	0.14
300	55.0	20	27.8	16.5	1396	11.27	0.14
400	54.0	20	35.7	21.7	1793	14.19	0.14
500	53.5	20	45.3	28.8	2276	18.45	0.14
600	53.0	20	55.0	31.9	2763	22.88	0.14
700	54.0	20	63.9	37.9	3210	25.99	0.14

Table 3.4 were taken with cathode spot attachment on the gas shield.

Gas shield modifications – Since the gas shield surrounding the cathode provided a high arc voltage and greater arc stability, it was decided to attempt modifications to this component. The initial design of the gas shield was marginal and required improvements in maintaining electrical isolation between the shield and cathode. Figure 3.8 shows a redesign of the gas shield and main anode-cathode insulator. The gas shield wall thickness was increased to 0.158 cm and the flared end was changed to a right angle flange. A tungsten washer pinned to the downstream end of the shield tube secured the shield to the main anode-cathode insulator. The washer has a diameter of 1.780 cm and serves to shield the anode-cathode insulator from arc radiation. This modification was fabricated and installed in the X–7 thruster with a 2.032 cm throat diameter. A test of this thruster was made at an ammonia mass flow rate of 0.020 g/sec. After approximately thirty minutes of operation at a current level of 300 amps and as the current was increased to 400 amps erosion of the tungsten gas shield was observed, after which the test was concluded. Inspection of the shield after thruster disassembly showed that melting occurred at approximately the mid-point of the shield leaving two ring

Table 3.3 Test data for X–7 MPD arc thruster

2.032 cm throat diameter				NH_3 – Propellant			
Arc current (A)	Arc voltage (V)	Flow rate (g/sec)	Thrust (g)	Power (kW)	Specific impulse (sec)	Thrust efficiency (%)	Magnetic field (tesla)
300	56.0	0.040	35.0	16.8	879	8.77	0.14
400	55.0	0.040	45.8	22.1	1150	11.47	0.14
500	56.0	0.040	56.0	28.1	1406	13.47	0.14
600	55.0	0.040	64.7	33.1	1625	15.26	0.14
700	47.5	0.040	71.0	33.4	1783	18.24	0.14
700	41.0	0.030	59.2	28.8	1983	19.58	0.14
600	41.0	0.030	53.1	24.7	1778	18.38	0.14
500	43.0	0.030	45.9	21.6	1537	15.71	0.14
400	46.0	0.030	37.8	18.4	1266	12.45	0.14
300	49.0	0.030	30.7	14.7	1028	10.28	0.14
300	51.0	0.040	32.3	15.3	811	8.20	0.10
400	44.0	0.040	38.0	17.6	954	9.87	0.10
500	41.0	0.040	46.0	20.6	1155	12.41	0.10
600	39.0	0.040	51.2	23.5	1286	13.47	0.10
700	38.0	0.040	58.1	26.7	1459	15.26	0.10
700	38.0	0.030	49.9	26.7	1671	15.01	0.10
600	38.0	0.030	45.5	22.9	1524	14.56	0.10
500	38.0	0.030	40.5	19.0	1356	13.84	0.10
400	40.0	0.030	34.4	16.0	1152	11.86	0.10
300	44.0	0.030	26.0	13.2	870	8.21	0.10
300	43.0	0.020	23.0	12.9	1155	9.86	0.10
400	40.0	0.020	28.4	16.0	1427	12.12	0.10
500	39.0	0.020	31.8	19.5	1597	12.47	0.10
600	38.0	0.020	38.3	22.9	1924	15.48	0.10
700	39.0	0.020	42.5	27.4	2135	15.92	0.10
700	40.0	0.020	43.0	28.1	2160	15.88	0.10

segments. A second test of this shield configuration was made to insure that the first failure was not due to a material defect. Observation of the shield assembly was made visually during this second test. Stable arc operation was achieved for a period of approximately one hour during which the arc current was varied between 300 and 500 amps. However, as the current level was increased to 600 amps a portion of the cathode emission spot wandered to the base of the cathode cone and intermittently attached to the shield. After several minutes at the 600 amp condition continuous arc attachment was observed on the shield with subsequent melting and erosion of the shield.

A third test was conducted, in which the retaining washer attached to the shield was removed. Arc attachment to the shield took place at a current level of 650 amps, and continued operation resulted in complete melting of the shield with the shield material being deposited in the throat.

Based upon the above tests and previous results of the X–7 thruster it is apparent that high current operation of an exposed gas shield is not feasible in a configuration such as the X–7 electrode geometry.

An unexposed shield design as shown in Fig. 3.9 was fabricated and tested in an X–7 thruster having a

Table 3.4 Test data for X–7 MPD arc thruster

2.286 cm throat diameter						NH_3 – Propellant	
Arc current (A)	Arc voltage (V)	Flow rate (g/sec)	Thrust (g)	Power (kW)	Specific impulse (sec)	Thrust efficiency (%)	Magnetic field (tesla)
300	75.0	0.040	42.1	22.6	1057	9.47	0.18
400	60.0	0.040	56.1	24.1	1409	15.77	0.18
500	55.0	0.040	58.8	27.6	1477	15.12	0.18
500	58.0	0.040	63.2	29.1	1587	16.57	0.18
600	55.0	0.040	71.0	33.1	1783	18.37	0.18
600	58.0	0.040	71.8	34.9	1803	17.82	0.18
600	56.0	0.040	71.7	33.7	1801	18.40	0.14
500	62.5	0.040	59.7	31.4	1499	13.72	0.14
500	61.0	0.040	59.4	30.6	1492	13.91	0.14
400	62.5	0.040	51.3	25.1	1288	12.66	0.14
300	60.0	0.040	39.8	18.0	999	10.58	0.14
300	62.5	0.040	35.2	18.8	1179	10.60	0.14
400	64.0	0.030	45.9	25.7	1537	13.20	0.14
500	63.0	0.030	57.9	31.6	1939	17.07	0.14
600	49.0	0.030	54.8	29.5	1835	16.38	0.14
700	49.0	0.030	65.0	34.4	2177	19.75	0.14

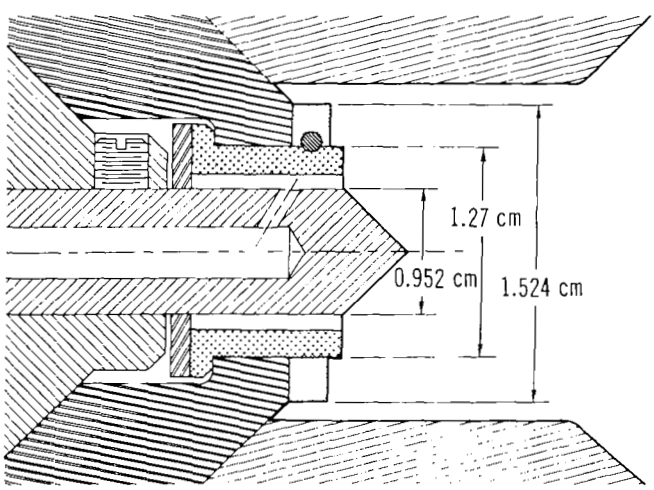

Fig. 3.8 X–7 Thruster gas shield design modification

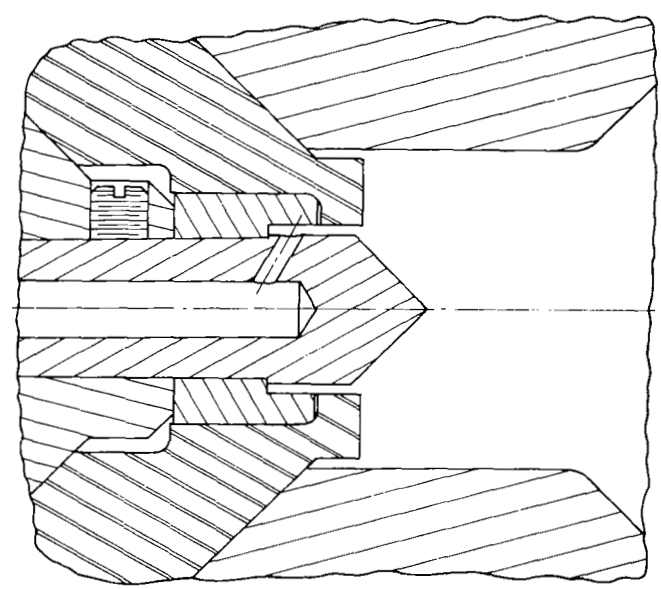

Fig. 3.9 Unexposed shield design

1.780 cm throat. This shield arrangement worked satis - factorily until erosion of the boron nitride by the propellant left a portion of the tungsten shield exposed; thereby, resulting in arc attachment to it.

X–7 Magnet heat transfer – Measurements of the thermal power recorded in the two magnet cooling circuits minus the dc power supplied the magnet are shown in Fig. 3.10 for each of the test conditions recorded during the parametric study. The excess power scales roughly as the thruster power ranging between 0.40 and 1.2 kW. There is considerable data scatter, some of which is due to recording small differences between two large numbers. The lower flow rate conditions generally produced higher excess power in the magnet.

There is some question whether the excess power absorbed in the magnet should be assigned as radiated power from the thruster. Two water circuits were involved in the above measurements, one circuit consisting of the 80 turns of copper tubing and a jacket circuit which completely surrounds the coil circuit and should, in theory, absorb the majority of radiated power to the magnet before it could enter the coil circuit. Approximately 66% of the excess thermal power was recorded in the coil circuit and between 100 and 300 watts recorded the jacket circuit, in general. In addition, the coil temperature increase was generally 3 to 6°K higher than the jacket water so that heat would be transferred from the coil to the jacket system. A possible explanation of the above results is that ac power components due to power supply ripple and interactions between the arc discharge and electromagnet (rotating arc spokes) were supplying additional power to the electromagnet which is not acoounted for in the power balance. Scheduling difficulties prevented a detailed investigation of this point and consequently the question has not yet been resolved.

X–7 Temperature measurements – Figure 2.7 shows a comparison between the numerical predictions for a heat input to the anode of 16 kW and the measured temperatures at several locations on the thruster for an arc power input of 35 kW. The predicted values are between 76 and 134°K higher than the measured values. Based upon previous calculations a heat input of 13.6 kW would produce good agreement.

The results of temperature measurements obtained at the downstream face of the graphite radiation flange are presented in Fig. 3.11. Data are presented for the four throat diameters tested and verify the calculations which show that for a constant power input the temperature distribution is lowered as the throat diameter is increased. There is only a slight dependence of mass flow rate on the measured temperatures.

Figure 3.12 shows a plot of the temperatures recorded on the outside diameter of the graphite radiation flange as a function of the input power to the 1.524 cm throat diameter thruster. Also shown on this plot is the calculated temperature at this location assuming a constant thermal efficiency of 50% and 60%. It can be seen that at 30 kW input power the thermal efficiency of this device is approximately 60%.

3.3 Parametric test conclusions

Several conclusions were made based upon the results of the parametric test phase:

- MPD thrust efficiency is a linear function of specific impulse over the range of interest and has a slope proportional to mass flow rate. The thrust to power ratio which is proportional to the slope of the η vs I_{sp} lines averaged 2.2 g/kW at 0.040 g/sec, 1.95 g/kW at 0.030 g/sec, and 1.7 g/kW at 0.020 g/sec.

- Some small variations of the thrust to power ratio were observed for different throat diameters and magnetic field strengths; however, these variations were within the experimental error. The data obtained on the X–4A thruster gave almost identical results. Thus changes in geometry and magnetic field serve mainly to affect the voltage level and consequently the power but not the thrust-to-power ratio.

- The measured thrust performance precluded operating at the contract design goal of 40%

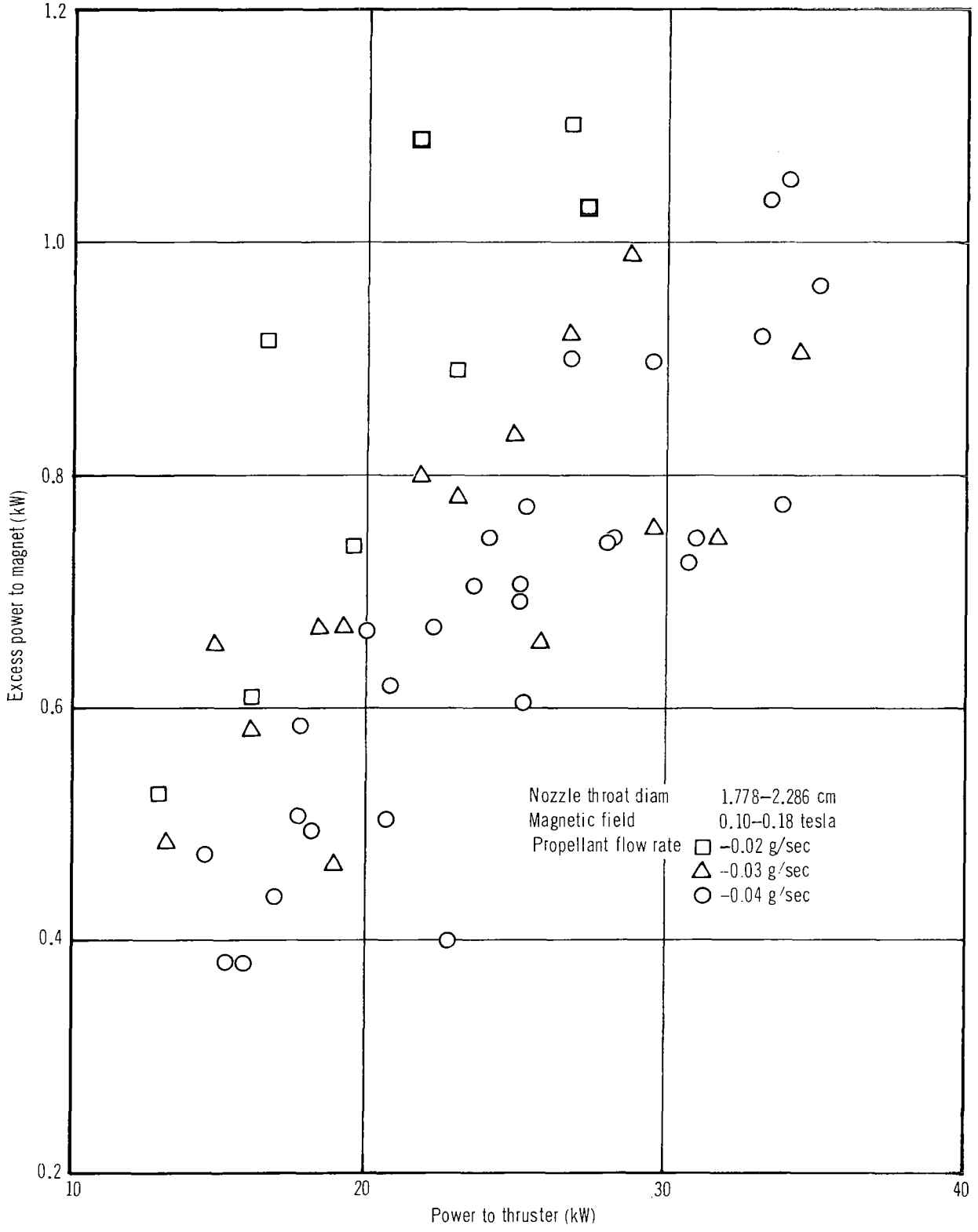

Fig. 3.10 Excess power to X–7 electromagnet

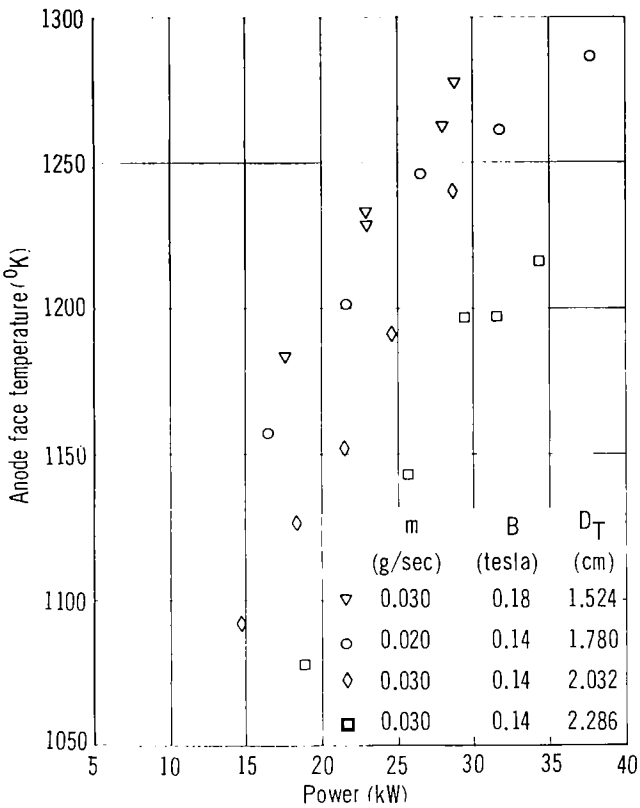

Fig. 3.11 Temperature measurements on X–7 radiation flange downstream face

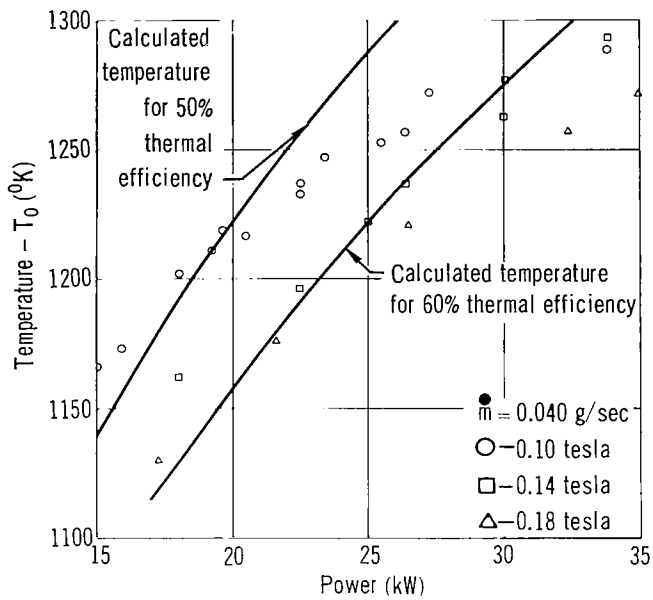

Fig. 3.12 Measured temperature on graphite radiation flange outer diameter

thrust efficiency, 25 kW input power and specific impulse between 2000 and 3500 seconds. To achieve the design efficiency in the specific impulse range specified, the input power must be raised above 25 kW.

- Attempts to raise the input power into the range of 40 kW for extended durations proved unsuccessful with the X–7 configuration. The current level of the X–7 unit was limited to approximately 700 amps. Thus higher power operation dictated a higher arc voltage. Higher MPD arc voltages could be effected by increasing the magnetic field (an undesirable technique due to magnet weight requirements), increasing the throat diameter and providing a gas shield around the cathode. Larger throat diameter operation was unstable without the gas shield and could not be maintained at high currents with the shield for long duration.

- Since attempts to increase the arc power capability of the X–7 thruster with a gas shield cathode proved unsuccessful, a decision to perform the 500 hour lifetest at a performance level below the contract design goal was made after a meeting between MDC and NASA contract personnel. The initial duration test was to be conducted at the following operating conditions:

Ammonia mass flow rate	– 0.030 g/sec
Arc current	– 650 amps
Magnet field	– 0.14 tesla
Throat diameter	– 1.780 cm.

Based upon previous performance tests this condition would provide a thrust efficiency of 22% at a specific impulse of 2200 seconds with an electrical power input of 28–32 kW depending upon the arc voltage recorded.

3.4 500 hour lifetest

A new X–7 tungsten nozzle, cathode and anode-cathode insulator were fabricated, and the vacuum chamber was prepared for duration testing. On 10 February 1969 at 9:00 a.m., a duration test of the X–7 thruster was initiated. The propellant mass flow rate was set at 0.030 g/sec and the magnetic field at 0.14 tesla. The arc current was increased gradually from a light-off value of 300 amps at t = 2.5 hours. The arc voltage at these current values ranged between 66.6 and 67.5 volts, suggesting that the arc was operating at the high mode. Cathode spot attachment was observed to occur on the cathode tip. As the test proceeded, the attachment spot moved sporadically off the tip to the shoulder of the cathode with a resultant drop in arc voltage to a value of 51 to 53 volts. It was found that a slight reduction in arc current would drive the attachment spot to the cathode tip and into the higher voltage mode.

Since a power level of approximately 30 kW could be supplied in the high voltage mode, it was decided to vary the arc current so as to maintain high voltage mode operation. After approximately 6 hours of operation a current range of 420 to 450 amps generally maintained the high voltage mode condition. The thrust to power level at this condition was measured to be 1.75 g/kW with a specific impulse value of 1750 sec. It was noted that during the thrust measurement arcing to the thrust "killer" occurred. Due to this arcing, thrust measurements were deferred until t = 73 hours; however, when a thrust measurement was attempted, arcing became quite severe and the drive motor failed to remove the "killer" from the exhaust flow. After approximately 5 minutes with the killer blocking the exhaust flow the test was terminated with power shutdown.

The vacuum was released and a visual inspection of the thruster was made. Slight erosion of the tungsten nozzle in the expansion region approximately 1 cm downstream of the throat was indicated. This erosion appeared as a rippling of the surface to a depth of several mils. The edge of the graphite radiation flange which forms a portion of the expansion nozzle was eroded uniformly about its circumference to a depth of approximately 2 mm. The main cathode to anode insulator suffered erosion of its downstream edge to a depth of 2 or 3 mm. The greatest erosion occurred about the propellant injection ports. The arc cathode appeared in good condition.

After the visual inspection had been completed it was concluded that the thruster was in a satisfactory condition and that testing could be continued. At 1:00 p.m., 13 February 1969, the X–7 was restarted at the following operating conditions:

Ammonia mass flow rate	– 0.030 g/sec
Arc current	– 650 amps
Magnet field	– 0.14 tesla
Throat diameter	– 1.780 cm

Approximately 5 hours after light-off the arc voltage dropped from a value of 55 volts to 44 volts with an attendant change in arc cathode attachment from the tip to the cathode shoulder. Continued operation at this condition revealed erosion of the cathode and the anode throat. The cathode tip appeared to be completely molten and the conical definition of the tip severely distorted. After 16.3 hours into the second test the thruster was shut down because the tip of the cathode was eroded to the point that a portion of the tip was ejected from the throat.

The thruster was disassembled and the following weights recorded.

Part	Weight prior to test (g)	Weight after test (g)
Graphite radiation flange	2194.2	2167.25
Tungsten anode nozzle	4725.2	4726.0
Cathode	27.24	–
Anode-cathode insulator	27.64	15.50

The increase of the nozzle weight was most probably due to deposition of a portion of the cathode material on the throat. The cathode could not be removed from the cathode holder and had to be machined out. The portion of the cathode tip retrieved in the vacuum chamber weighed 5.6 gm. The main anode-cathode insulator suffered the greatest percentage erosion and was due to the proximity of the cathode arc attachment.

Upon inspection of the thruster and after a discussion of the problem with the NASA Project Manager, it was decided to enlarge the cathode diameter and to provide the connection to the cathode holder as shown in Fig. 3.13. A new tungsten nozzle, cathode and anode-cathode insulator were fabricated and the X–7 thruster was reassembled for testing.

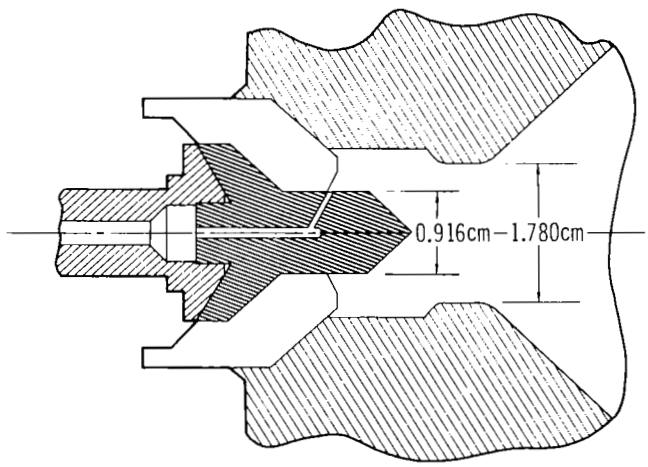

Fig. 3.13 X–7 Cathode modification

The third duration test of the X–7 thruster was initiated at 8:30 a.m., 26 February 1969, at the following operating conditions:

Ammonia mass flow rate	– 0.030 g/sec
Arc current	– 560 amps
Magnetic field	– 0.14 tesla
Throat diameter	– 1.780 cm

This test was terminated at 1:04 p.m., 19 March 1969, for a total uninterrupted test duration of 508.5 hours. Termination of the test was made for the purpose of inspection of the thruster. After the inspection had been completed, the thruster was restarted and operated for an additional 45.5 hours, providing an accumulated operating test time of 554 hours. Shutdown of the unit was voluntary and was made when a shift from a high voltage to low voltage mode had occurred. Previous duration tests in the low voltage mode indicated that electrode erosion is greater in the low voltage mode; thus, shutdown was ordered so that erosion measurements applicable to the previous 554 hours of test time could be made.

During the lifetest the thruster operated in a high voltage mode condition, which through photographic evidence appears to be associated with cathode spot emission from the extreme tip of the cathode. Figure 3.14 presents the voltage and power time history of the lifetest. Photographs of the arc discharge region obtained during the lifetest are presented in Figs. 3.15 and 3.16. Up to t = 2.0 hours the cathode attachment periodically moved to the base of the cathode, and this is shown in the first picture on Fig. 3.15. Evidence is seen in this picture of a small melted area at the top of and upstream of the nozzle throat which occurred some time within the first two hours of run time. The arc voltage did not remain steady but increased from 51 volts at an elapsed time of several hours to 62 volts after 30 hours of operation. At that time the magnetic field was reduced until the voltage decreased to 56 volts. Then a gradual increase in voltage was observed reaching a value of 63–64 volts at 425 hours elapsed time. During this period, the cathode tip appeared to grow a nodule or tit which was approximately 2 mm in diameter. The formation of this nodule is clearly evident in the photographs of Fig. 3.15. It is noted that the different intensity levels of the photos are not due to temperature changes on the thruster but to changes in camera settings required to offset clouding of the observation port which increased as the test progressed. At t = 428 hours a portion of the tit left the cathode and was deposited on the anode expansion angle; there was an attendant decrease in arc voltage to a level of 58 to 60 volts. The voltage remained between 58 and 61 volts until t = 505 hours when upon insertion of the thrust killer into the exhaust flow the voltage decreased to 51 to 52 volts. Due to variation in arc voltage the thruster input power ranged between 28 and 35 kW.

Figures 3.17, 3.18 and 3.19 are photographs of the thruster looking upstream after the shutdown at 508.5 hours. Figure 3.17 shows the general conditions of the unit and the erosion which occurred on the graphite radiation flange. The shape of the cathode and anode

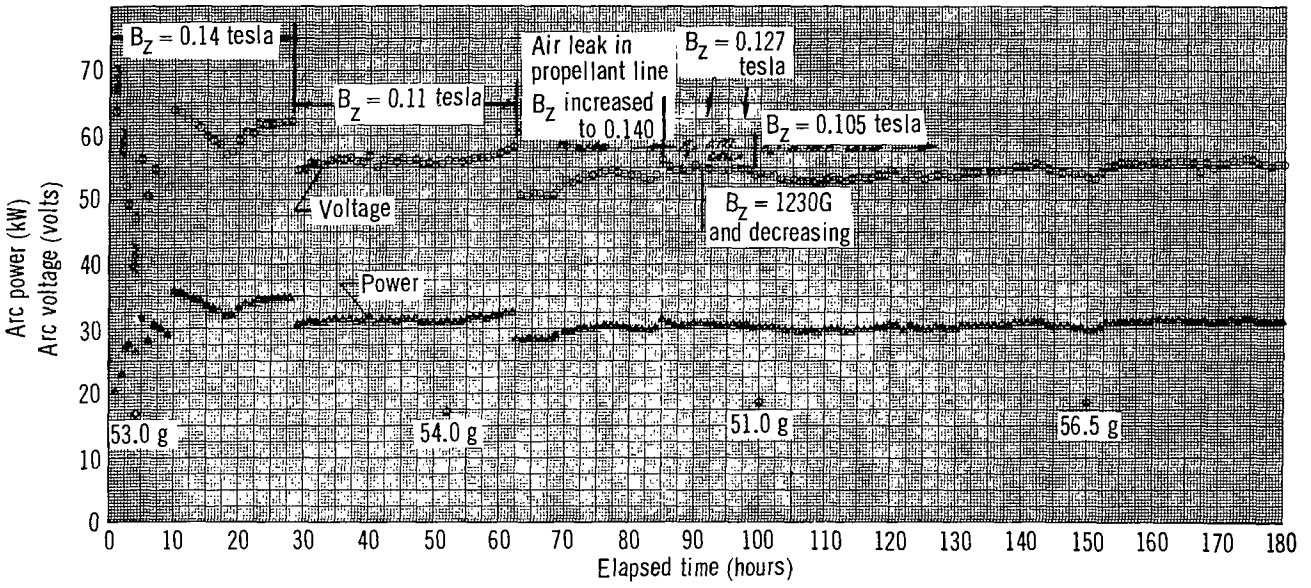

Fig. 3.14 Lifetest arc voltage and power histogram

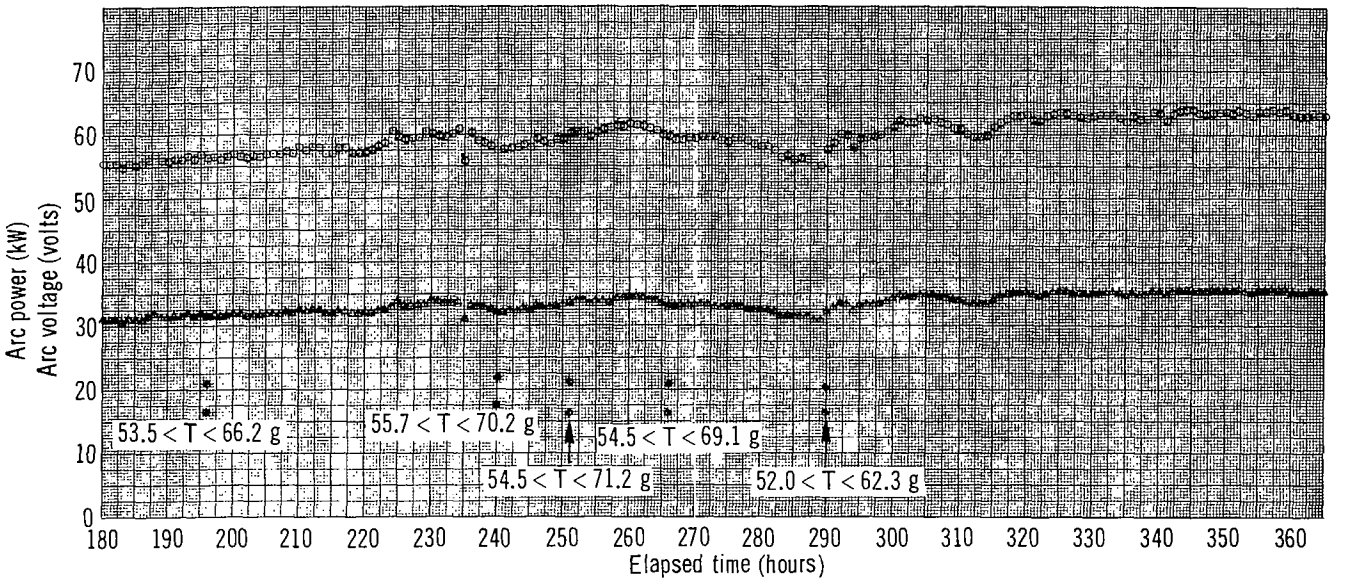

Fig. 3.14 Lifetest arc voltage and power histogram (Continued)

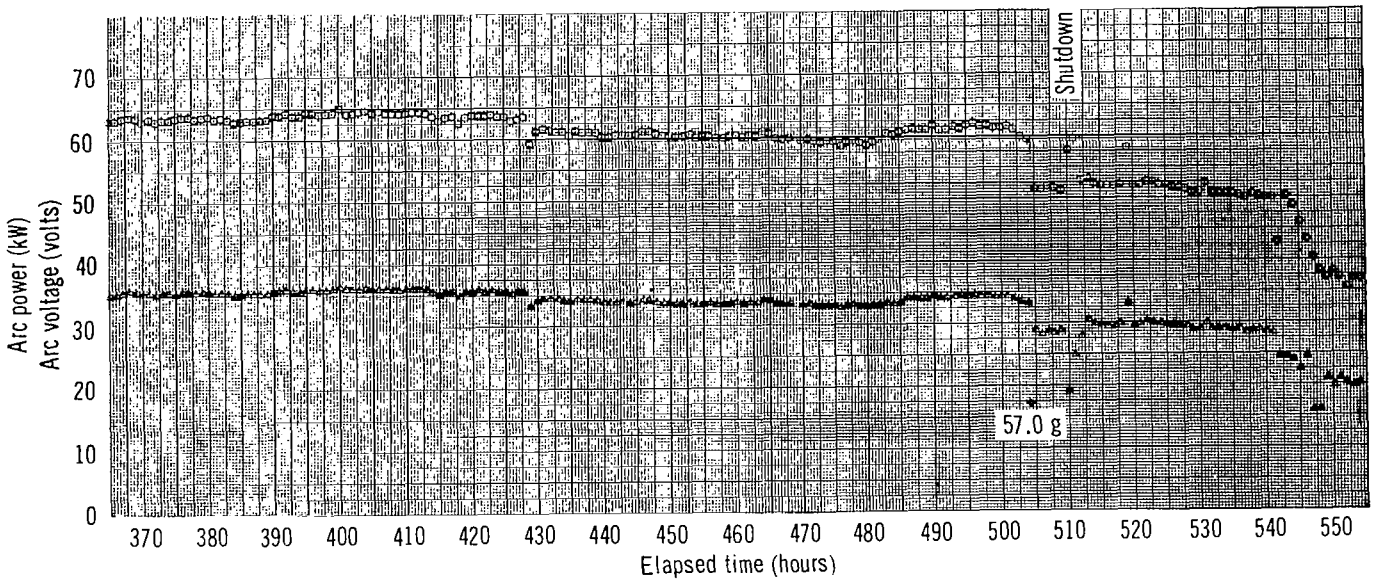

Fig. 3.14 Lifetest arc voltage and power histogram (continued)

throat are shown in Fig. 3.18 whereas Fig. 3.19 shows the downstream edge of the boron nitride cathode-anode insulator.

After the inspection of the thruster was completed the unit was restarted and brought to the same conditions as immediately prior to shutdown. The arc voltage remained fairly constant near 52 volts up to 529 hours when oscillations to a slightly lower voltage mode appeared. The pictures taken at this time indicate that the cathode attachment no longer was completely on the tip as in the high voltage mode but appeared to be emitting from an annular ring at the base of the cathode and also from the tip. The third row of pictures on Fig. 3.16 shows a sequence during one of these voltage oscillations. At t = 543 hours the arc attachment appeared to move completely to the base and rod section of the cathode and a definite increase in visible radiation from the cathode was observed. This increased radiation is shown in the last two photos taken during operation. Since the erosion was suspected to be greater in this mode the test was terminated at t = 554 hours.

Erosion – Figure 3.20 shows the dimensional changes to the tungsten nozzle which occurred during the lifetest. A net increase in weight of 0.6 g was recorded on this component which is due in part to the deposition of a portion of the cathode tip on the nozzle expansion angle (see Fig. 3.17). The nozzle suffered an elongation of 0.33 to 0.35 mm from its initial length and a reduction of 0.23 to 0.35 mm on the outer diameter. The original 2.032 cm internal diameter was decreased by 0.38 to 0.76 mm, and since this surface did not appear to be eroded, it can be assumed that further sintering of the pressed and sintered tungsten material is responsible for the reduction. The throat region (original 1.780 cm internal diameter) underwent a reduction in diameter of 1.01 to 1.27 mm of which approximately

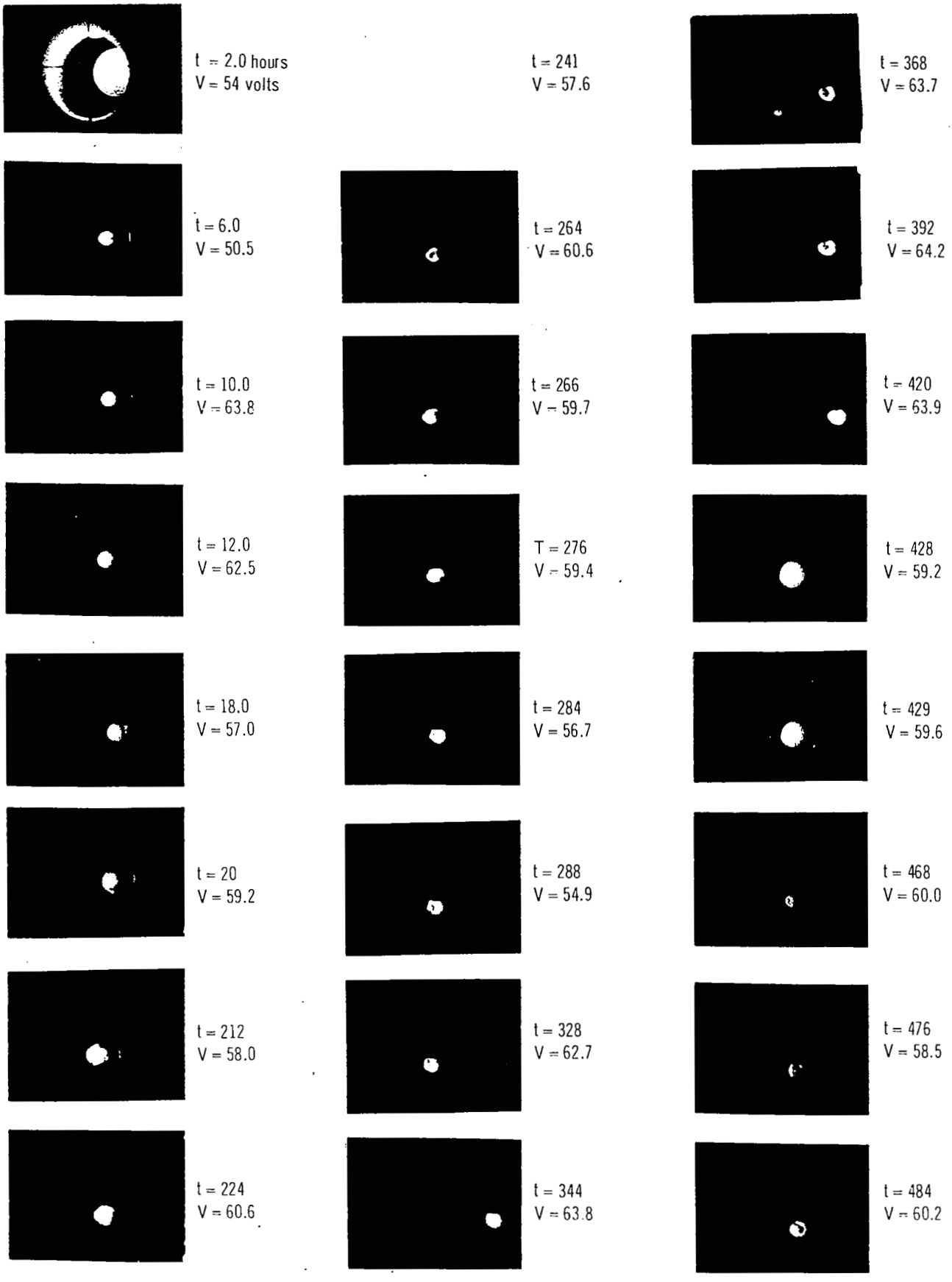

Fig. 3.15 Photographs of arc discharge during life test

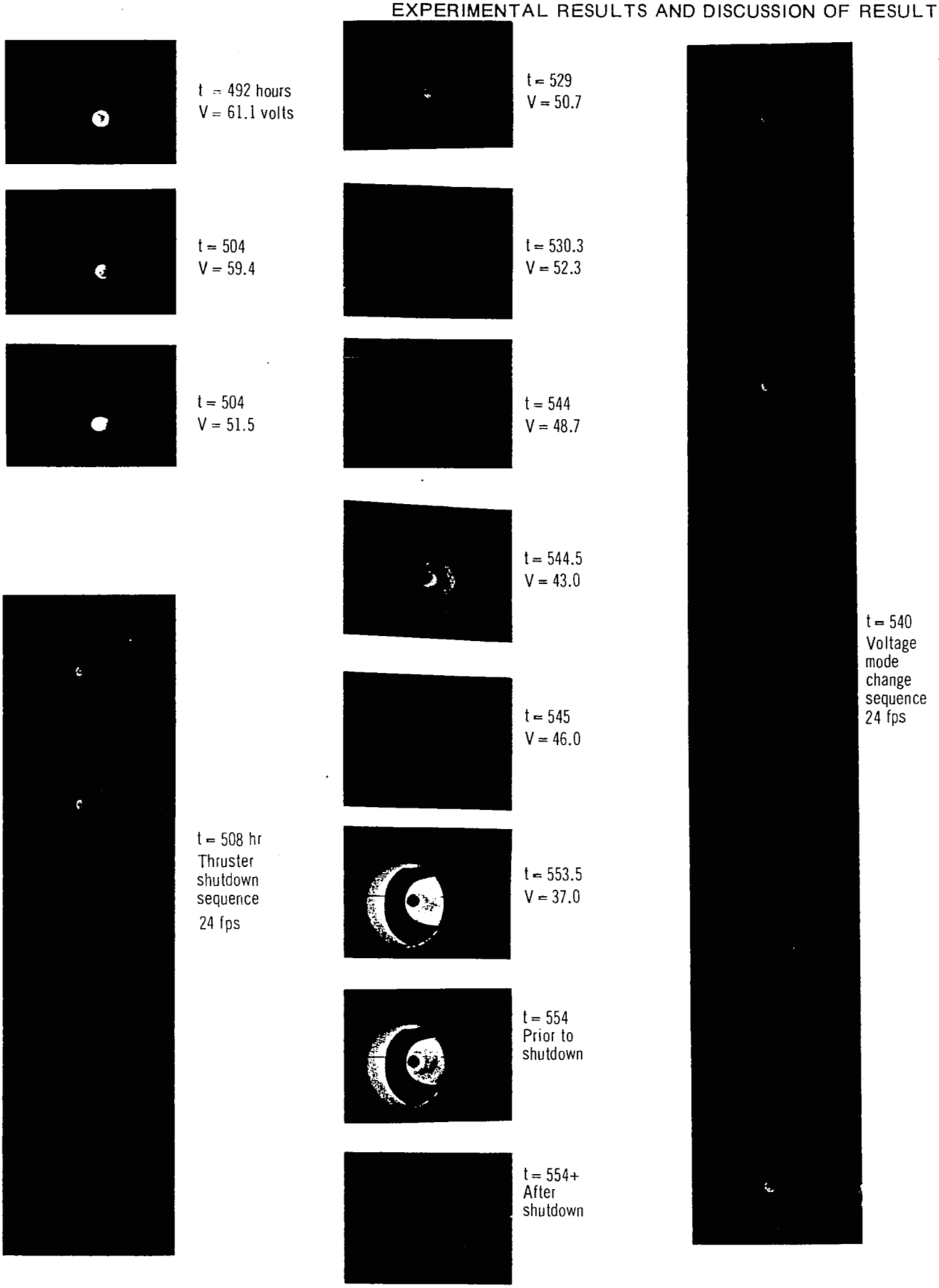

Fig. 3.16 Photographs of arc discharge during lifetest

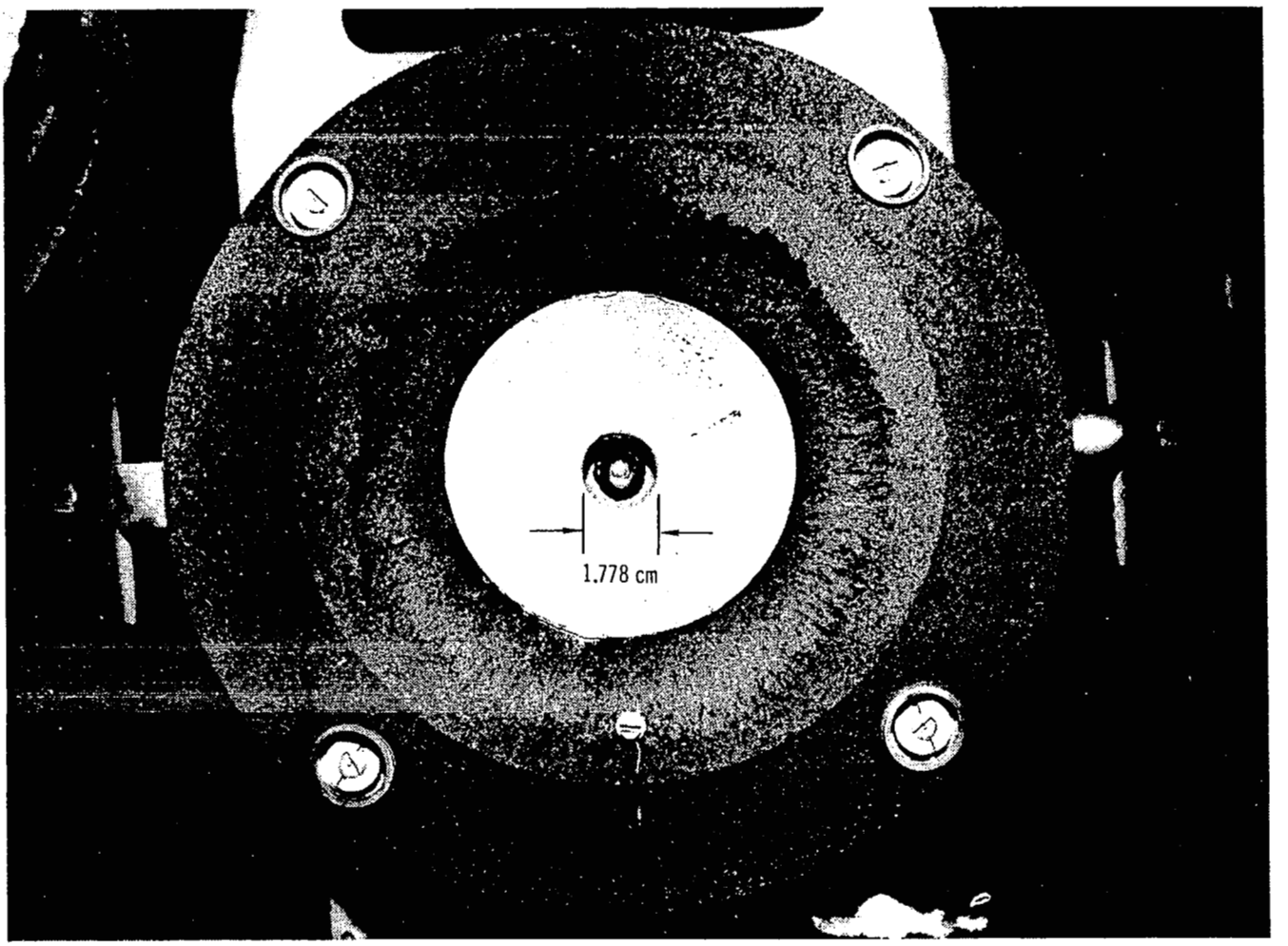

Fig. 3.17 X–7 Thruster after 508.5 hr life test

0.35 mm may be attributed to sintering while the remainder is most likely due to deposition of cathode material and recrystallization of the base metal. Two small radial fractures occurred in the throat which appear to be approximately 1 mm in depth. The final shape of the cathode is shown in Fig. 3.21. A decrease in weight of 2.4377 g represents an erosion of 2.9% of its initial weight. The erosion occurred mainly on the diameter of the cathode which was reduced by 1.55 mm on its downstream end and in the injection ports which increased in diameter by almost 50%. The tit which formed at the cathode tip had an average diameter of 2.54 mm and a length of 1.5 mm which at times during the lifetest appeared longer. Figure 3.22 shows the lifetest cathode and a newly machine cathode. Figures 3.23 and 3.24 are microphotographs of the lifetest cathode after it was sectioned along its length. The structure of the cathode tip for a distance of 2–3 mm appears to be more dense than the base metal with a fairly sharp zone separating the two regions. The cathode-insulator surface reveals a structure characteristic of a tungsten boride eutectic to a depth of several millimeters. Again a sharp division is observed between the base metal and the column-like structure of the eutectic.

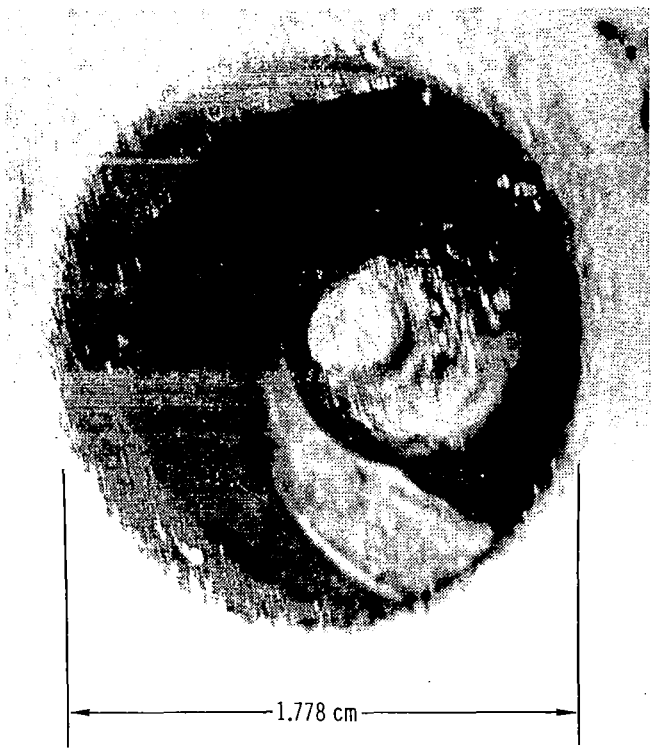

Fig. 3.18 X–7 Thruster after 508.5 hr. life test

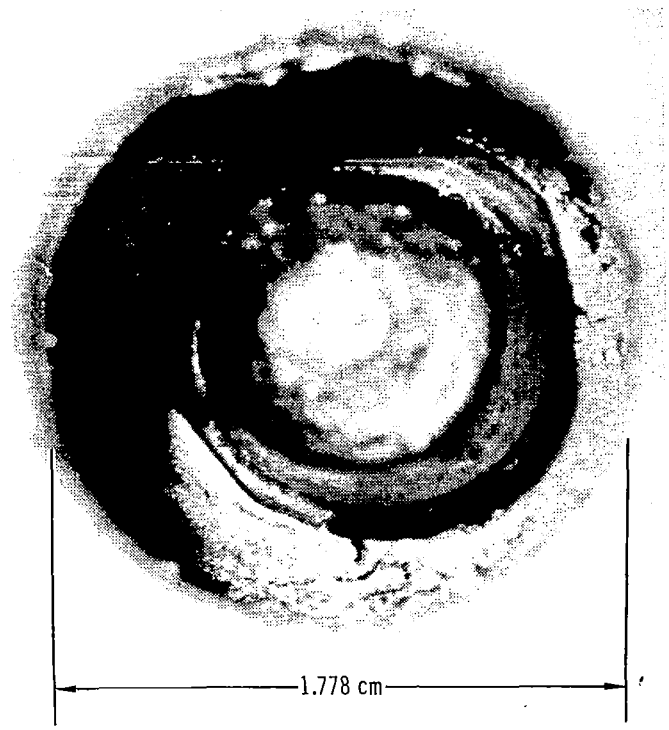

Fig. 3.19 X–7 Thruster after 508.5 hr. life test

Figure 3.25 shows the geometry of the graphite radiation flange which lost a net weight of 164.1 grams. The majority of this erosion occurred on the downstream internal surface and would appear to be due to shear effects of the exhaust propellant. The external surfaces of the flange were reduced in depth by approximately 0.9 mm and can be attributed to surface vaporization and/or sintering of the material. A significant reduction in erosion of the radiation flange should be possible by removing the flange from the expansion region of the exhaust.

The erosion which occurred on the main cathode-to-anode insulator is depicted in Fig. 3.26. This component suffered the greatest percentage erosion with a value of 41.4% of the initial 24.55 g. A significant amount of this erosion took place during the last 45 hours of test operation. A measurement of the distance between the downstream edge of the insulator and the front surface of the radiation flange at t = 508.5 and at t = 554 hours indicated that an erosion of 1.47 mm of insulator length took place during this period. Inspection of the cathode assembly before the unit was disassembled revealed that the insulator and cathode were firmly seated, thus indicating that the compression springs moved the cathode and insulator forward as the forward edge of the insulator eroded. This forward movement of the cathode probably served to effect the arc voltage; however, it is unknown whether this movement would increase or decrease the arc voltage since the effects of cathode position on the high voltage mode condition are not well known.

If the total material loss of these four components is divided by their initial weight, then the erosion rate per 500 hours would be 2.22%.

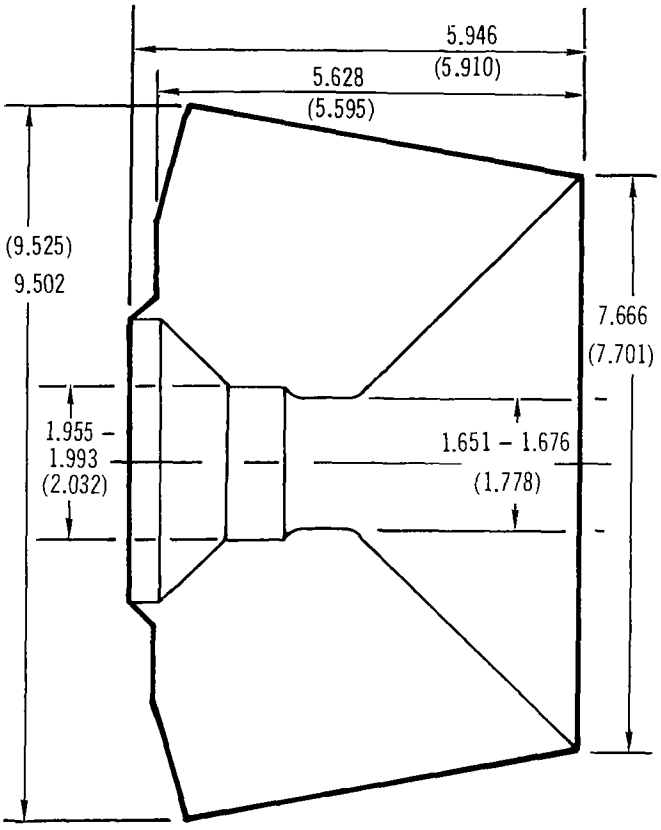

Notes

1. All dimensions in centimeters
2. Original dimensions shown in parentheses
3. Original mass - 4781.2g
4. Final mass - 4781.8g

Fig. 3.20 X–7 Tungsten nozzle geometry before and after 500 hour life test

Notes

1. All dimensions in centimeters
2. Original dimensions shown in parenthesis
3. Orginal mass - 82.8543g
4. Final mass - 80.4166g

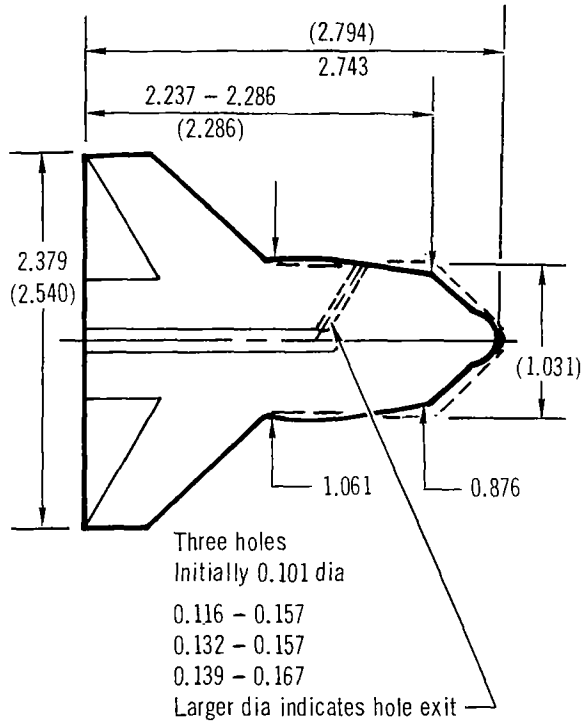

Fig. 3.21 X–7 Tungsten cathode geometry before and after 500 hour life test

Lifetest thrust performance – Thrust measurements were recorded during the 500 hour lifetest at intervals of approximately 50 hours. More frequent measurements were not made due to sporadic arcing to the thrust killer while it was in the flow blocking position and also because the thrust killer drive motor had difficulty positioning the killer. This latter condition appeared only during the duration tests and was probably due to heat warpage in the drive gear train. It is noted that the first duration test was terminated because of this condition.

The times at which thrust measurements were taken are shown on Fig. 3.14 and also in Appendix D. The first measurement was obtained at t = 4.0 hours and yielded the following values:

Thrust	– 53.0 g
Specific impulse	– 1767 seconds
Thrust efficiency without magnet power	– 17.1 %
Thrust efficiency with magnet power	– 14.9 %

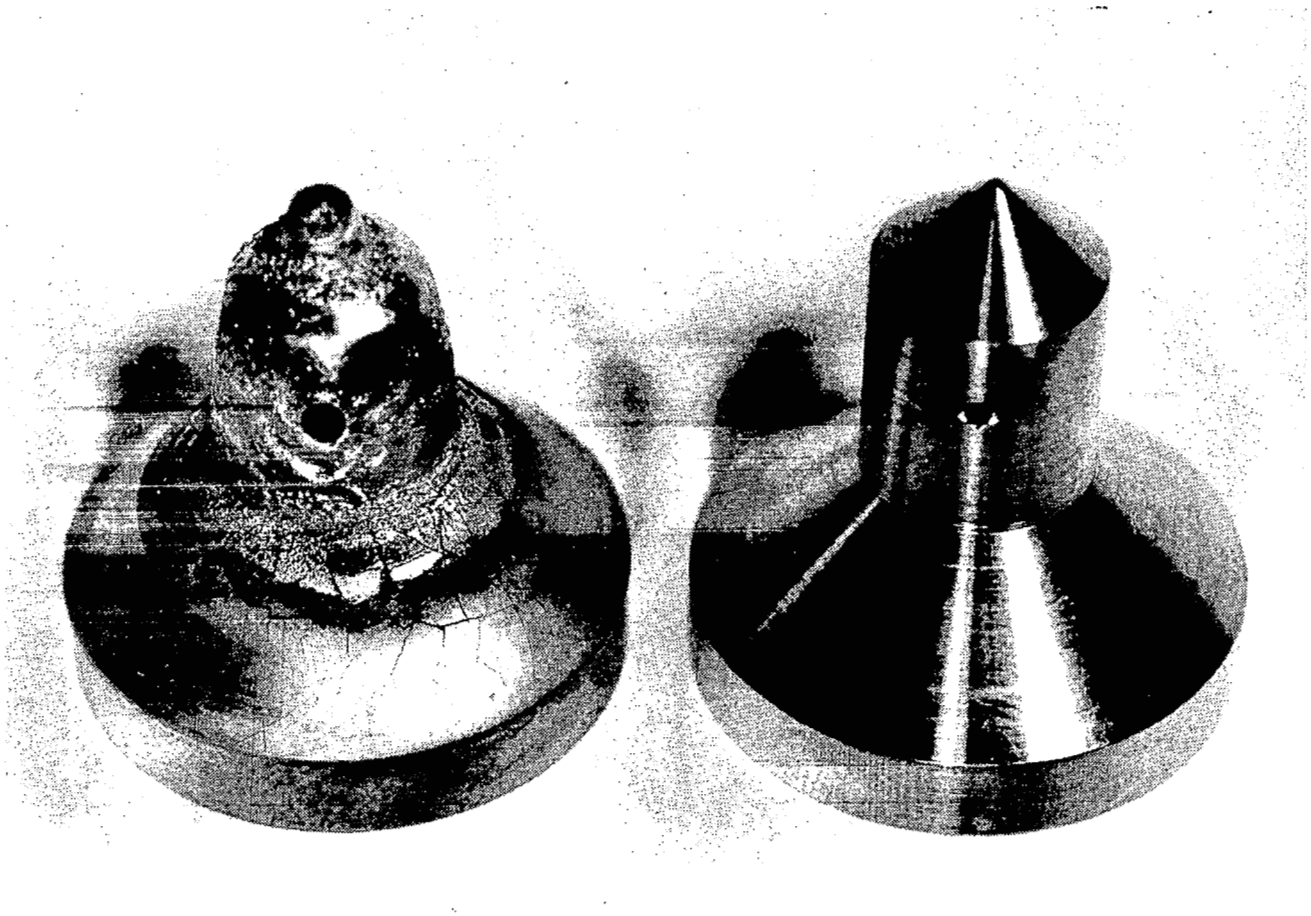

Fig. 3.22 X–7 Life test cathode and new cathode

These data are close to the average values recorded during the parametric testing phase and are representative of a low voltage mode condition. Shortly after this first thrust measurement the voltage began to increase to the level shown in Fig. 3.14 and indicate the thruster moved gradually into a high voltage mode condition. The second thrust measurement, taken at t = 52 hours, showed only one gram increase in thrust for approximately 4 kW increase in power. The specific impulse increased to 1800 seconds; however, the thrust-to-power ratio dropped to 1.72 g/kW, and the thrust efficiency without magnet power decreased to 14.9 %. The thrust efficiency with magnet power was 13.9%. These values are characteristic of the high voltage conditions.

The thrust measurements taken at t = 100 and 150 hours show a slightly improved performance; however, a gradual decrease in thrust stand sensitivity was observed during this period. The drop in thrust stand sensitivity increased slowly with time, and the measurements at t = 196, 240, 251, 266 and 290 hours were taken with this condition. After some experimentation with the stand, which involved loading and unloading the calibration weights, it became clear that the oil used for damping low frequency vibrations had formed a high viscosity surface layer. It was found that the deflection per 25 g weight increased with the number of times the weight was loaded and unloaded. The initial sensitivity was attained after 45 to 50 weight drops and suggested

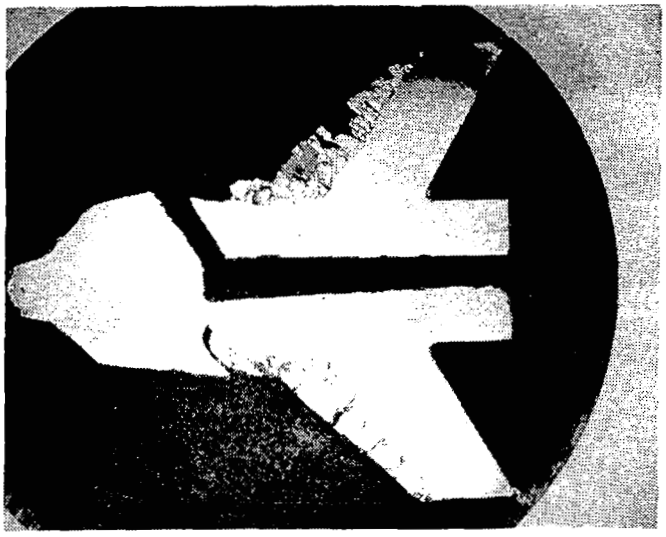

Sectioned Cathode

Position Opposite Propellant Injection Port

Cathode Tip

Fig. 3.23 Microphotographs of life test cathode

Cathode – Insulator Surface

Fig. 3.24 Microphotographs of life test cathode

that the pendulum had to be swung through the oil a sufficient number of times to break up the surface layer. This procedure was followed for the last thrust measurement taken at t = 504 hours. The thrust measurements reported at t = 100 and 150 hours are most likely several grams too high while the measurement at t = 196, 240, 251, 266 and 290 hours indicate the maximum and minimum thrust which could be inferred. The minimum values are those obtained from the initial sensitivity values, and the maximum values are those derived using the reduced sensitivity values obtained for one weight drop after the thrust measurement. The correct value of

Notes

1. All dimensions in centimeters
2. Original dimensions shown in parenthesis
3. Original mass – 2049.8g
4. Final mass – 1885.7g

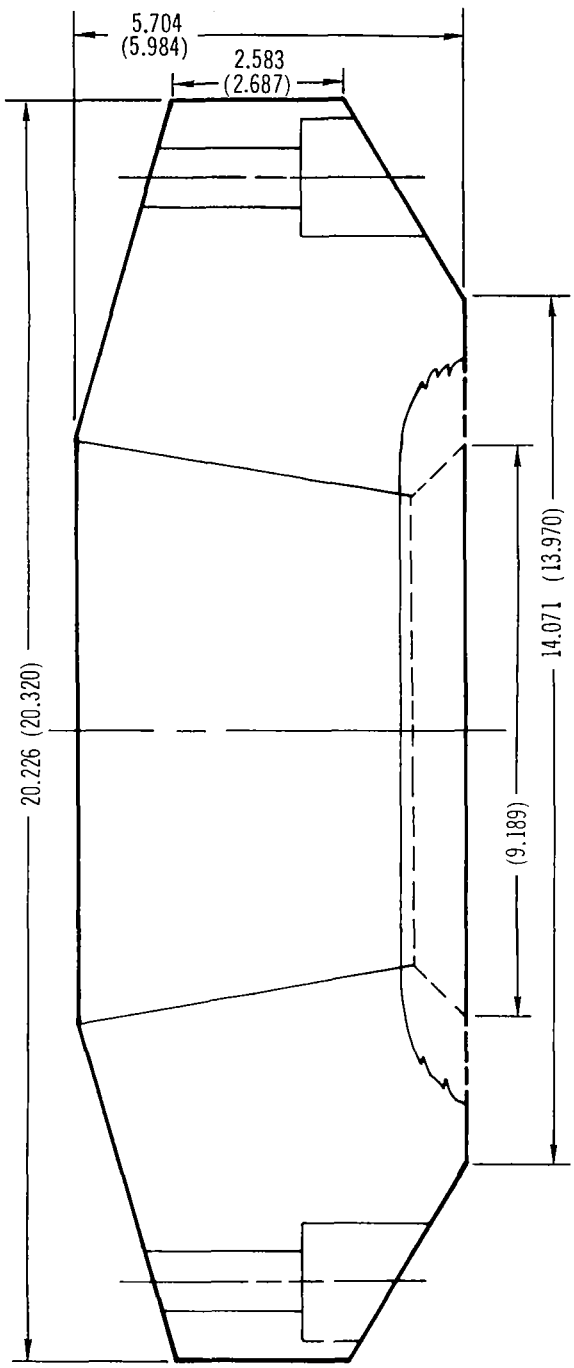

Fig. 3.25 X–7 Graphite radiation flange before and after 500 hour life test

Notes

1. All dimensions in centimeters
2. Original dimensions shown in parentheses
3. Original mass – 24.5531g
4. Final mass – 13.6050g

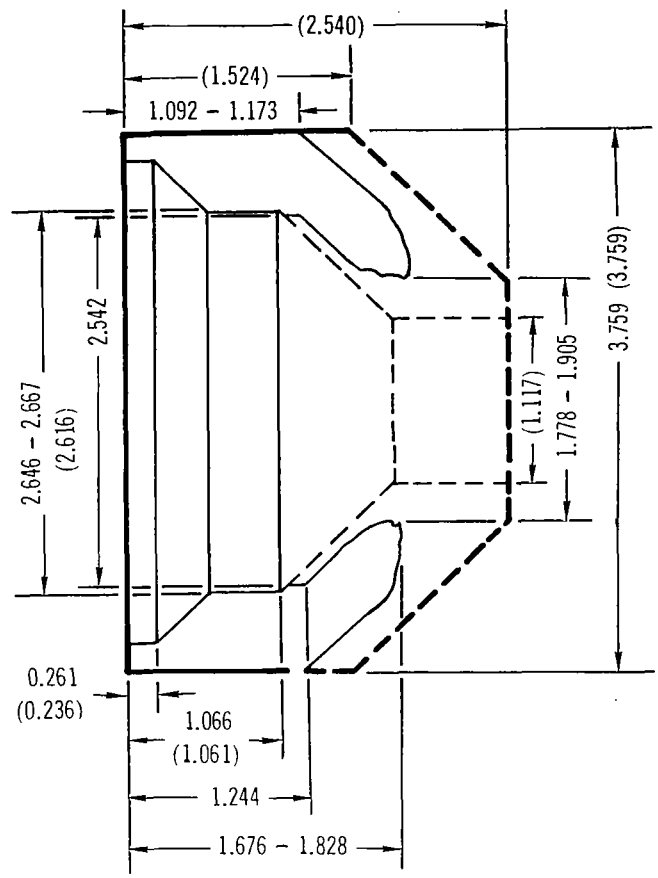

Fig. 3.26 X–7 Boron nitride cathode insulator geometry before and after 500 hour life test

thrust lies within the range shown and most probably is 57–58 g. The performance recorded at t = 504 hours was:

Thrust	– 57.0 g
Specific impulse	– 1900 seconds
Thrust efficiency without magnet power	– 15.6 %
Thrust efficiency with magnet power	– 14.5%

Assuming an average thrust value of 57 grams over the lifetests, then for the 504 hours of operation a total impulse level of 2.29×10^5 lb-sec was developed.

Lifetest thruster measurements – Temperature measurements on the radiation flange outer diameter and downstream face were recorded during the lifetest. Figure 3.27 shows the temperature-time history for these two locations. These data exhibit significant scatter and fluctuations, some of which correlate with the changes in magnetic field mode during the first 100 hours of operation. The rather abrupt rise in the face temperature during the period between t = 100 and 300 hours is unexplained. It is noted that the erosion of the graphite flange at the termination of the lifetest had proceeded to the thermocouple location and this loss of material would affect radiative heat transfer at this location. Referring to Fig. 3.12 a temperature of 1250°K on the radiation flange face would infer a thermal efficiency of 60%.

The power to the electromagnet and excess power recorded in the two magnet cooling circuits are shown in Fig. 3.28. The excess power ranged between 0.7 and 0.1 kW with a nominal value of 0.3 kW. Figure 3.29 shows the thermal power received by the magnet cooling jacket, which is the cooling circuit surrounding the coil circuit. A nominal value of 80 watts was recorded in the circuit and it is conjectured that this measurement is more indicative of the heat transfer which would be recorded on a permanent magnet thruster (see Section 2.2).

At t = 460 hours erratic readings were encountered on the jacket cooling water flow rates and temperatures, which were due to a hole which had developed in the coil circuit within the magnet. This hole evidently caused by electrochemical erosion served to place the two cooling circuits in parallel.

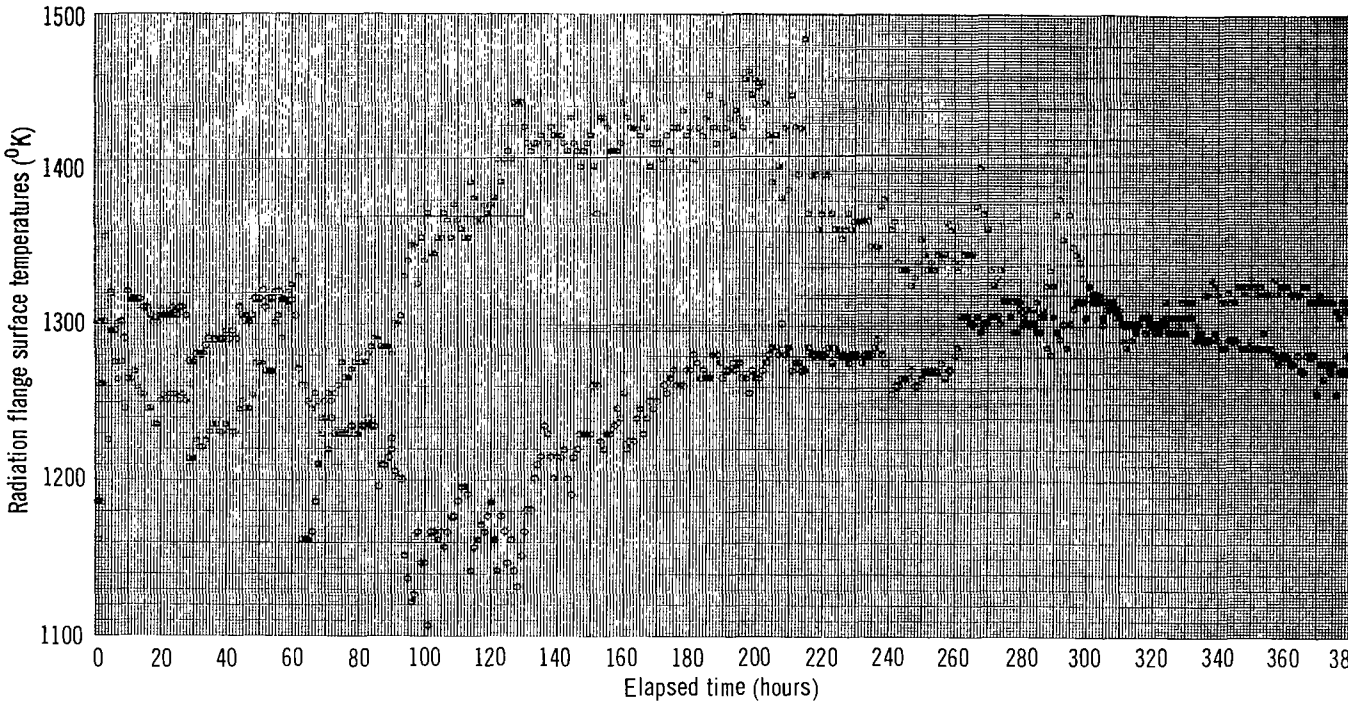

Fig. 3.27 Radiation flange temperature histogram

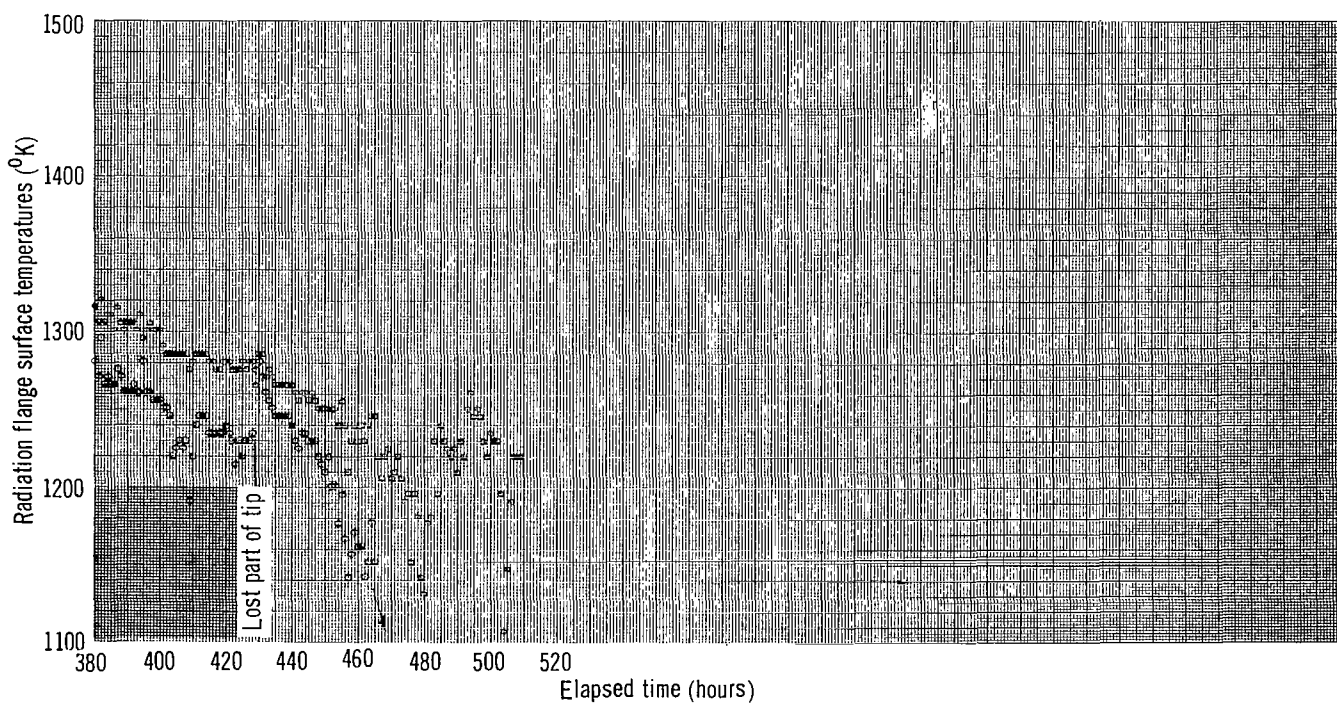

Fig. 3.27 Radiation flange temperature histogram (continued)

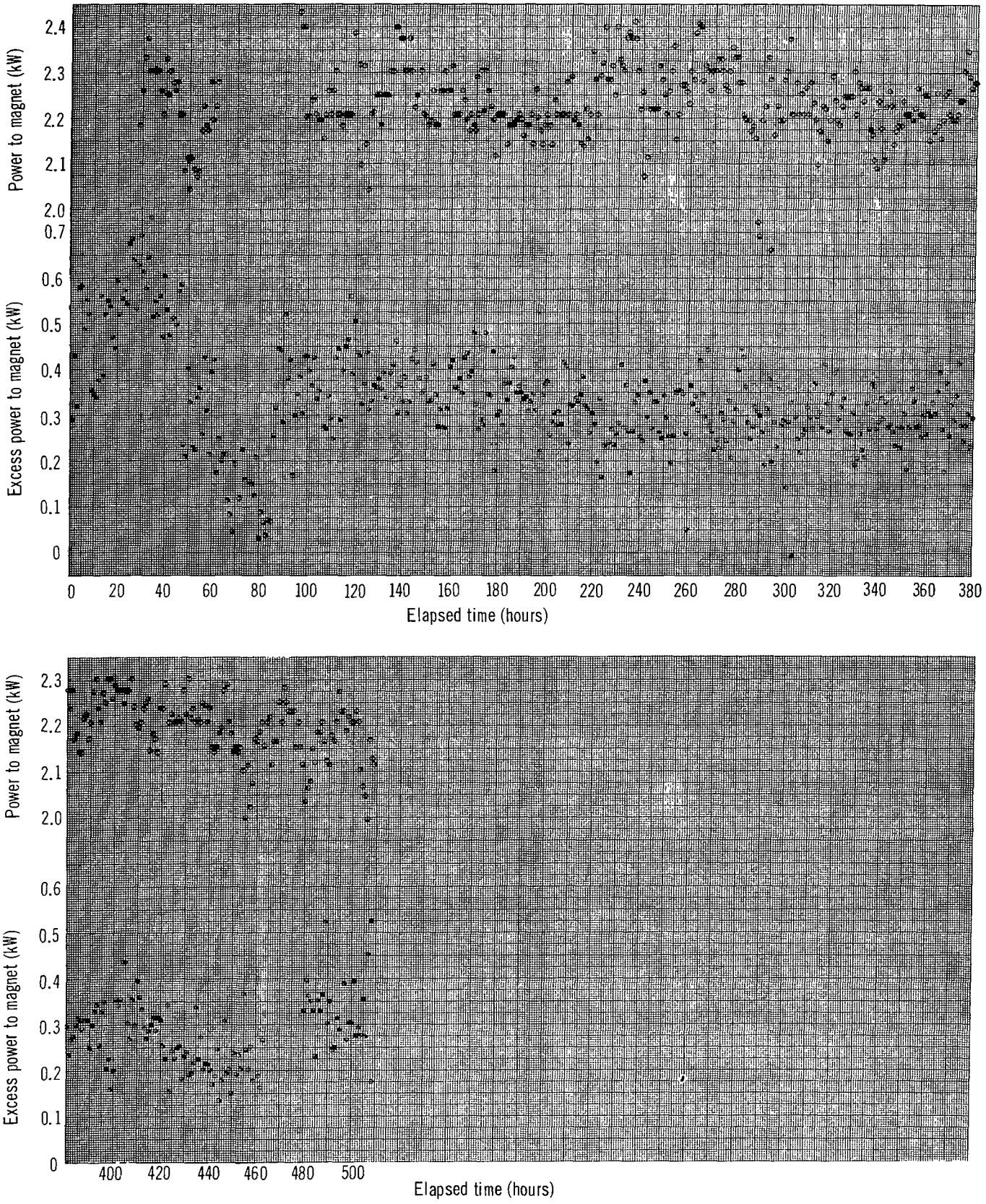

Fig. 3.28 Magnet power and excess power histogram

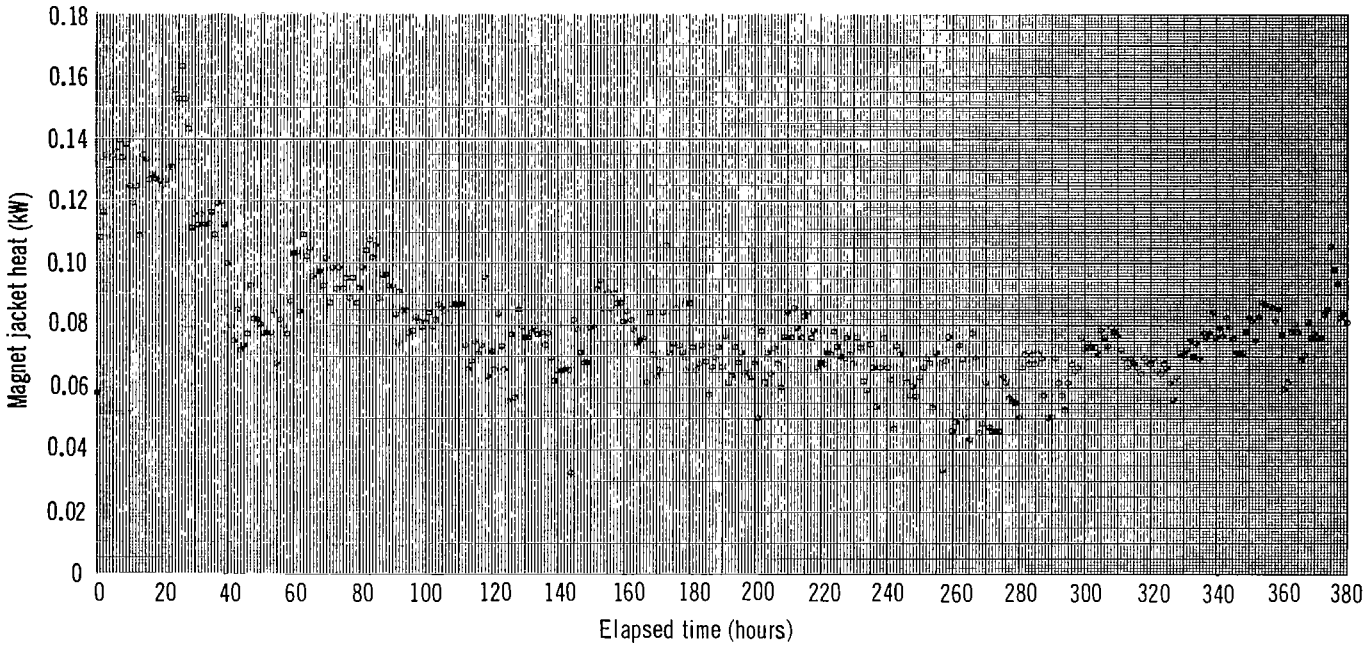

Fig. 3.29 Power to magnet cooling jacket histogram

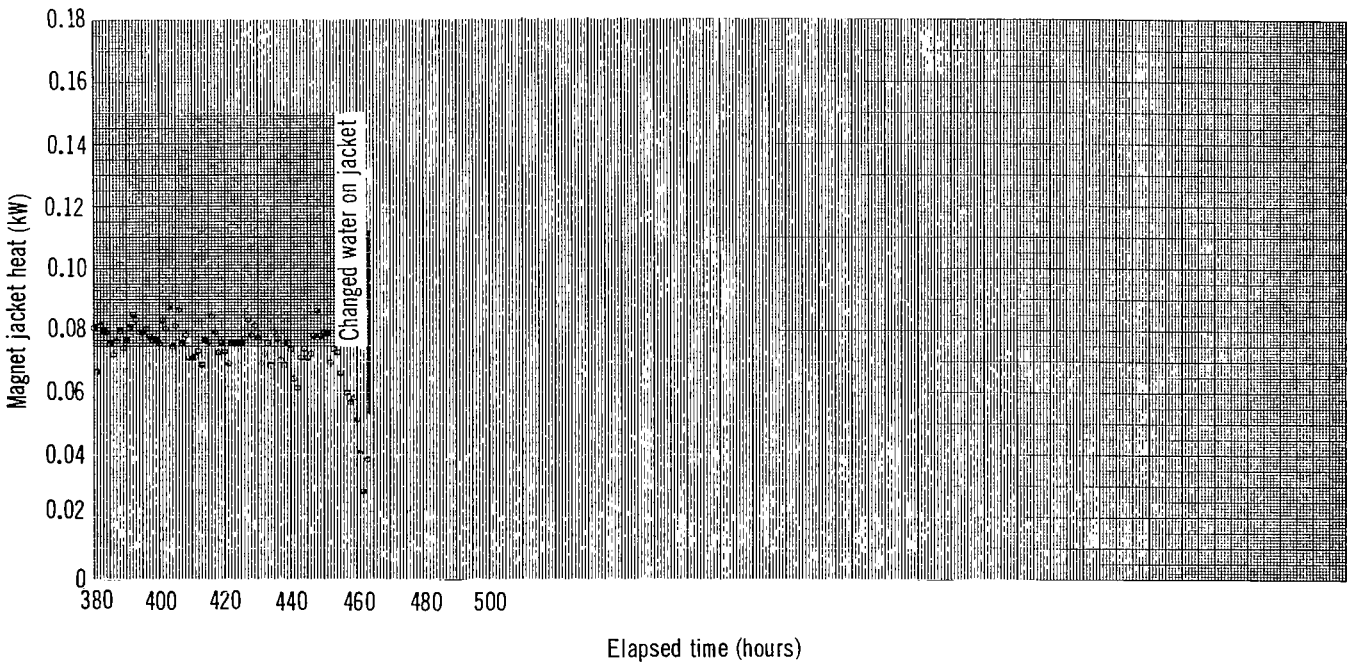

Fig. 3.29 Power to magnet cooling jacket histogram (Continued)

EXPERIMENTAL RESULTS AND DISCUSSION OF RESULTS

4 Conclusions

The following conclusions are made on the basis of the results of this study program.

Thruster design

- A radiation-cooled thruster configuration has been established which is capable of extended operating duration of over 500 hours at a nominal power level of 32 kW.

- Use of a composite tungsten-graphite anode with a simulated permanent magnet located to the rear of the anode-cathode insulator assembly provides a relatively lightweight thruster geometry. The total weight of the lifetest thruster with electromagnet is 17.2 kg, yielding a specific weight of 0.54 kg/kW.

- Replacement of the electromagnet with an annular Columax–9 permanent magnet should reduce the specific weight to near 0.45 kg/kW. Little or no additional thermal insulation between the permanent magnet and the anode assembly would be required to convert the present thruster design to a completely radiation-cooled configuration.

- Specification of minimum weight annular permanent magnet geometry was made which involved an assumption of uniform magnetization. The design curves generated for this case provide a qualitative estimate of permanent magnet weight for comparison with other magnet systems. Exact magnet weight design information can be provided if the magnetic field distribution of an actual permanent magnet could be accurately predicted. Comparisons between predicted and measured distribution on several Alnico–5 magnets yielded fairly good agreement, provided an empirical M/H curve was used.

Thruster performance

- Thrust performance recorded during short term tests (approximately 3 to 6 hours) on radiation-cooled thrusters of several different thermal diameters gave results comparable to water-cooled thruster performance previously reported. MPD thrust efficiency was a linear function of specific impulse with a slope proportional to mass flow rate. The thrust-to-power ratio averaged 2.2 g/kW at 0.040 g/sec, 1.95 g/kW at 0.030 g/sec and 1.7 g/kW at 0.020 g/sec.

- Changes in thruster geometry and external magnetic field serve mainly to affect the voltage and power level but not the thrust-to-power ratio. Some small variations of the thrust to power ratio were observed for different throat diameters and magnetic fields; however, these were within the experimental error.

- The performance attained during the short term tests was not duplicated in the 500 hour lifetest due to a time variation of the arc voltage. A

change from low voltage to a high voltage mode occurred after some 4 hours of test time, and a lower thrust efficiency associated with the high voltage mode was recorded.

- Photographic evidence of the cathode arc spot during the lifetest suggests that the high voltage mode is associated with arc attachment at the cathode tip, and low voltage mode operation occurs when the attachment area is at the base of the rod cathode. An intermediate voltage mode consisting of spot attachment on both the tip and base of the cathode was also observed.

- Cathode erosion was greater in the low voltage mode than in the high voltage mode and indicates that reliability is best in the high voltage mode while thrust performance is lower. The difference in arc voltage with and without a cathode gas shield and the increase in current level (while maintaining the high voltage mode) afforded by enlarging the cathode geometry indicate that the cathode temperature and consequently the cathode heat balance is a major factor in determining whether high or low mode operation is attained.

- The critical thruster component which determines the performance level and power capability is the cathode. The cathode configuration was the significant factor in setting the maximum possible current level and also the voltage mode. Cathode erosion rather than anode erosion appears predominant in determining thruster electrode life.

- The main cathode to anode insulator erosion was the highest of all critical thruster components. Based upon the insulator erosion rate recorded during the lifetest the projected life of the thruster was 1000 hours. The insulator erosion rate is a function of the cathode temperature level and mode of arc attachment with insulator erosion greatest in the low voltage mode condition.

- On the basis of measured and calculated temperatures of the radiation flange, the thrust efficiency of the radiation-cooled unit at the lifetest condition was approximately 60%. The agreement between measured and calculated temperature distribution indicates that the assignment of heat transfer into the anode at the downstream end of the anode throat for the purpose of calculating temperature distributions and thermal design analysis appears to be valid.

5 Recommendations for future work

The MPD arc thruster has been brought to an intermediate stage of development where duration testing of the device up to 500 hours has been accomplished. While power levels up to 40 kW have been tested for short periods, problems associated with the present cathode electrode configuration limit significant improvements in thrust performance, power capability and operational life beyond 1000 hours. Thus it is suggested that the next stage of work be focused upon the development of a high current MPD cathode configuration and the lifetest of a complete radiation-cooled thruster and magnet assembly.

To accomplish the above task the following future work is recommended:

- An experimental parametric study of high current MPD cathode electrode configurations be conducted within a radiation-cooled thruster design. Geometries to be investigated should include at least solid conical, hollow and gas-shielded or buffered cathodes with special attention to voltage and arc attachment modes. The test duration should be at 4–5 hours to ascertain thermal transient effects.

- An analytical and experimental study of annular permanent magnets be made with attention focused on the prediction of the magnetic field distribution away from the magnet and the effects of geometry on the distribution. Upon completion of this task a weight optimization study should be conducted to provide design curves of minimum mass magnet systems.

- A lifetest should be conducted of a radiation-cooled thruster incorporating an optimized high current cathode and a radiation-cooled minimum weight permanent magnet.

RECOMMENDATION FOR FUTURE WORK

Appendix A
X-4A radiation cooled thruster

Two radiation-cooled MPD thrusters of the McDonnell X–4A design were delivered to NASA on 13 May 1968. The X–4A thruster was developed under McDonnell's independent R&D program and is shown in Fig. A–1. This unit incorporates a composite tungsten-graphite anode assembly and a rod cathode electrically isolated from the anode by a cylindrical boron nitride insulator. Propellant is introduced into the discharge region through the cathode, and the arc chamber is sealed by means of lapped taper joints. The cathode is held in compression by means of six molybdenum screws attaching to the anode. The magnetic field coil is placed to the rear of the thruster. Radiation shields of 0.0254 cm molybdenum sheet are located between the magnet and the graphite radiation flanges to reduce the radiation flux to the magnet. The throat diameter of this thruster is 1.524 cm (0.6 inch) and the cathode tip is located at the convergence point of the tungsten nozzle.

The initial X–4A thrust performance data were obtained on a linear bushing thrust stand which did not possess a thrust killer or flow deflection bucket. This stand exhibited thermal drifts in the thrust reading over a period of several hours. Consequently, thrust measurements were obtained by shutdown tests. These measurements were determined by operating the thruster for approximately 30 to 45 minutes at the condition desired, abruptly killing the power to the thruster and recording the difference in thrust stand deflection between power on and power off. A calibration of deflection as a function of force (graduated weights) was obtained immediately after power was terminated and was used to convert the deflection to thrust. A thrust reading correction varying between 0 and 3 g (depending upon current level) was made to account for current "lead in" and magnetic field interactions. The correction curve was established for the current range tested by shorting the anode and cathode with a copper bar. Data obtained with the linear bushing stand were suspected of being in error due to thermal drift, and since this stand was also inadequate for long duration tests, a new single pendulum stand which incorporated a thrust killer was designed and fabricated. This stand is described in Section 3 and was used to measure the X–4A performance. Figure A–2 shows the thrust efficiency and specific impulse characteristics of the X–4A unit obtained with the new thrust balance. Also shown as a shaded region is the performance recorded with the linear bushing stand. The effect of mass flow rate on thrust efficiency is clearly evident whereas it was absent in the earlier measurements with the linear stand. The single pendulum measurements are in very good agreement with the performance obtained at the NASA Lewis Research Center on an identical X–4A unit.[10]

The results of the X–4A thrust measurement serve to emphasize the importance of having flexibility designed into the stand;whereby,the effects of thermal drift,magnetic,and cooling water tare forces may be effectively cancelled during the thrust measurement.

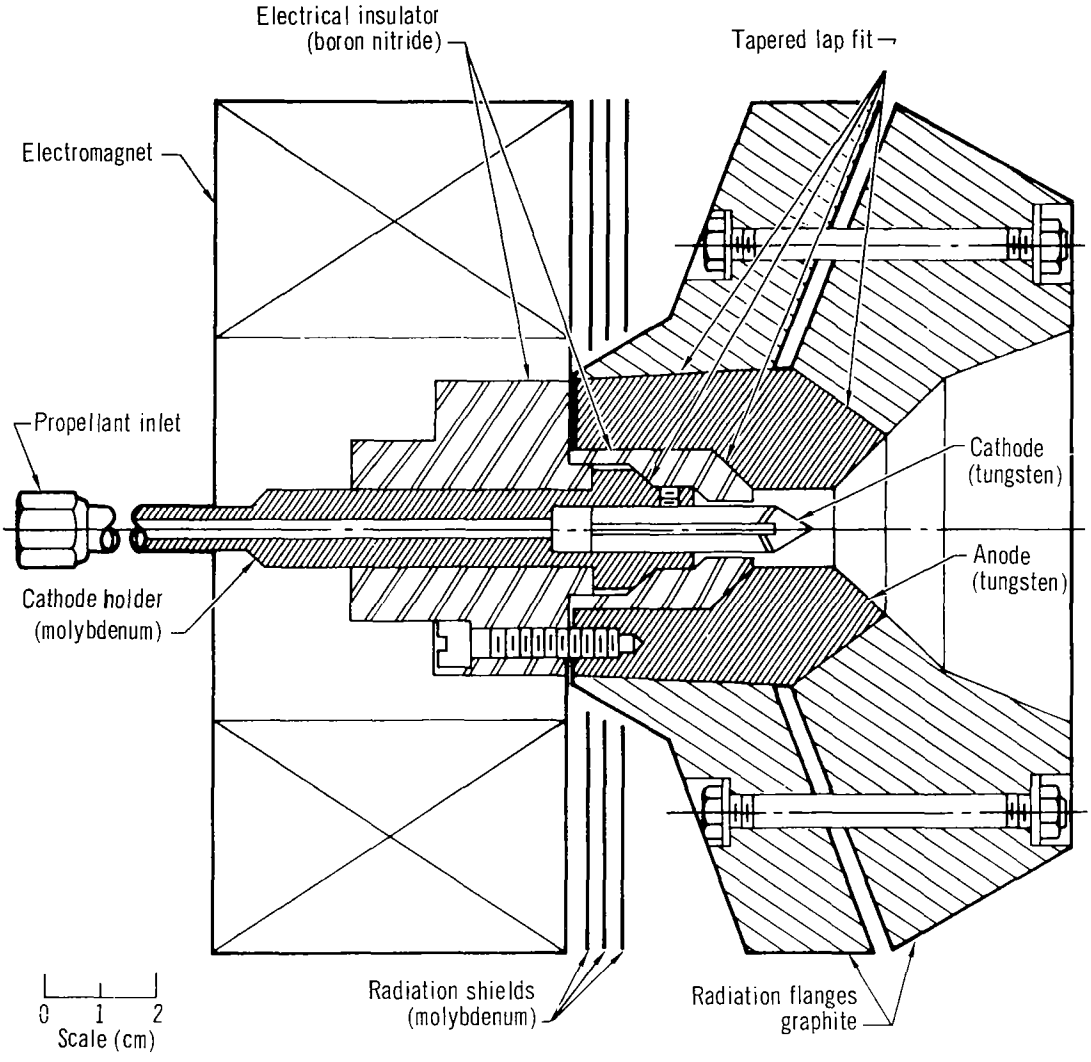

Fig. A–1 X–4A Radiation cooled thruster

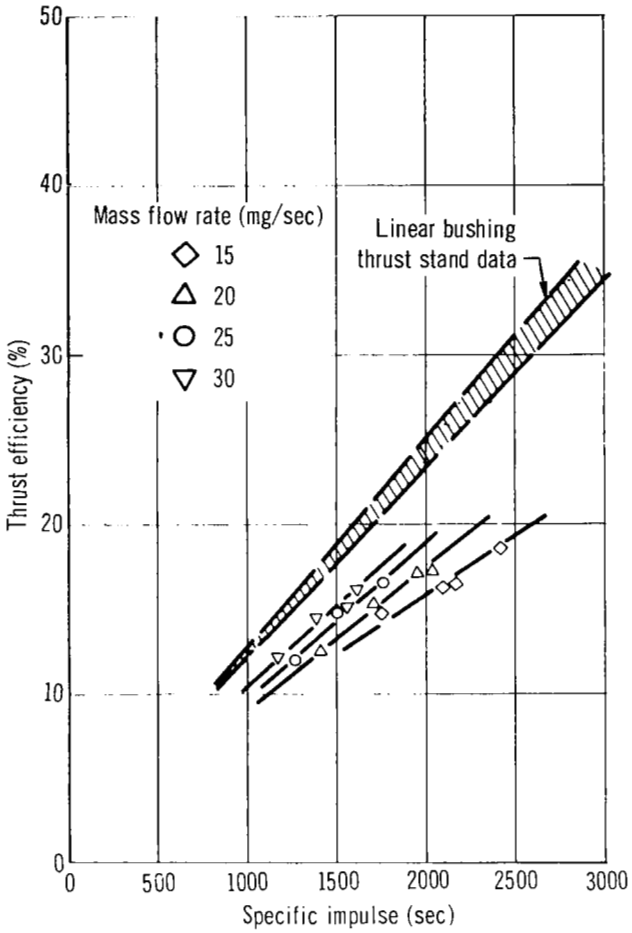

Fig. A–2 X–4A thrust performance on ammonia

APPENDICES

Appendix B
Design study guidelines

The guidelines used in the design study were establisted upon the following rationale:

Thruster parameters

- **Mass flow rate** – The mass flow rate range was determined quite simply from the thrust efficiency equation

$$\eta = \frac{4.81 \times 10^{-5}\, \dot{m}\, I_{sp}}{P_{in}} \qquad \text{B.1}$$

where η = thrust efficiency, (%),
$\dot{m}$ = mass flow rate (g/sec),
I_{sp} = specific impulse (sec),
P_{in} = input power (kW).

For specific impulses between 3500 and 2000 seconds at a constant thrust efficiency of 40% with 25 kW of input power, Equation (B.1) requires the mass flow rate to be within 17 to 52 mg/sec.

- **Arc current** – For MPD thrusters the arc voltage is a function of arc current, applied magnetic field, mass flow rate, and electrode geometry; however, past experimental results on a variety of configurations, propellant flow rates and field levels show that generally the arc voltage will be between 35 and 60 volts. Thus, to provide a power input of 25 kW the arc current is required to be within the range of 400–750 amps.

- **Power radiated from anode assembly** – The anode power loss which is radiated from the engine structure was estimated from thermal efficiency data obtained on water-cooled thrusters. Figure B–1 presents thermal efficiency measurements for several different ammonia MPD thruster configurations as a function of specific impulse. Data obtained in the 7 to 50 kW power range in this laboratory, AVCO RAD[11] and NASA Lewis Research Center[12] laboratories are plotted on Fig. B–1. In general, the thermal efficiency shows little sensitivity to thruster geometry and

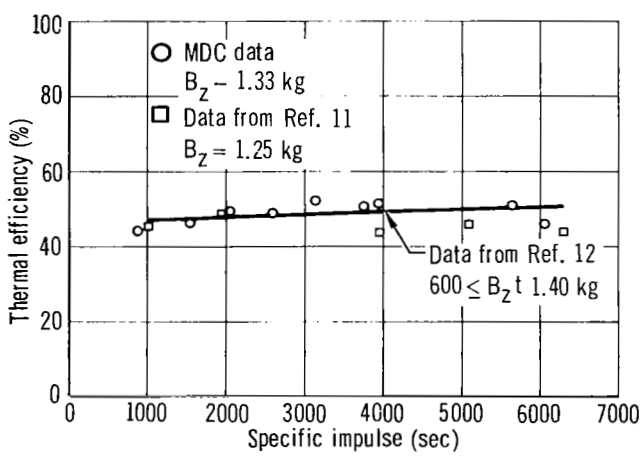

Fig. B–1 Thermal efficiency for various MPD ammonia thrusters

is only a slight function of applied magnetic field. The majority of reported data fall within the range of 45 to 55%. Thus for a thruster operating at an I_{sp} between 2000 and 3500 seconds, a thermal efficiency of 50% is anticipated and consequently 12.5 kW of power must be radiated from the anode structure.

- **External magnetic field at cathode tip** – The external magnetic field required is not simply specified since the performance of MPD thrusters is not particularly sensitive to field strength or shape as long as a solenoidal field is used. A minimum field would be desired for power and weight considerations; however, a sufficiently large field must be maintained to provide arc stability and to maintain the arc voltage at a level where excessive current levels are not required. Laboratory experience has shown that external fields at the cathode tip between 0.05 and 0.2 tesla are required. In the design study this range was assumed to be necessary although the final choice was determined in the parametric testing phase.

Thruster geometry considerations

Figure B–2 shows the typical axisymmetric configuration of the MPD thruster with critical design dimensions identified. The dimensions can be roughly divided into design groups. Dimensions D_m and L_c determine the size and weight of the radiation-cooled magnet assembly once the field shape and strength have been established. Studies[8] on radiation-cooled magnets indicate that the mass of the magnet for a fixed value of B at the cathode tip varies approximately as the cube of L_c and also as the cube of D_m. Since the magnet mass is generally greater than the anode-cathode-insulator assembly hence:

- the diameter of the cathode rod or support exterior to the thruster should be minimized so that the inner radius of the magnet may be as small as possible, and
- the distance between the cathode tip and the downstream face of the magnet should be minimized.

The dimensions D_t and L_g, the throat diameter and electrode gap respectively, determine to a large degree the interaction volume of the accelerating J x B forces which are the predominant thrust-producing mechanisms in the MPD arc thrusters. However, the precise J x B terms (i.e., Hall current effects, self-induced field effects, or thermal expansion through a magnetic nozzle), are not clearly understood at the present time. Moreover, there is a body of evidence that indicates the current discharge acts in the manner of a rotating spoke.[6,13,14,15] Since there is no satisfactory theory concerning the MPD accelerating mechanism which allows a calculation of the optimum interaction volume, D_t and L_g must be empirically determined. Therefore,

- provisions for changing the electrode gap and nozzle throat diameter should be incorporated so that thruster performance may be optimized with respect to these dimensions.

For a one piece solid anode as shown in Fig. B–2, the dimensions D_a and L_a are determined by the requirement

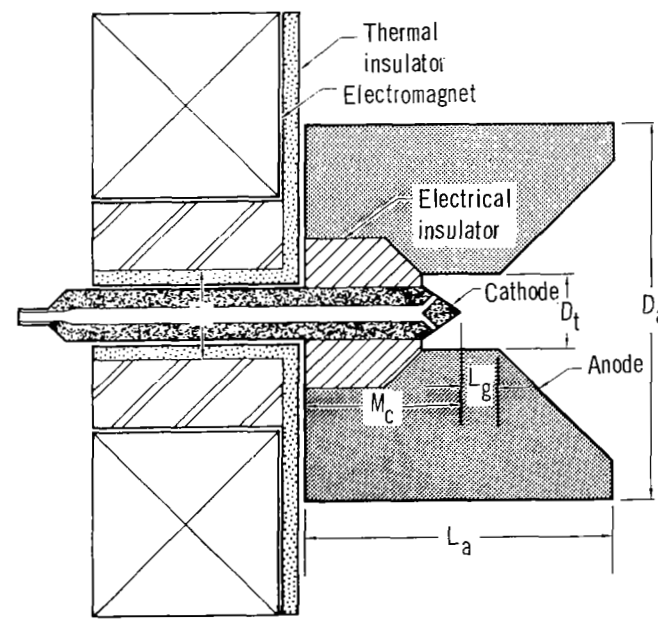

Fig. B–2 Radiation cooled MPD thrustor geometry

of conducting the anode heat (approximately 12.5 kW) from the throat region to the surface, where it would be radiated from the anode structure. However, the requirement of a minimum weight configuration and maintaining the heat transfer from the thruster assembly to the magnet below 100 watts eliminates the simple cylindrical anode from consideration.

Operation of a 7.62 cm diameter composite tungsten-graphite anode in this laboratory (X–4 thruster) has resulted in a maximum power capability (30.8 kW) which is approximately 10% lower than that obtained on a 7.62 cm tungsten engine[1]; however, the weight of this unit (7 lb) was approximately one-third that of the tungsten engine. Thus it is apparent that a significant weight reduction can be accomplished through the use of a composite anode structure. Consequently, a composite anode assembly consisting of a tungsten inner core and a graphite radiation flange should be utilized to provide a low thruster weight.

The heat transfer condition of 100 watts between the anode assembly and the magnet coupled with the 1200°K anode assembly operating temperature requires that thermal conduction paths between the magnet and the rear surface of the anode be minimized.

Tests conducted in the laboratory on a regeneratively-cooled anode injection MPD thruster showed no performance advantage to anode injection and a disadvantage in terms of gas sealing difficulties. Cathode injection results in less severe seal problems between anode, cathode and insulator. Consequently, the propellant should be introducted through the cathode. The high current operation requires that the limited regenerative-cooling capability of ammonia be utilized in the cathode to reduce erosion.

APPENDICES

Appendix C
Radiation cooled magnet study

Past analyses[1,2,8] of the weight of MPD magnet systems have assumed the electromagnet can be located such that the maximum field region coincides with the cathode electrode. For a single solenoid this requires the electromagnet to surround the cathode and have a bore large enough to accommodate the anode assembly. For MPD operation in the 15 to 50 kW range an anode outer diameter of at least 10 cm is necessary to radiate the anode heat loss. In view of the large bore requirements and the high temperatures encountered near the anode, relocation of the magnet upstream of the thruster appears to present fewer problems in terms of radiation-cooling and reliability. The field distribution of an annular permanent magnet is particularly well suited for magnet location upstream of the thruster, and therefore an analysis of optimum permanent magnet weight was conducted.

Mass optimization

The general centerline field distribution of an annular permanent magnet is shown in Fig. C–1. The field distribution of the axis possesses a maximum at a distance z_0 from the magnet face located at $z = 0$. The optimization problem involves a determination of minimum mass magnet dimensions for a required axial magnet field value and distance from the magnet end face. The thruster design and performance dictate the selection of magnetic field and (z) distance. For this study a range of magnetic field values between 0.1 and 0.2 tesla and (z) distances between 2.4 and 5.08 cm were considered. Conventional thrusters utilizing a rod cathode and holder place an additional design constraint on the analysis requiring a minimum internal magnet diameter which will accept the cathode holder. A range of internal radii between 0.95 cm and 1.9 cm was also considered in this study. Specification of B_z, z and R_i provides sufficient conditions to determine a minimum mass magnet, and for the range of values considered the cathode tip or z distance is located in a field region downstream of the B_z maximum.

Johansen and Palmer[8] have calculated optimum permanent magnet weights with the constraint that the cathode tip be coincident with the field maximum at $z = z_0$. With this condition, only specification of B_z and z is required to obtain a minimum mass; however, as will be shown, this condition results in heavier magnets than if R_i is specified and operation off the field maximum is allowed.

The analysis has been performed for only one magnet material, Columax–9, since this material has the highest energy density product. The demagnetization curve for Columax–9 is shown in Fig. C–2, and is essentially the same material as Alnico–9. It is noted that the demagnetization curve for Alnico–9 used in Ref. 9 shows a larger coercive force than Columax-9 and was based upon a vendor's estimate of the material's performance. Subsequent verification of Alnico–9 performance shows it identical to the Columax–9 curve in Fig. C–2.

The magnetic potential ϕ at a point in space due to a volume v of magnetized material is given by

$$\phi = \frac{1}{4\pi}\left\{\int_S \frac{\overline{M}\cdot d\overline{s}}{R} - \int_V \frac{\overline{\nabla}\cdot\overline{M}\,dv}{R}\right\} \qquad \text{(C–1)}$$

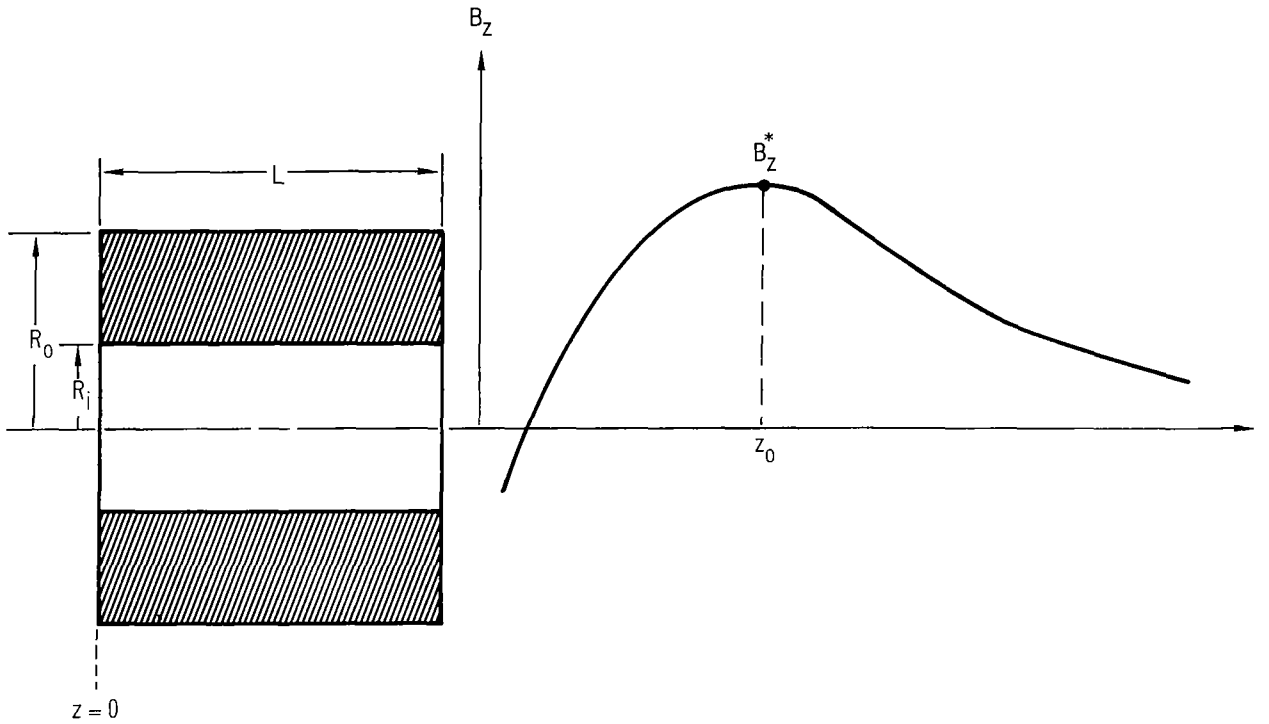

Fig. C–1 Permanent magnet geometry and centerline field distribution

where M is the magnetization vector, R is the distance between the point in space and the volume element, μ_0 is the permeability of free space, and s is the surface area of the magnet. The magnetizing field (H) is related to ϕ through

$$H = -\overline{\nabla}\phi. \qquad \text{(C–2)}$$

The magnetic induction is given by

$$\overline{B} = \mu_0 (\overline{H} + 4\pi\overline{M}). \qquad \text{(C–3)}$$

If we make the assumption that M is uniform and parallel to the axis of the annular magnet, then the expression for ϕ simplifies to a surface integral over the end faces of the magnet, and application of Eqs. (C-2) and (C-3) results in the following expression for the centerline field distribution of the magnet

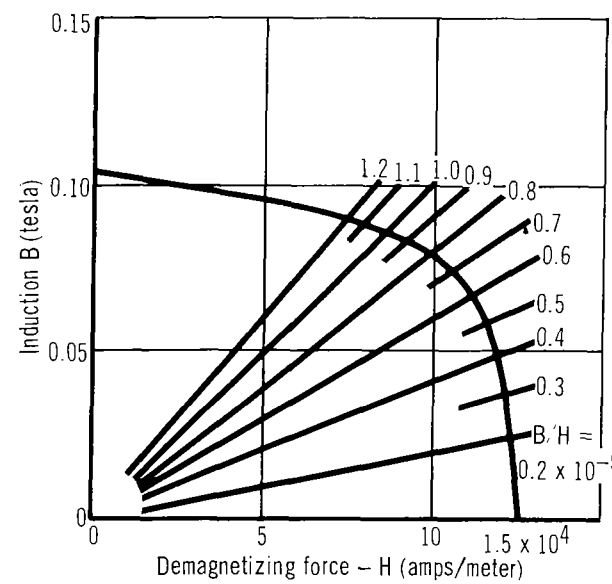

Fig. C–2 Demagnetization curve for Columax –9

$$B_z = \frac{M}{2}\left\{\frac{z-L}{[R_o^2+(z-L)^2]^{1/2}} - \frac{z}{[R_o^2+z^2]^{1/2}} - \frac{z-L}{[R_i^2+(z-L)^2]^{1/2}} + \frac{z}{[R_i^2+z^2]^{1/2}}\right\}. \quad \text{(C–4)}$$

The magnetization (M) is a function of the magnet material and geometry and is determined by the intersection of the M/H line on the demagnetization curve, Fig. C–2. The demagnetization coefficient(M/H)is derived from the free pole formula of Evershed[9] and is given by the expression

$$M/H = \frac{L_e}{(R_o^2 - R_i^2)}\left\{(R_o+R_i)(R_o-R_i+L)\right\}^{1/2}, \quad \text{(C–5)}$$

where L_e is an effective length which varies between L and 0.7 L, depending upon the ratio of end surface area to lateral surface area, and was assumed constant at a value of 0.7 L for the present calculations. The final equation required is that of the permanent magnet mass M_p, which is given by

$$M_p = \rho_m \pi (R_o^2 - R_i^2) L, \quad \text{(C–6)}$$

where ρ_m is the mass density of the magnet material. The mass optimization procedure was as follows:

(1) Choose values for R_i, z, and B_{z_o}. The values of R_i and z are chosen so as to be consistent with the thruster geometry. B_{z_o} is chosen to be a value that results in satisfactory thruster performance.

(2) Plot B_z and R_o for various values of L. The values of R_o and L are chosen such that the calculated B_z values are in the range containing B_{z_o}.

(3) From the graph in (2) above, obtain values for plotting R_o versus L for $B_z = B_{z_o}$.

(4) On the R_o versus L for constant B_{z_o} graph, plot R_o against L for constant M_p values. The minimum value of M_p is that which gives a curve tangent to the R_o versus L for $B_z = B_{z_o}$ curve.

Figures C–3, C–4, and C–5 represent design curves which provide Columax–9 magnet mass and length as a function of axial magnetic field, magnet internal radius and z distance.

Use of the design curves is illustrated for the following set of conditions: B_z = 0.1 tesla, z = 2.54 cm and R_i = 0.952 cm. From the solid curve of Fig. C–3 at B_z = 0.1 tesla and R_i = 0.952 cm the magnet mass is

$$M_p = 1.60 \text{ kg}.$$

From the dashed curve of Fig. C–3 at B_z = 0.1 tesla, R_i = 0.952 cm, the magnet length is

$$L = 10.7 \text{ cm}.$$

From Eq. (C–6) for the magnet mass, inserting a mass density of 0.00728 kg/cm^3, the magnet outer radius is

$$R_o = 2.73 \text{ cm}.$$

The results presented in Figs. C–3 to C–6 show that for a given set of B_z and z values a bar magnet provides the lowest permanent magnet mass and increasing R_i produces a corresponding increase in the mass. Thus for a low weight thruster system it is necessary to minimize the cathode holder or rod diameter which passes through the magnet. It is also clear that the value of z should be minimized.

The results of Johansen and Palmer[8] for a system producing 0.096 tesla at a z distance of 2.5 cm from the magnet follow, for comparison. A combined permanent magnet-Bitter electromagnet was found to be optimum with the permanent magnet supplying 0.075 tesla having a mass of 2.57 kg, while the electromagnet supplied the remaining 0.021 tesla with a mass of 0.91 kg. The total system mass of 3.48 kg is significantly higher than the 1.6 kg required by the Columax–9 magnet illustrated above, which provides a higher field. The difference in

mass between the two systems is a penalty imposed by the condition that the cathode tip coincide with the magnet field maximum.

After completing the mass optimization study discussed above, the calculation method was changed. A computer program was written to determine the minimum mass magnet for given R_i, z and B_{z_0} values. This program is discussed below.

Experimental magnet measurements

In order to check the validity of the mass optimization study, twelve Alnico–5 magnets were purchased and their axial and radial field distributions were measured. Figures C–6 and C–7 show typical field distributions for an annular magnet. These distributions were obtained before the magnet was remagnetized to saturation, but the essential features of the distributions are not greatly affected by the level of magnetization. Table C–1 gives the magnet dimensions, the z location and magnitude of the calculated field peak obtained using Eqs. (C–4) and (C–5). It is noted that the measured and calculated locations of the peak are in approximate agreement; however, the magnitudes of the measured and calculated maximum field points differ widely. Comparison of magnetic field measurements on several Columax–9 bar magnets showed Eqs. (C–4) and (C–5) to over-predict the centerline field. In the actual magnet since uniform magnetization is not realized due to leakage effects, it is expected that the uniform calculations would over-predict the field as observed for bar magnets. For annular magnets, a uniform magnetization calculation should over-predict the field at the magnet face; however, on the axis of the magnet, the leakage through the inner lateral surface serves to increase the axial field at the peak above the uniform magnetization calculations as observed for the Alnico–5 magnets.

As a result of these measurements it was concluded first that the design curves of Figs. C–3, C–4 and C–5 do not provide true minimum weight values. Hence the weights for bar magnets will be low whereas high weights for annular magnets are predicted. Secondly, true optimum weight calculations require a more accurate field distribution than afforded by Eqs. (C–4) and (C–5).

Table C–1 Alnico–5 magnet dimensions and maximum field values

Magnet No.	R_0 (cm)	R_i (cm)	L (cm)	Measured B_z (tesla)	Measured z_0 (cm)	Calculated (Equations 2.4 and 2.5) B_z (tesla)	Calculated (Equations 2.4 and 2.5) z_0 (cm)
1	3.80	3.17	3.81	6.4	2.8	3.61	3.04
2	3.55	1.00	1.90	8.0	2.0	5.54	1.72
3	4.55	3.60	3.30	4.4	3.5	1.92	3.78
4	3.80	2.38	9.52	26.6	2.1	26.1	2.20
5	5.54	2.57	4.76	11.2	2.9	5.35	3.22
6	3.50	2.00	12.41	46.8	1.6	54.4	1.88
7	5.16	3.65	4.45	7.3	3.6	3.23	3.86
8	3.52	2.54	2.86	6.2	2.5	2.75	2.70
9	3.80	3.17	3.81	6.6	2.8	3.61	3.04
10	4.44	3.21	4.28	7.4	3.1	4.08	3.28
11	5.08	1.90	5.55	16.9	2.3	9.65	2.45
12	4.76	3.99	3.10	3.3	4.0	1.35	4.18

Field calculations including leakage

In order to take flux leakage effects into account the distribution of M, the magnetization, must be specified. Once M is known, the integration of Eq. (C–1) may be carried out.

In the absence of any demagnetizing effects the magnetization of a sample which has been saturated is equal to the saturation value. However there is always present the self-demagnetizing field of the magnet which results from the formation of surface poles during the magnetizing process. Therefore when the magnetizing field is removed the magnetization at a point in the material will move along the hysteresis curve into the second quadrant to a point where the self-demagnetizing field and the magnetization are compatible. This operating point is a function of the geometry of the magnet, the magnet material and the reluctance of the magnetic circuit. For a magnet operating with no external circuit other than air the operating point is a function only of the material and the magnet dimensions because the

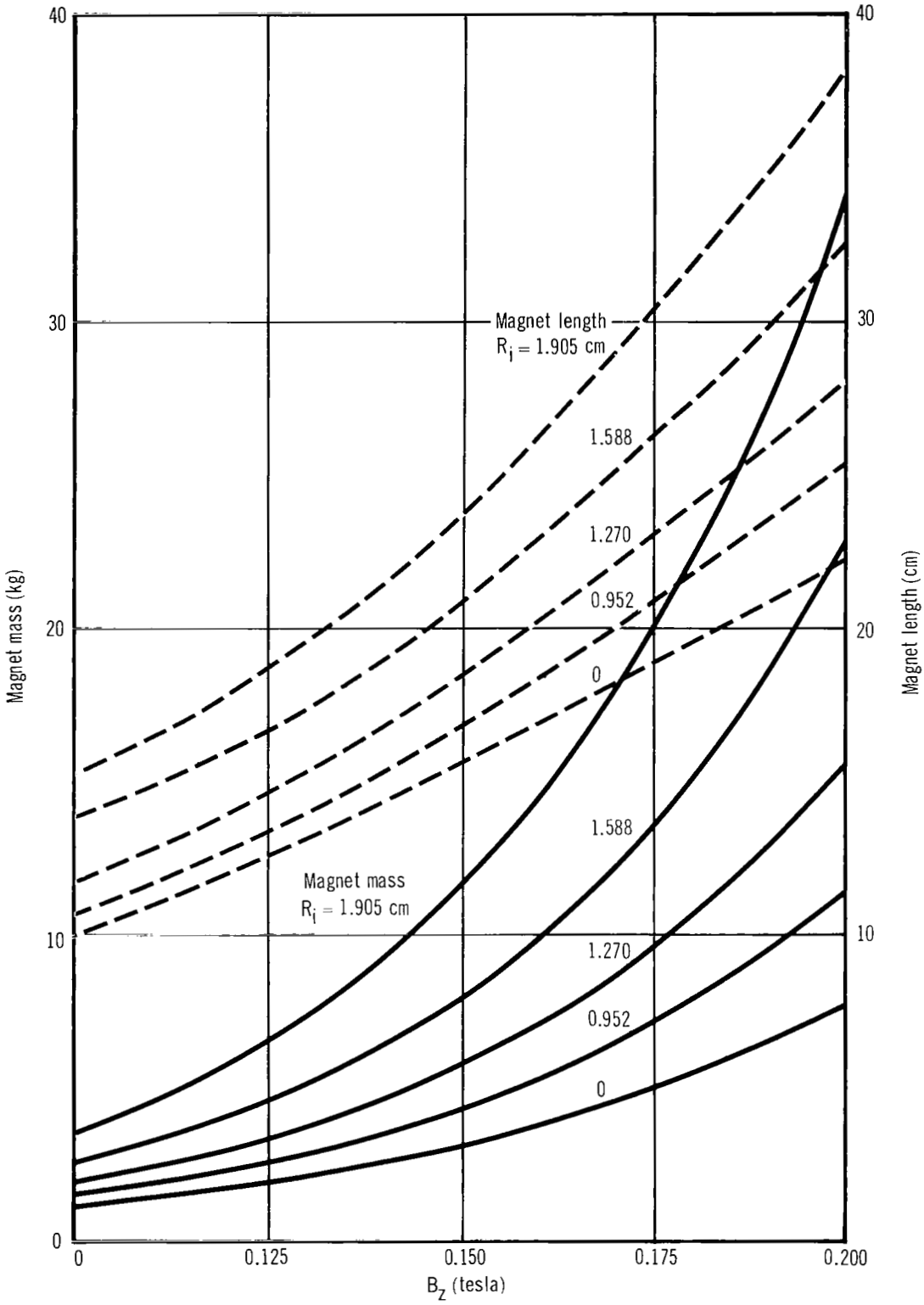

Fig. C–3 Optimum magnet mass for z = 2.54 cm (Columax–9)

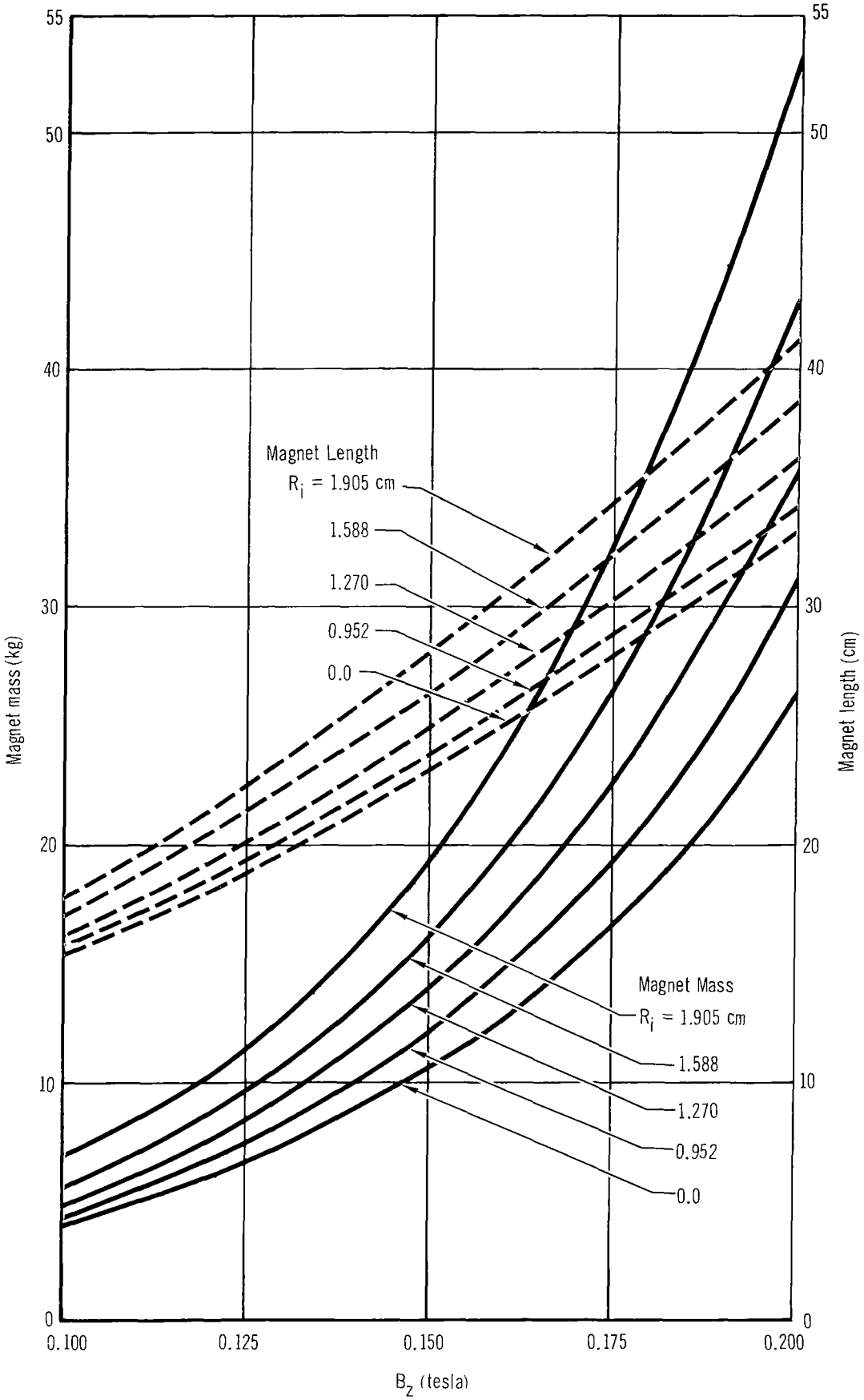

Fig. C–4 Optimum magnet mass for z = 3.81 cm (Columax–9)

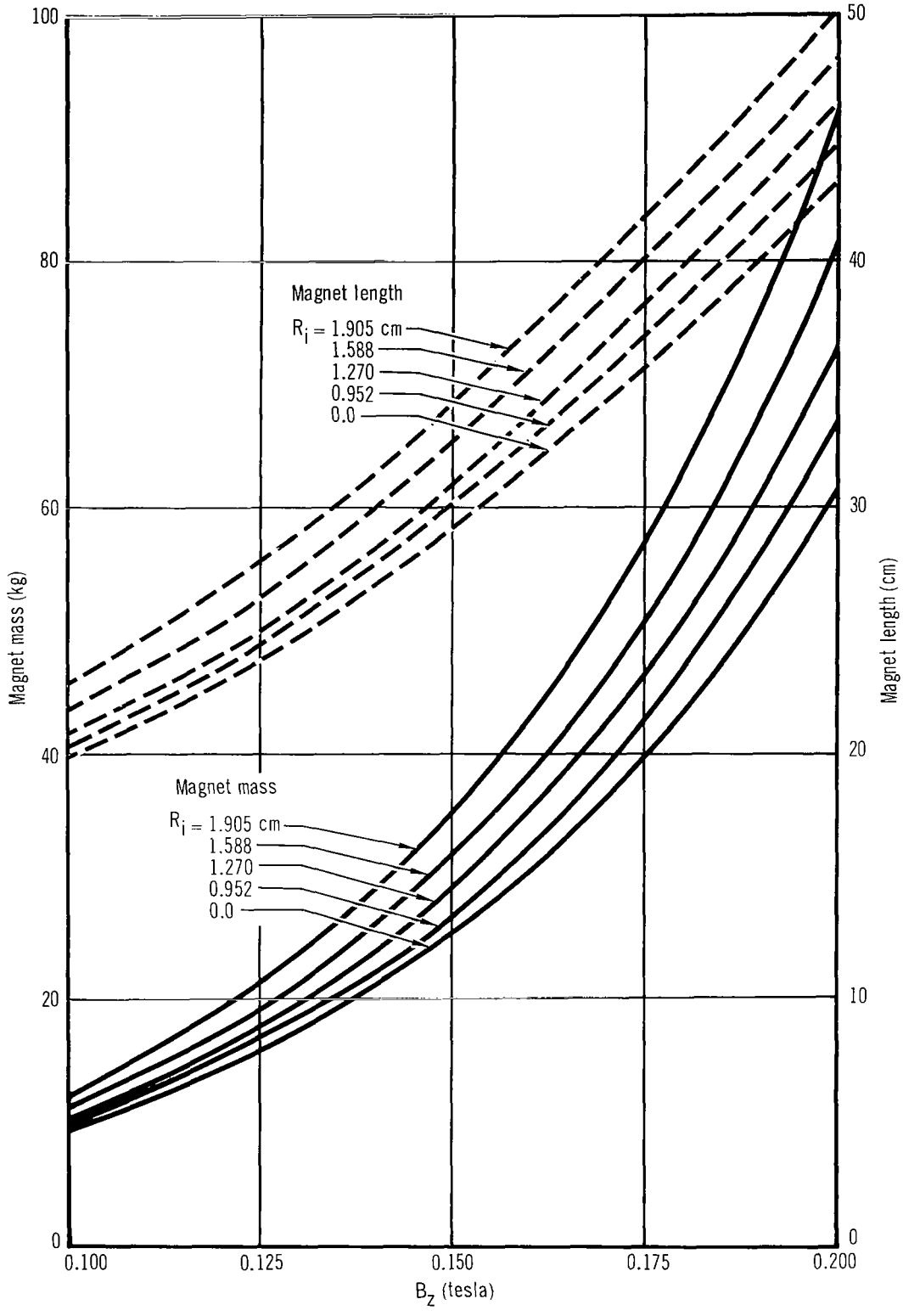

Fig. C–5 Optimum magnet mass for z = 5.08 cm (Columax–9)

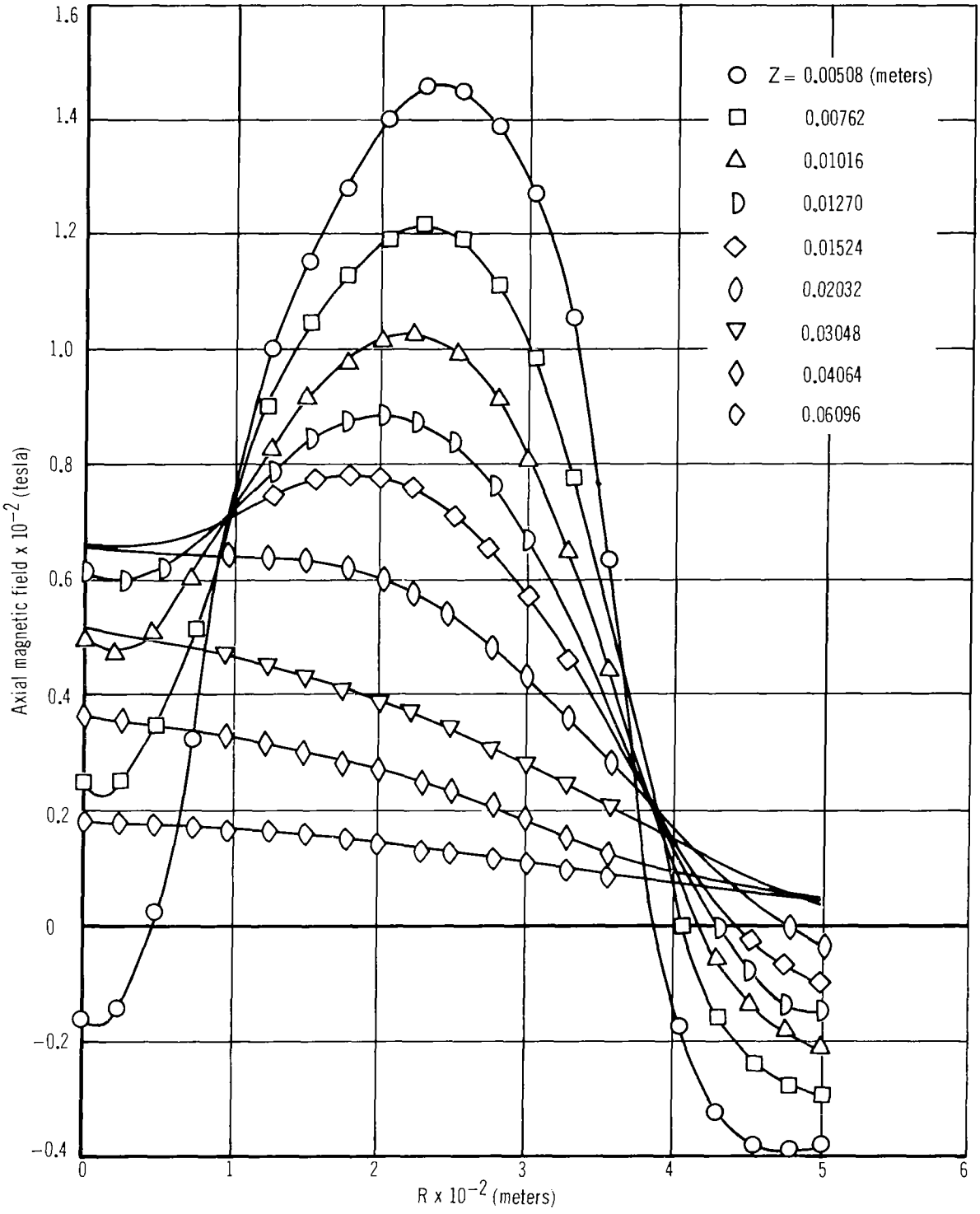

Fig. C–6 Measured B_z distribution for Alnico 5, magnet No. 2

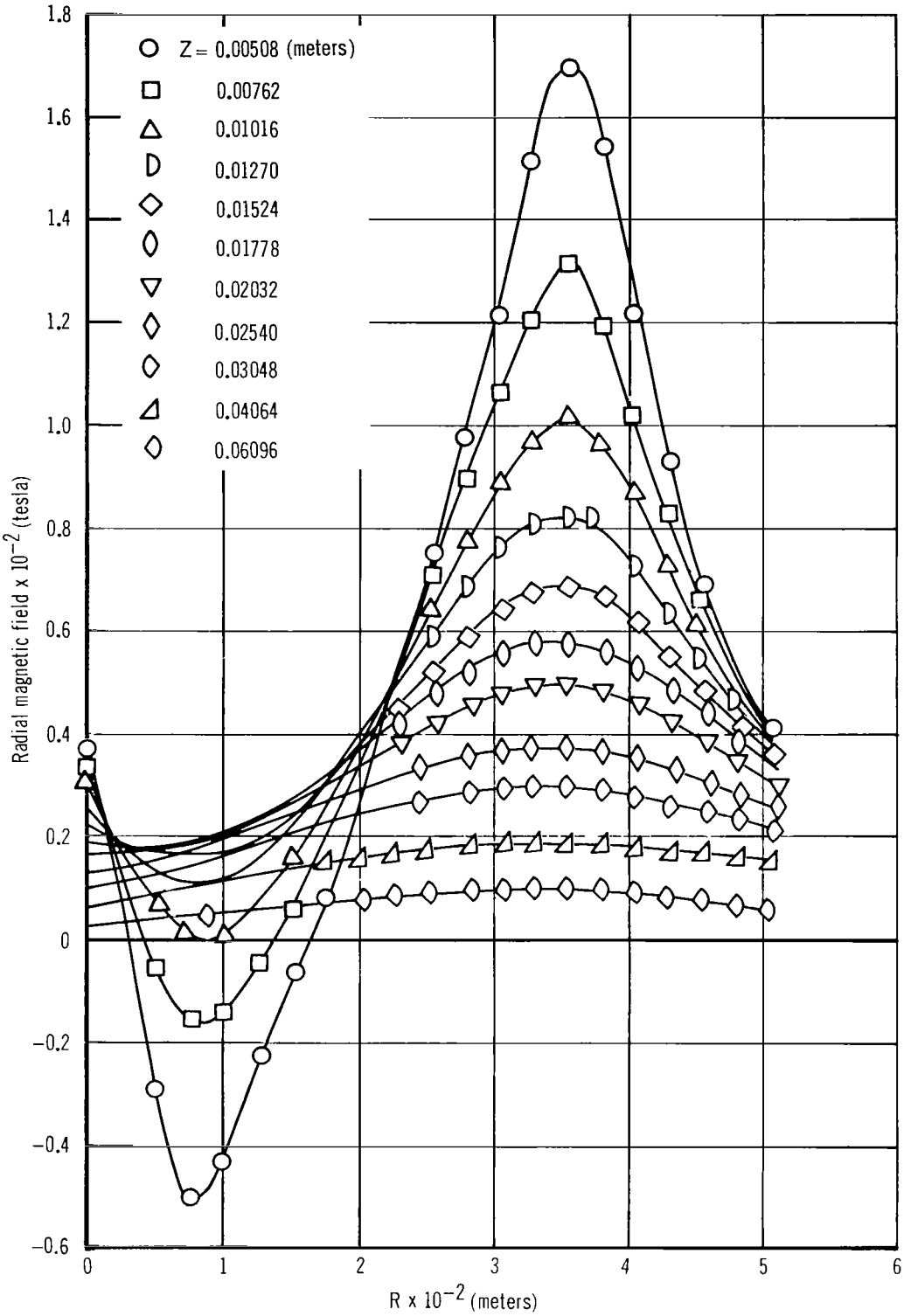

Fig. C–7 Measured B_r distribution for Alnico 5, magnet No. 2

reluctance of the external circuit is a function only of the magnet dimensions.

Before the field of the magnet can be calculated the magnetization must be determined at all points within the volume. One method of doing this is to determine the magnetization at a particular volume or plane over which the magnetization is assumed to be constant and then by some extrapolation procedure calculate the magnetization throughout the volume.

One such extrapolation technique was proposed by Evershed.[9] His method assumes that the length of the magnet may be subdivided into shorter length zones over which the magnetization is constant. The magnetomotive force can then be calculated at the junction between each pair of zones and then related to the leakage flux. The permeance to be used in this procedure is the leakage permeance of the lateral surfaces. All leakage is assumed to take place at the junctions between the zones. This method of extrapolation produces a parabolic variation in magnetization along the length of the magnet. An example of the Evershed technique is given below. The length of the magnet is divided into four pairs of zones, i.e., four on either side of the neutral section as shown in Fig. C–8.

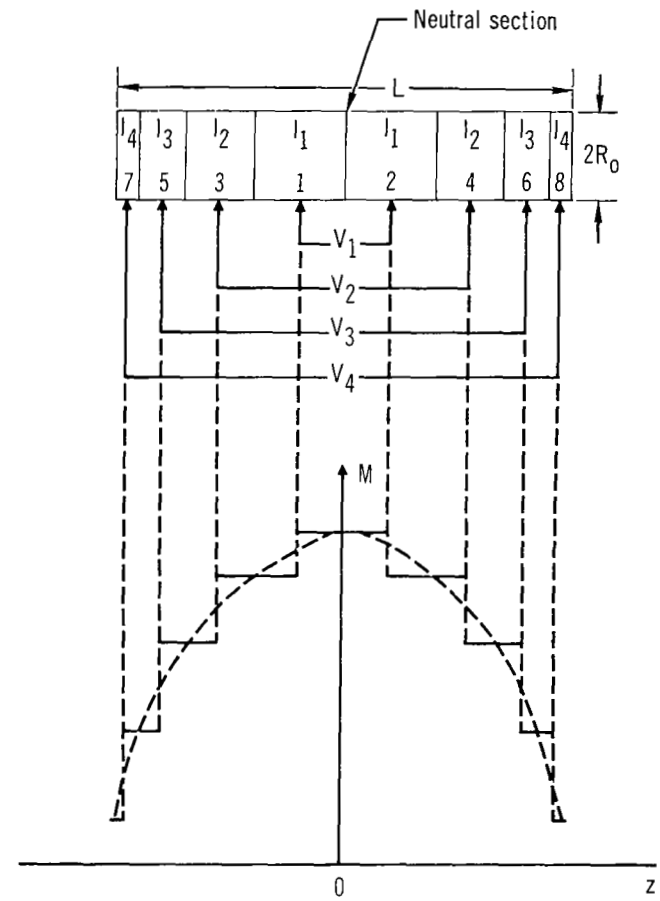

Fig. C–8 Schematic of magnet for Evershed extrapolation technique

The flux is considered to be uniform in the region from $z = -\frac{l_1}{2}$ to $+\frac{l_1}{2}$ and from $z = +\frac{l_1}{2}$ to $+(\frac{l_1}{2} + \frac{l_2}{2})$ etc., i.e., from points 1 to 2 and 2 to 4. etc. A value of M at the neutral section is chosen. For purposes of this discussion it is arbitrary: however, Eq. (C–5) provides a good initial choice. H at the neutral section is obtained from the demagnetization curve. The mmf (V_1) between points 1 and 2 is computed from

$$V_1 = H_{12}\,(l_1). \qquad \text{(C–7)}$$

The leakage flux can then be computed from

$$F_1 = V_1\,(P_1). \qquad \text{(C–8)}$$

P_1 is the leakage permeance of the z_1. For this discussion it need not be defined, but it is usually calculated by considering the total leakage permeance to be given by the free pole formula

$$P = \pi S. \qquad \text{(C–9)}$$

S here is the leakage surface area, i.e., the pole face is excluded. For a round bar magnet

$$S = 2L\,\pi\,R_0. \qquad \text{(C–10)}$$

Then P_1 is taken to be the leakage permeance per unit length times the length of the zone.

$$P_1 = \frac{\pi S}{L}\,L_1. \qquad \text{(C–11)}$$

The loss in magnetization at the end of the first zone is then

$$SM = H_{12}\,\frac{\pi S}{L}\,L_1^2/A \qquad \text{(C–12)}$$

Table C–2 Magnetic field calculation method of Evershed

M of zone	H of zone	Length of zone	mmf at zone junction	Leakage permeance of zone	ΔM at zone junction
M_1	H_1	L_1	$V_1 = H_1 L_1$	$P_1 = \frac{\pi S}{L} L_1$	$\Delta M_1 = V_1 P_1 / A$
$M_2 = M_1 - \Delta M_1$	H_2	$L_1 + L_2$	$V_2 = H_2 (L_1 + L_2) + V_1$	$P_2 = \frac{\pi S}{L} (L_1 + L_2)$	$\Delta M_2 = V_2 P_2 / A$
$M_3 = M_2 - \Delta M_1$	H_3	$L_2 + L_3$	$V_3 = V_2 + H_3 (L_2 + L_3)$	$P_3 = \frac{\pi S}{L} (L_2 + L_3)$	$\Delta M_3 = V_3 P_3 / A$
$M_4 = M_3 - \Delta M_3$	H_4	$L_3 + L_4$	$V_4 = V_3 + H_4 (L_3 + L_4)$	$P_4 = \frac{\pi S}{L} (L_3 + L_4)$	$\Delta M_4 = V_4 P_4 / A$
$M_5 = M_4 - \Delta M_4$					

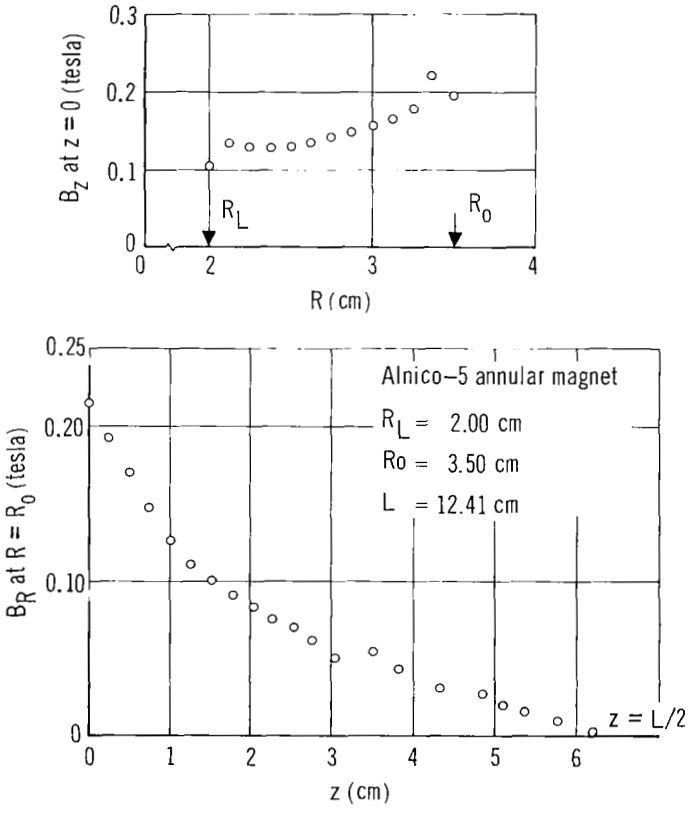

Fig. C–9 End and outer lateral surface normal magnetic field distributions for magnet No. 6

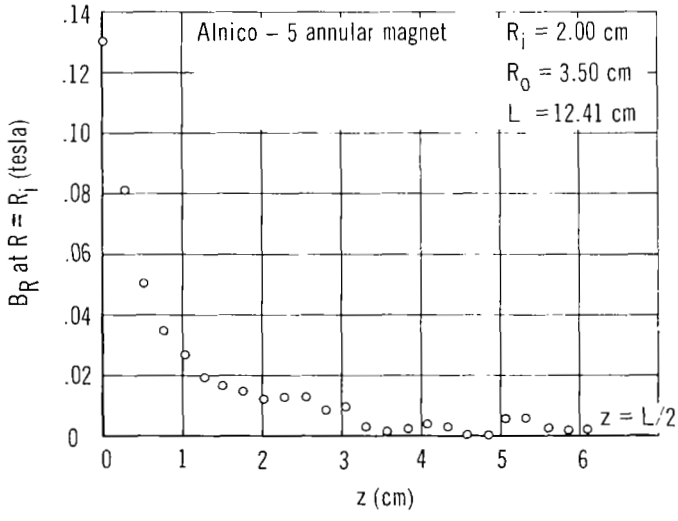

Fig. C–10 Inner lateral surface normal magnetic field distribution for magnet No. 6

where A is the cross-sectional area of the magnet. This decrease is then subtracted from the neutral section magnetization to obtain M in second zone. The procedure is then repeated along the length of the magnet until the face is reached. The value of B obtained at the face is checked by insertion into the following equation:

$$B \cdot A = H \cdot L \cdot P \qquad \text{(C–13)}$$

with P equal to the over-all air gap permeance. If Eq. (C–13) is not satisfied, then the initial choice of B at the neutral section must be rechosen until agreement is obtained. The use of Eq. (C–5) for the initial choice of the neutral section B value usually expedites this iteration. The graph in Fig. C–8 is then plotted and a smooth curve drawn through the steps as illustrated by the dashed curve. The entire calculation for the example magnet is shown in Table C–2. The above procedure provides a method by which the axial variation of B and M within the magnet may be estimated. Thus from the M(z) curve, the axial gradient $\delta M/\delta z$ may be determined.

As a check on the validity of the Evershed technique the normal field distribution on several of the Alnico–5 magnets were measured over the pole face, inner and outer lateral surfaces. The distributions obtained on magnet No. 6 are shown in Figs. C–9 and C–10. Using the above surface distribution and a macroscopic application of $\nabla \cdot B = 0$, the B_z distribution inside the magnet was inferred and is shown in Fig. C–11. The distribution is nearly parabolic and qualitatively agrees with the results of the Evershed extrapolation technique. Thus it is reasonable to assume that $\partial M/\partial z = \nabla \cdot M$ is given by this method.

Specification of the surface distribution of M is not straightforward; however, as an approximation it was assumed that the flux density surface distributions were the same as the magnetization distribution. The experimental measurements were used to obtain functions of the distributions as follows:

$$M\,(z = 0, R) = Q, \qquad \text{(C–14)}$$

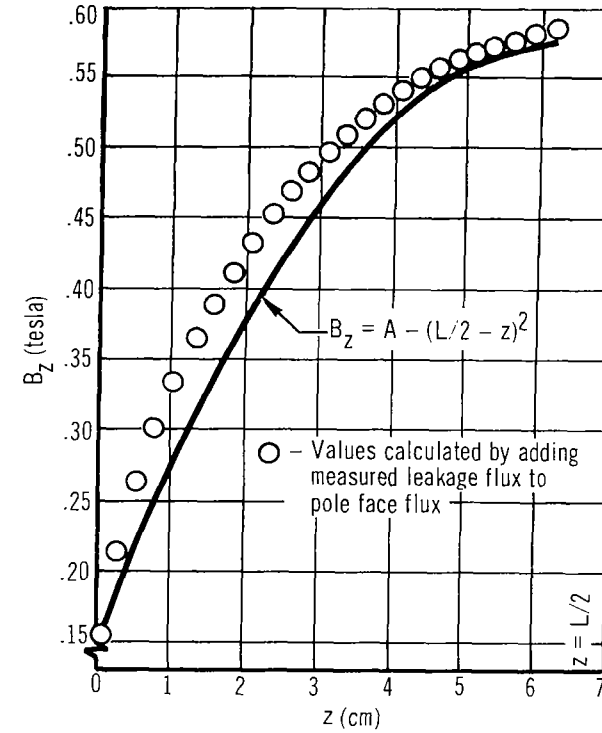

Fig. C–11 Calculated axial magnetic field within magnet No. 6

$$M_R\,(z, R = R_o) = \frac{Q}{(L/2)^2}\,(L/2 - z)^2,\ z \leq L/2, \qquad \text{(C–15)}$$

$$= \frac{-Q}{(L/2)^2}\,(L/2 - z)^2,\ z \geq L/2, \qquad \text{(C–16)}$$

$$M_R\,(z, R = R_i) = \frac{-Q}{(L/2)^7}\,(L/2 - z)^7, \qquad \text{(C–17)}$$

where Q is the average value of the magnetization at z = 0 and is related to the neutral section M through the extrapolation procedure.

The functions of Eqs. (C–14) through (C–17) were inserted into Eq. (C–1) and the indicated integrations carried out over the magnet volume to yield a calculated centerline field distribution.

Figure C–12 shows the results of a sample calculation with the contributions from each of the integrals in

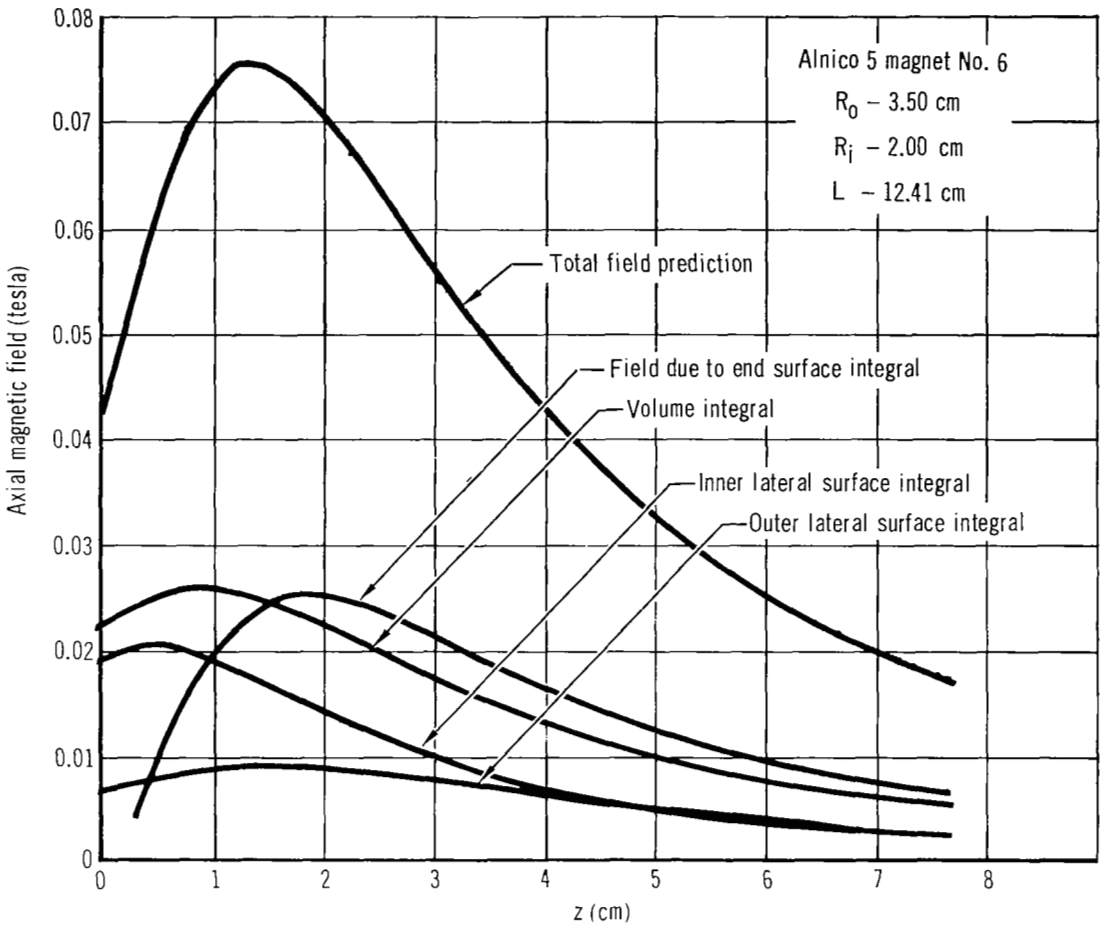

Fig. C–12 Calculated centerline field distribution for Alnico 5 magnet No. 6

Eq. (C–11) identified. As indicated, inclusion of the volume and surface contributions to the field preserves the essential features of the centerline axial field distribution. The initial results of these calculations showed good agreement with measured field distributions on several of the magnets; however, good agreement could not be obtained for all the magnets. The requirement of satisfying Eq. (C–13) at the end of the extrapolation scheme was then released and the following form for M_z was assumed

$$M_z = M_0 - \left(\frac{2}{L}\right)^2 (M_0 - Q)(L/2 - z)^2, \qquad \text{(C–18)}$$

where M_0 is the neutral section magnetization. This relation preserves the functional form of the Evershed extrapolation scheme. Equation (C–18) was used in the integration of Eq. (C–1) with the value of Q as a free parameter. The value of Q was then chosen such that the calculated peak and the measured peak in the centerline distribution agreed. A partial check on the validity of the calculations is the agreement obtained between measured and predicted values of z_0, the location of the field maximum. Table C–3, gives the results for all the Alnico–5 magnets.

Agreement within ± 15% is obtained for all the magnets and in terms of the previous calculations it is the best agreement to date.

The values of $(M_0/H)^*$ required to match the field maxima were compared with the expression for M/H

Table C–3 Measured and calculated location of magnetic field maximum

Magnet No.	Measured z_0 (cm)	Calculated z_0 (cm)
1	2.8	2.9
2	2.0	1.7
3	3.5	3.7
4	2.1	1.8
5	2.9	3.2
6	1.6	1.4
7	3.6	3.8
8	2.5	2.8
9	2.8	2.9
10	3.1	3.3
11	2.3	2.3
12	4.0	4.2
13*	2.4	2.3

* Magnet 13 is formed by joining 1 and 9 end to end

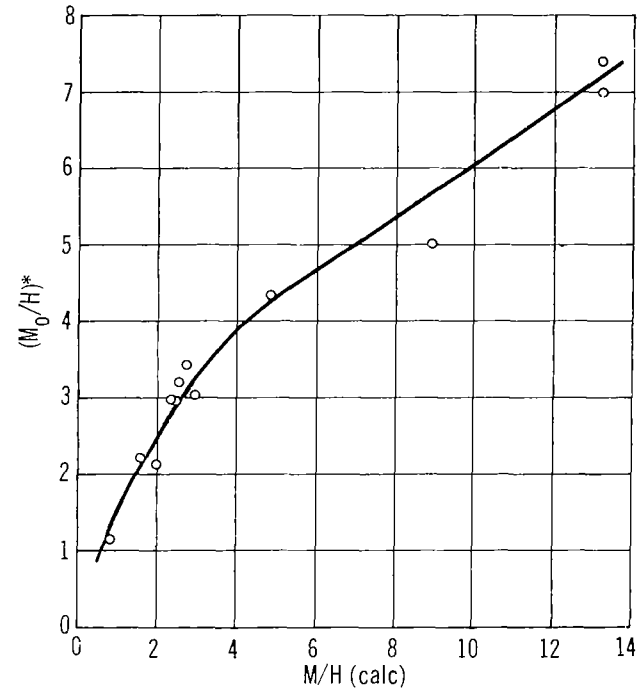

Fig. C–13 $(M_0/H)^*$ versus M/H calculated by Eq. (2.6)

based upon Evershed's free pole formula given by Eq. (C–5). Figure C–13 shows this comparison for the case $L_e = 1$. If $(M_0/H)^*$ is substituted into Eq. (C–5) and a value of L_e extracted, we find a range of L_e between 1.4 and 0.6; however, no systematic correlation of L_e with the ratio of lateral to end surface could be established.

The above procedure was carried out for several Columax–9 bar magnets; however, poor agreement was obtained between measured and predicted field values. Since leakage effects produce opposite contributions to the centerline field for annular and bar magnets it is not too surprising that the empirical M/H curve (Fig. C–13) obtained for annular magnets did not produce good agreement. It is quite possible that the procedure is adequate for annular Columax–9 magnets and a different B/H curve is required for bar magnets.

Computer program for mass optimization

The computer program for the determination of the geometry of a minimum mass annular magnet is given in Table C–4. The program is written in the BASIC language and represents the case of a uniformly magnetized Columax–9 magnet with an effective length value of 0.7 times the actual magnet length.

The design equations for the magnet mass and the centerline magnetic field distributions are given by Eqs. (C–4), (C–5), and (C–6). Statement 160 of Table C–4 is the mass Eq. (C–6) and statements 205, 210 and 215 provide the magnetic field distribution given in Eq. (C–4). Statement 165 represents Eq. (C–5) and the demagnetization curve is tabulated via statements 515 through 885.

```
5 PRINT "THIS PROGRAM DETERMINES THE GEOMETRY FOR A FIXED ID ANNULAR"
10 PRINT "MAGNET OF MINIMUM MASS, GIVEN THE VALUES OF Z, BZØ, RI, RØ,"
15 PRINT "DELTA RØ, L, AND DELTA L, RESPECTIVELY."
20 PRINT
25 PRINT "WHAT ACCURACY IS DESIRED--1, 2, OR 3":
30  INPUT A
35 PRINT
40 PRINT "INPUT VALUES OF Z, BZØ, RI, RØ, DELTA RØ, L, AND"
45 PRINT "DELTA L, RESPECTIVELY."
50 PRINT
55 INPUT Z,BØ,R1,RØ,R3,L,L3
60 PRINT
65 PRINT "Z=";Z;"BZØ=";BØ;"R1=";R1
70 ON A GO TO 75, 95, 115
75  LET A1=1.
80 LET A2=10.
85 LET A3=100.
90 GO TO 130
95 LET A1=10.
100 LET A2=100.
105 LET A3=1000.
110 GO TO 130
115 LET A1=100.
120 LET A2=1000.
125 LET A3=10000.
130 LET D9=0.0
135 LET D=0.0
140 LET D2=0.0
145  LET D3=0.0
150 LET D1=R3
155 LETR3=D1
160 LET W=.8325*(RØ^2-R1^2)*L
165 LET M=(.7*L/(RØ^2-R1^2))*SQR((RØ+R1)*(RØ-R1+L))
170 LET U=INT(M)
175 IF U<1.0 THEN 875
180 IF U>18 THEN 200
185 GO TO 515
190 LET B=Q+(S-Q)*(M-U)
195 GO TO 205
200 LET B=4840
205 LET K3=(Z+L)/SQR(RØ^2+(Z+L)^2)-Z/SQR(RØ^2+Z^2)
210 LET K3=K3+Z/SQR(R1^2+Z^2)-(Z+L)/SQR(R1^2+(Z+L)^2)
215 LET B=B*K3
220 IF INT(B*A1)=INT(BØ*A1) THEN 285
225 IF INT(B*A1)>INT(BØ*A1) THEN 250
230 LET D=RØ
235 LET RØ=RØ+R3
240 IF RØ>10.0 THEN  475
245 GO TO 160
```

Table C–4 Mass optimization computer program

```
250 LET R3=R3/10.0
255 IF D=0 THEN 505
260 IF R3>E-10 THEN 275
265 LET R0=D6
270 GO TO 155
275 LETR0=D+R3
280 GO TO 160
285 IF D3 =0 THEN 325
290 IF INT(L*A2)=INT(D4*A2) THEN 450
295 IF INT(W*A3)=INT(D3*A3) THEN 450
300 IF INT(W*A3)>INT(D3*A3) THEN 375
305 LET D5=D3
310 LET D7=D6
315 LET D8=D4
320 LET D2=1.0
325 LET D9=D9+1.
330 LET D4=L
335 LET D6=R0
340 LET L=L-L3
345 IF D5=0.0 THEN 365
350 IF ABS(D7-D6)<5.0E-5 THEN 365
355 LET M=(D8-D4)/(D7-D6)
360 LET R0=(L+M*D7-D8)/M
365 LET D3=W
370 GO TO 155
375 IF D2=0.0 THEN 495
380 LET L3=L3/10.0
385 IF D5<>0.0 THEN405
390 LET D5=D3
395 LET D7=D6
400 LET D8=D4
405 LET L=D8-L3
410 LET D3=D5
415 LET D6=D7
420 LET D4=D8
425 LET D5=0
430 LET D7=0
435 LET D8=0
440 LET R0=D6
445 GO TO 155
450 PRINT "MIN MASS(LBS)=";W
455 PRINT "L(IN)=";L
460 PRINT "R(IN)=";R0
465 PRINT "B(GAUSS)=";B
470 GO TO 50
475 IF D9=1. THEN 485
480 IF D2=0.0 THEN 495
485 PRINT "DELTA L IS TO LARGE, OR L IS BELOW MIN MASS POINT"
490 GO TO 50
```

Table C–4 Mass optimization computer program (continued)

```
495 PRINT "L IS BELOW MIN MASS POINT"
500 GO TO 50
505 PRINT"RØ IS TO LARGE"
510 GO TO 50
515 IF U=1 THEN 605
520 IF U=2 THEN 620
525 IF U=3 THEN635
530 IF U=4 THEN 650
535 IF U=5 THEN 665
540 IF U=6 THEN 680
545 IF U=7 THEN 695
550 IF U=8 THEN 710
555 IF U=9 THEN 725
560 IF U=10 THEN 740
565 IF U=11 THEN 755
570 IF U=12 THEN 770
575 IF U=13 THEN 785
580 IF U=14 THEN 800
585 IF U=15 THEN 815
590 IF U=16 THEN 830
595 IF U=17 THEN 845
600 IF U=18 THEN 860
605 LET Q=920
610 LET S=1570
615 GO TO190
620 LET Q=1570
625 LET S=2245
630 GO TO 190
635 LET Q=2245
640 LET S=2920
645 GO TO 190
650 LET Q=2920
655  LET S=3470
660 GO TO 190
665 LET Q=3470
670 LET S=3870
675 GO TO 190
680 LET Q=3870
685 LET S=4130
690 GO TO 190
695 LETQ=4130
700 LET S=4300
705 GO TO 190
710 LET Q=4300
715 LETS=4415
720  GO TO 190
725 LET Q=4415
730 LET S=4505
735 GO TO 190
740 LET Q=4505
745 LETS=4570
750 GO TO 190
755 LET Q=4570
760 LET S=4620
765 GOTO 190
770 LET Q=4620
775 LETS=4660
780  GO TO 190
785 LETQ=4660
790 LET S=4710
795 GO TO  190
800  LET Q=4710
805 LETS=4740
810 GO TO 190
815 LET Q=4740
820 LET S=4770
825 GO TO 190
830 LET Q=4770
835 LET S=4800
840 GO TO 190
845 LET Q=4800
850 LET S=4820
855 GO TO 190
860 LET Q=4820
865 LET S=4840
870 GOTO 190
875 LET Q=0.0
880 LETS=920
885 GOTO 190
890 END

00.0 SECS  READY
```

Table C–4 Mass optimization computer program (continued)

The inputs for the program are given below. All dimensions are in inches and the field is in gauss.

Accuracy – 1, 2, or 3 . . . The desired degree of accuracy – "3" is the most accurate and "1" is the least.

z . . . . . Selected distance from the pole face to the point at which B_z (centerline axial field) is to be calculated.

B_{z_o} . . . . . Selected design value of B_z.

R_i . . . . . Selected inner radius of annular magnet.

R_o . . . . . Initial estimate of outside radius of minimum mass annular magnet.

ΔR_o. . . . . Initial increment by which R_o is varied in the iteration scheme.

L. . . . . Initial estimate of length of minimum mass annular magnet.

ΔL. . . . . Initial increment by which L is varied in the iteration.

The analysis then proceeds as follows:

(1) Choose values for B_z, z and R_i. These chosen values will be called B_{z_o}, z_o, and R_{i_o}.
(2) Choose a value for L.
(3) Find the value of R_o which satisfies Eq. (C–5) for $B_z = B_{z_o}$. This step usually requires an iteration due to the functional form of Eq. (C–5) and (C–6).
(4) Calculate M_p.
(5) Choose a new value of L.
(6) Repeat steps 3 through 5 until M_p passes through a minimum value.

Figure C–14 is a plot of L versus R_o for $B_z = B_{z_o}$. This graph is not actually used in the program and is only included here to clarify the procedure. The input values of R_o and L must be chosen to be in the shaded region of Fig. C–14 and ΔL must be small enough that L is not taken below L^* on the first iteration. This limitation on ΔL is caused by the fact that the $B_z = B_{z_o}$ curve is very nearly parallel to the R_o axis for values of L less than L^* which causes the iteration time to become indefinitely long.

The following example illustrates the use of the computer program. All user inputs are underlined in Table C–5. Upon starting the run sequence of the program, a brief summary of the program's purpose is stated. The accuracy to which results are desired is then requested. When this information has been supplied, values of z, B_{z_o}, R_i, R_o, ΔR_o, L, and ΔL are requested by the computer. z, B_{z_o}, and R_i are, of course, design parameters, i.e., they are fixed, and values of R_o and L are to be found. In Table C–5 the first estimate values produced the error message that L was below the minimum mass point. In the second estimate L was increased, but apparently the initial estimate of R_o was too large. In the third estimate R_o is

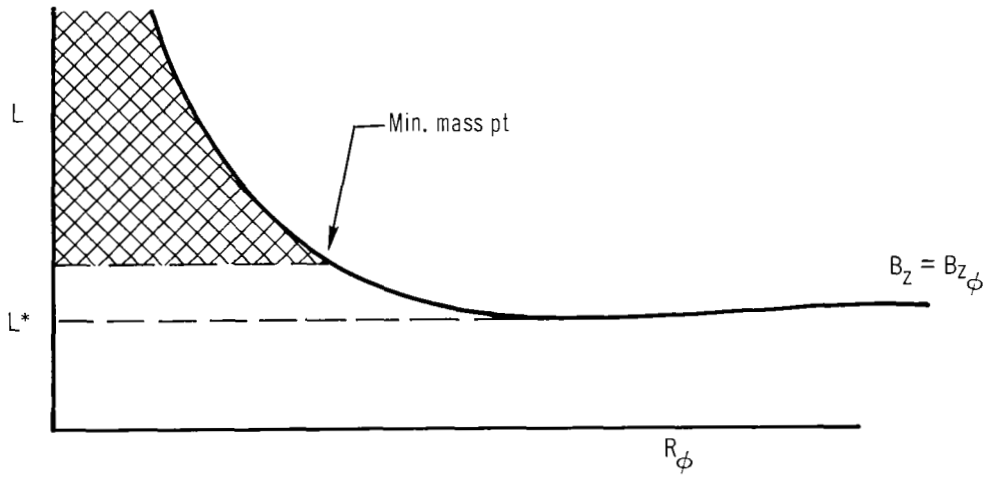

Fig. C–14 Magnet length vs outer diameter for constant B_L, R_i and z

```
THIS PROGRAM DETERMINES THE GEOMETRY FOR A FIXED ID ANNULAR
MAGNET OF MINIMUM MASS, GIVEN THE VALUES OF Z, BZØ, RI, RØ,
DELTA RØ, L, AND DELTA L, RESPECTIVELY.

WHAT ACCURACY IS DESIRED--1, 2, OR 3 ? 1

INPUT VALUES OF Z, BZØ, RI, RØ, DELTA RØ, L, AND
DELTA L, RESPECTIVELY.

 ? 1,1000,.75,2,.1,5,1 <------- 1st Estimate

Z= 1 BZØ= 1000 RI= .75
L IS BELOW MIN MASS POINT

 ? 1,1000,.75,2,.1,6,1 <------- 2nd Estimate

Z= 1 BZØ= 1000 RI= .75
RØ IS TO LARGE

 ? 1,1000,.75,1,.1,6,1 <------- 3rd Estimate

Z= 1 BZØ= 1000 RI= .75
DELTA L IS TO LARGE, OR L IS BELOW MIN MASS POINT

 ? 1,1000,.75,1,.1,6,.2 <------- 4th Estimate

Z= 1 BZØ= 1000 RI= .75
MIN MASS(LBS)= 7.95739
L(IN)= 5.98
R(IN)= 1.47
B(GAUSS)= 1000.63

 ? S
   07.0 SECS  READY

THIS PROGRAM DETERMINES THE GEOMETRY FOR A FIXED ID ANNULAR
MAGNET OF MINIMUM MASS, GIVEN THE VALUES OF Z, BZØ, RI, RØ,
DELTA RØ, L, AND DELTA L, RESPECTIVELY.

WHAT ACCURACY IS DESIRED--1, 2, OR 3 ? 3

INPUT VALUES OF Z, BZØ, RI, RØ, DELTA RØ, L, AND
DELTA L, RESPECTIVELY.

 ? 1,1000,.75,1,.1,6,.2

Z= 1 BZØ= 1000 RI= .75
MIN MASS(LBS)= 7.93472
L(IN)= 5.92
R(IN)= 1.47394
B(GAUSS)= 1000.

 ? S
   04.7 SECS  READY
```

Results

Table C–5 Sample readout for mass optimization computer program

decreased, but the error message indicates the ΔL was chosen too large. The fourth estimate gives results to the accuracy requested (in this case "1", the least accurate). Greater accuracy may be obtained by changing the "1" to a "3". To do this it is necessary to reinitiate the run sequence. The initial estimates of R_0, L, ΔR_0, and ΔL can be taken from the results of the less accurate calculation.

Magnet study conclusions

In summary, it is clear that the work is far from complete and the results obtained should be considered tentative until checked with further experimental measurements. The results to date are summarized below.

1. A computer program has been devised which will calculate the minimum mass magnet for a given centerline field value and location once an expression for the field distribution is available.
2. Design curves for minimum mass magnets using the uniform magnetization field expression have been constructed.
3. The uniform magnetization calculations over-predict the field of bar magnets and under-predict the field of annular magnets.
4. A calculational procedure which accounts for leakage effects has been devised which when used with an empirical M/H curve (Fig. C–13) predicts the field distribution of thirteen (13) Alnico–5 annular magnets with fair accuracy. Additional measurements are required to further check the validity of this procedure.
5. The above procedure does not apply to bar magnets and implies that a separate M/H curve would be required for bar magnets.

Appendix D
500-hour lifetest data

Table D–1 Test data for 500 hour lifetest

Time (hr)	Current (amps)	Voltage (volts)	m (g/sec)	Thrust (g)	Power (kW)	I_{sp} (sec)	T/P (g/kW)	η (%)	B_z (tesla)	Input magnet power (kW)	Output magnet power (kW) (jacket)	Output magnet power (kW) (coil)	Heat to magnet (kW)	Background pressure (10^{-3} Torr)	Surface temperature Face (°K)	Surface temperature Outer diameter (°K)
0	0	0	0		0				0.14	3.7994	0.0580	3.4515	−0.2899	6		
1	320	63.7	0.03		20.4				0.14	3.7994	0.1077	3.9825	0.2908	10	1162	1186
2	430	54.0	0.03		23.2				0.14	3.7994	0.1162	4.1152	0.4320	10	1186	1261
2.5	520	52.0	0.03		27.0				0.14	3.7994	0.1346	3.9825	0.3177	10	1236	1281
3	560	49.2	0.03		27.6				0.14	3.7994	0.1346	4.2480	0.5832	10	1357	1301
4	560	47.0	0.03	53	26.3	1767	2.01	17.11	0.14	3.7994	0.1298	4.2480	0.5784	10	1226	1321
5	560	56.4	0.03		31.6				0.14	3.7994	0.1346	4.2480	0.5832	10	1321	1296
6	560	50.5	0.03		28.3				0.14	3.7994	0.1358	4.1522	0.4886	10	1276	1296
7	570	54.7	0.03		30.6				0.14	3.7994	0.1394	4.2116	0.5516	9	1265	1301
8	560	54.0	0.03		30.2				0.14	3.7994	0.1334	4.1872	0.5212	8.8	1276	1301
9	560	52.0	0.03		29.1				0.14	3.7994	0.1381	4.0181	0.3568	8.7	1246	1291
10	560	63.9	0.03		35.8				0.14	3.7994	0.1243	4.0181	0.3430	8.6	1265	1321
11	560	63.5	0.03		35.6				0.14	3.7994	0.1193	4.0181	0.3380	8.8	1265	1316
12	560	62.4	0.03		34.9				0.14	3.7994	0.1247	4.0521	0.3774	8.8	1270	1316
13	560	61.7	0.03		34.6				0.14	3.7994	0.1087	4.2519	0.5612	8.9	1260	1316
14	560	61.1	0.03		34.2				0.14	3.7994	0.1346	4.0521	0.3873	8.9	1255	1316
15	560	59.9	0.03		33.5				0.14	3.7994	0.1331	4.1872	0.5209	8.9	1255	1311
16	565	59.1	0.03		33.1				0.1406	3.8997	0.1267	4.3223	0.5499	8.9	1246	1311
17	560	58.6	0.03		32.8				0.1402	3.8430	0.1285	4.2519	0.5374	8.8	1246	1306
18	560	57.0	0.03		31.9				0.1402	3.8430	0.1267	4.1872	0.4709	8.8	1236	1301
19	560	57.5	0.03		32.2				0.1406	3.8674	0.1267	4.1872	0.4465	8.9	1236	1301
20	560	59.3	0.03		33.2				0.1400	3.7837	0.1247	4.2519	0.5929	8.8	1251	1306
21	560	60.5	0.03		33.9				0.1392	3.7200	0.1263	4.1148	0.5211	8.9	1255	1306
22	560	60.2	0.03		33.7				0.1392	3.6890	0.1304	4.1148	0.5562	8.8	1251	1306
23	560	61.6	0.03		34.5				0.1385	3.6108	0.1306	4.0521	0.5719	9.0	1255	1306
24	560	61.7	0.03		34.6				0.1400	3.7994	0.1552	4.1872	0.5430	9.0	1255	1311
25	560	61.7	0.03		34.6				0.1400	3.2994	0.1524	4.3223	0.6753	9.0	1255	1306
26	560	61.9	0.03		34.7				0.1400	3.7994	0.1630	4.3223	0.6859	9.0	1251	1311
27	560	62.1	0.03		34.8				0.1400	3.7984	0.1524	4.2860	0.6390	9.0	1255	1311
28	560	62.2	0.03		34.8				0.1400	3.7994	0.1429	4.1872	0.5307	9.0	1251	1306
29	560	54.7	0.03		30.6				0.1107	2.1840	0.1111	2.7014	0.6285	9.0	1214	1276
30	560	54.8	0.03		30.7				0.1120	2.2599	0.1155	2.8367	0.6923	9.0	1214	1276
31	560	55.7	0.03		31.2				0.1137	2.3341	0.1121	2.8365	0.6145	9.0	1226	1281
32	560	55.6	0.03		31.1				0.1148	2.3750	0.1155	2.8367	0.5772	8.7	1221	1281
33	560	55.3	0.03		31.0				0.1128	2.3030	0.1121	2.8367	0.6458	8.7	1221	1281
34	560	56.2	0.03		31.5				0.1120	2.2599	0.1123	2.8805	0.7329	8.7	1226	1286
35	560	56.4	0.03		31.6				0.1128	2.3030	0.1161	2.7016	0.5147	8.7	1231	1291
36	560	56.2	0.03		31.5				0.1128	2.3030	0.1089	2.7433	0.5492	8.7	1236	1291
37	560	56.4	0.03		31.6				0.1128	2.3030	0.1191	2.7016	0.5177	8.6	1236	1291
38	560	55.8	0.03		31.2				0.1120	2.2599	0.1196	2.7016	0.5613	8.6	1231	1291
39	560	55.4	0.03		31.4				0.1107	2.2080	0.1121	2.5665	0.4706	8.6	1231	1291
40	570	56.8	0.03		31.8				0.1141	2.3312	0.0997	2.8367	0.6052	8.6	1236	1296
41	560	55.0	0.03		30.8				0.1115	2.2506	0.0794	2.7016	0.5304	8.6	1231	1291
42	565	56.2	0.03		31.5				0.1128	2.3030	0.0747	2.7016	0.4733	8.6	1231	1296
43	560	56.0	0.03		31.4				0.1128	2.2785	0.0847	2.7016	0.5078	8.6	1231	1291
44	560	55.8	0.03		31.2				0.1120	2.2599	0.0715	2.7016	0.5132	8.6	1246	1311
45	560	56.5	0.03		31.6				0.1128	2.2785	0.0732	2.7016	0.4963	8.6	1251	1306
46	560	56.0	0.03		31.4				0.1107	2.2080	0.0770	2.7016	0.5706	8.6	1246	1306
47	560	56.2	0.03		31.5				0.1107	2.2080	0.0924	2.7016	0.5860	8.8	1246	1301

Table D–1 Test data for 500 hour lifetest (continued)

Time (hr)	Current (amps)	Voltage (volts)	m (g/sec)	Thrust (g)	Power (kW)	I_{sp} (sec)	T/P (g/kW)	η (%)	B_z (tesla)	Input magnet power (kW)	Output magnet power (kW) (jacket)	Output magnet power (kW) (coil)	Heat to magnet (kW)	Background pressure (10^{-3} Torr)	Surface temperature Face (°K)	Surface temperature Outer diameter (°K)
48	560	55.6	0.03		31.1				0.1086	2.0844	0.0814	2.2385	0.2355	8.8	1255	1306
49	560	55.7	0.03		31.2				0.1090	2.1122	0.6814	2.2385	0.2077	8.8	1275	1317
50	560	55.3	0.03		31.0				0.1074	2.0416	0.0799	2.3629	0.4012	8.8	1275	1317
51	560	55.6	0.03		31.1				0.1090	2.1122	0.6772	2.3629	0.3279	8.8	1275	1322
52	560	56.1	0.03	54.0	31.4	1600	1.72	14.90	0.1086	2.0868	0.6773	2.2385	0.2290	8.7	1270	1311
53	560	55.8	0.03		31.2				0.1082	2.0709	0.0771	2.2385	0.2247	8.7	1270	1317
54	560	55.9	0.03		31.3				0.1086	2.0845	0.0843	2.3394	0.3392	8.8	1270	1317
55	560	56.2	0.03		31.5				0.1107	2.1720	0.0672	2.4626	0.3578	8.8	1301	1321
56	560	56.7	0.03		31.8				0.1116	2.2264	0.0814	2.4043	0.2593	8.6	1306	1321
57	560	56.7	0.03		31.8				0.1107	2.1840	0.0744	2.5309	0.4263	8.6	1291	1316
58	560	56.5	0.03		31.6				0.1107	2.1720	0.0770	2.4043	0.3093	8.7	1316	1316
59	560	57.2	0.03		32.0				0.1129	2.2785	0.0873	2.4043	0.2131	8.6	1321	1311
60	560	57.3	0.03		32.1				0.1107	2.1960	0.1029	2.4872	0.3941	8.6	1326	1316
61	560	57.8	0.03		32.4				0.1116	2.2264	0.1032	2.5438	0.4206	8.8	1341	1306
62	560	58.3	0.03		32.6				0.1129	2.2765	0.0842	2.3683	0.1740	8.8	1331	1271
63	560	50.7	0.03		28.4				0.1414	3.8478	0.1089	3.9875	0.2486	8.7	1261	1162
64	560	50.6	0.03		28.3				0.1414	3.8796	0.1019	3.9791	0.2014	8.7	1261	1162
65	560	51.0	0.03		28.6				0.1423	3.9360	0.1046	4.0447	0.2133	8.6	1251	1162
66	555	50.8	0.03		28.4				0.1342	3.7440	0.0953	3.8634	0.2147	8.7	1246	1167
67	560	50.6	0.03		28.3				0.1404	3.8430	0.0972	3.8589	0.1135	8.7	1256	1186
68	560	50.7	0.03		28.4				0.1423	3.9360	0.0972	3.9215	0.0827	8.7	1251	1210
69	565	52.0	0.03		29.1				0.1423	3.9680	0.0424	3.9215	0.0454	8.7	1240	1230
70	565	53.0	0.03		28.7				0.1420	3.8308	0.1016	3.9215	0.1923	8.8	1251	1240
71	560	52.7	0.03		29.5				0.1354	3.5334	0.0871	3.3444	0.1019	8.8	1256	1220
72	560	53.3	0.03		30.0				0.1400	3.7994	0.0983	3.8189	0.1170	8.8	1251	1240
73	560	53.8	0.03		35.1				0.1400	3.7994	0.0913	3,8589	0.2248	8.8	1256	1230
74	560	53.7	0.03		30.1				0.1400	3.7994	0.0983	3.8589	0.1578	8.8	1261	1230
75	560	54.2	0.03		30.4				0.1400	3.7994	0.0913	3.8589	0.2248	8.8	1276	1230
76	560	54.5	0.03		30.5				0.1400	3.7994	0.0451	3.8584	0.1546	8.8	1266	1230
77	560	54.6	0.03		30.6				0.1400	3.7994	0.0883	3.8589	0.1478	8.8	1266	1230
78	560	54.2	0.03		30.4				0.1400	3.7994	0.0451	3.8276	0.1233	8.8	1271	1235
79	560	54.0	0.03		30.2				0.1400	3.7994	0.0870	3.9215	0.2091	8.8	1276	1230
80	560	53.8	0.03		30.1				0.1385	3.7200	0.0919	3.6601	0.0320	8.7	1281	1230
81	560	53.6	0.03		30.1				0.1400	3.7994	0.0985	3.7908	0.0899	8.7	1275	1235
82	560	53.4	0.03		29.9				0.1400	3.7994	0.1040	3.7605	0.0651	8.7	1276	1235
83	560	53.2	0.03		29.8				0.1400	3.1994	0.1074	3.7303	0.0383	8.7	1281	1240
84	560	53.9	0.03		30.2				0.1400	3.7994	0.1018	3.7303	0.0727	8.7	1286	1235
85	560	56.3	0.03		31.5				0.1400	3.7994	0.1054	3.7605	0.0665	8.8	1291	1235
86	560	55.2	0.03		30.9				0.1268	2.9960	0.0885	3.1636	0.2561	8.7	1291	1196
87	560	54.6	0.03		30.6				0.1268	2.9966	0.0961	3.2157	0.3158	8.7	1286	1210
88	560	54.9	0.03		30.7				0.1268	2.9960	0.0961	3.3444	0.4445	8.6	1286	1210
89	560	54.6	0.03		30.6				0.1268	2.9960	0.0924	3.3444	0.4408	8.6	1286	1215
90	560	55.4	0.03		31.0				0.1268	3.0240	0.0924	3.2157	0.2841	8.8	1281	1220
91	560	55.0	0.03		30.8				0.1229	2.9080	0.0833	3.2443	0.5196	8.8	1301	1206
92	560	54.8	0.03		30.7				0.1250	2.8738	0.0905	3.1636	0.3803	8.8	1301	1201
93	560	54.8	0.03		30.7				0.1224	2.8080	0.0848	3.1443	0.4211	8.8	1306	1201
94	560	54.5	0.03		30.5				0.1190	2.5740	0.0848	2.6574	0.1682	8.8	1331	1152
95	560	54.5	0.03		30.5				0.1190	2.5610	0.0775	2.7889	0.3004	8.8	1341	1137
96	560	54.9	0.03		30.7				0.1157	2.4318	0.0780	2.7012	0.3474	8.8	1351	1122

Table D–1 Test data for 500 hour lifetest (continued)

Time (hr)	Current (amps)	Voltage (volts)	m (g/sec)	Thrust (g)	Power (kW)	I_{sp} (sec)	T/P (g/kW)	η (%)	B_z (tesla)	Input magnet power (kW)	Output magnet power (kW) (jacket)	Output magnet power (kW) (coil)	Heat to magnet (kW)	Background pressure (10^{-3} Torr)	Surface temperature Face (°K)	Surface temperature Outer diameter (°K)
97	560	54.8	0.03		30.7				0.1148	2.4000	0.0826	2.7012	0.3838	8.8	1351	1127
98	560	54.8	0.03		30.7				0.1148	2.4000	0.0809	2.6226	0.3035	8.8	1326	1167
99	560	53.7	0.03		30.1				0.1107	2.2032	0.0792	2.5517	0.4277	8.8	1356	1147
100	560	54.1	0.03	57	30.3	1900	1.88	17.19	0.1107	2.2032	0.0809	2.5517	0.4244	8.8	1341	1147
101	560	53.8	0.03		30.1				0.1116	2.2385	0.0841	2.5517	0.3973	8.8	1372	1107
102	560	53.7	0.03		30.1				0.1116	2.2458	0.0792	2.5309	0.3643	8.7	1346	1167
103	560	53.3	0.03		29.8				0.1107	2.2080	0.0817	2.5517	0.4254	8.7	1346	1167
104	560	53.0	0.03		29.7				0.1107	2.1960	0.0867	2.4440	0.3347	8.6	1356	1162
105	560	53.2	0.03		29.8				0.1107	2.1960	0.0852	2.4638	0.3530	8.6	1356	1167
106	560	52.7	0.03		29.5				0.1098	2.1539	0.0848	2.4241	0.3550	8.6	1372	1157
107	560	52.8	0.03		29.6				0.1107	2.2080	0.0502	2.4043	0.2765	8.7	1367	1167
108	560	52.8	0.03		29.6				0.1120	2.2599	0.0867	2.4440	0.2708	8.7	1356	1177
109	560	52.3	0.03		29.3				0.1107	2.2080	0.0867	2.4638	0.3425	8.7	1377	1177
110	560	53.2	0.03		29.8				0.1120	2.2599	0.0867	2.4628	0.2906	8.7	1367	1187
111	560	53.5	0.03		30.0				0.1128	2.3030	0.0867	2.4638	0.2475	8.6	1362	1196
112	560	53.2	0.03		29.8				0.1107	2.2080	0.0734	2.5590	0.4244	8.6	1356	1196
113	560	52.9	0.03		29.6				0.1107	2.2080	0.0654	2.5871	0.4445	8.6	1356	1191
114	560	53.3	0.03		29.4				0.1107	2.1840	0.0685	2.4043	0.2888	8.6	1392	1142
115	560	53.5	0.03		30.0				0.1107	2.2080	0.0744	2.5309	0.3973	8.7	1382	1157
116	560	53.4	0.03		29.9				0.1107	2.2080	0.0704	2.5871	0.4495	8.7	1367	1162
117	560	53.4	0.03		29.9				0.1107	2.2080	0.0734	2.6012	0.4666	8.8	1367	1172
118	560	53.8	0.03		30.1				0.1107	2.2080	0.0954	2.6726	0.5600	8.6	1377	1167
119	560	53.7	0.03		30.1				0.1148	2.3875	0.0634	2.7136	0.3895	8.8	1372	1177
120	560	54.7	0.03		30.6				0.1148	2.4000	0.0713	2.8341	0.5054	8.8	1377	1186
121	560	54.5	0.03		30.5				0.1132	2.3173	0.0654	2.6879	0.4360	8.8	1382	1162
122	560	53.1	0.03		29.7				0.1094	2.0975	0.0833	2.4436	0.4294	8.8	1407	1142
123	560	54.9	0.03		30.7				0.1128	2.3153	0.0730	2.5658	0.3235	8.8	1392	1177
124	560	53.8	0.03		30.1				0.1099	2.1420	0.0653	2.4436	0.3669	8.8	1407	1167
125	560	53.2	0.03		29.8				0.1073	2.0416	0.0553	2.4227	0.4364	8.8	1412	1147
126	560	53.4	0.03		29.9				0.1108	2.2080	0.0769	2.4436	0.3125	8.8	1407	1162
127	560	53.7	0.03		30.1				0.1108	2.2128	0.0565	2.4872	0.3309	8.8	1443	1142
128	560	53.9	0.03		30.2				0.1116	2.2506	0.0848	2.5309	0.3651	8.9	1443	1132
129	560	53.5	0.03		30.0				0.1116	2.2506	0.0795	2.5309	0.3598	8.9	1443	1152
130	560	53.5	0.03		30.0				0.1108	2.1840	0.0759	2.4872	0.3791	8.8	1427	1167
131	560	54.3	0.03		30.1				0.1116	2.2506	0.0759	2.5309	0.3562	8.9	1417	1181
132	560	54.3	0.03		30.4				0.1116	2.2506	0.0777	2.5638	0.3909	8.9	1412	1181
133	560	54.2	0.03		30.4				0.1116	2.2506	0.0795	2.5081	0.3370	9.0	1417	1201
134	560	54.4	0.03		30.5				0.1128	2.3030	0.0769	2.4645	0.2384	8.8	1417	1210
135	560	54.3	0.03		30.4				0.1128	2.3030	0.0773	2.6116	0.3859	8.8	1402	1215
136	560	54.3	0.03		30.4				0.1148	2.4000	0.0734	2.7359	0.4093	8.8	1387	1235
137	560	54.6	0.03		30.6				0.1148	2.4000	0.0773	2.7839	0.4612	8.8	1397	1230
138	560	54.7	0.03		30.6				0.1148	2.3750	0.0693	2.6116	0.3059	8.8	1407	1215
139	560	55.2	0.03		30.9				0.1148	2.3750	0.0618	2.6807	0.3675	8.8	1402	1201
140	560	55.2	0.03		30.9				0.1128	2.3030	0.0654	2.5658	0.3282	8.8	1402	1215
141	560	55.1	0.03		30.9				0.1128	2.3030	0.0654	2.6207	0.3831	8.8	1402	1215
142	560	55.6	0.03		31.1				0.1148	2.3750	0.0655	2.6116	0.3021	8.8	1397	1220
143	560	55.4	0.03		31.0				0.1128	2.3030	0.0655	2.5563	0.3188	8.8	1412	1201

Table D–1 Test data for 500 hour lifetest (continued)

Time (hr)	Current (amps)	Voltage (volts)	m (g/sec)	Thrust (g)	Power (kW)	I_{sp} (sec)	T/P (g/kW)	η (%)	B_z (tesla)	Input magnet power (kW)	Output magnet power (kW) (jacket)	Output magnet power (kW) (coil)	Heat to magnet (kW)	Background pressure (10^{-3} Torr)	Surface temperature Face (°K)	Surface temperature Outer diameter (°K)
144	560	54.7	0.03		30.6				0.1112	2.2220	0.0324	2.6114	0.4218	8.8	1433	1191
145	560	54.5	0.03		30.5				0.1116	2.2506	0.0815	2.6114	0.4423	8.9	1417	1215
146	560	54.2	0.03		30.4				0.1116	2.2506	0.0785	2.5876	0.4155	8.9	1412	1220
147	560	54.4	0.03		30.5				0.1128	2.3030	0.0711	2.6114	0.3795	8.7	1402	1230
148	560	53.9	0.03		30.2				0.1168	2.2080	0.0679	2.4870	0.3469	8.7	1412	1230
149	560	54.0	0.03		30.2				0.1108	2.2032	0.0680	2.4870	0.3518	8.7	1417	1230
150	560	53.4	0.03	56.5	29.9	1883	1.89	17.12	0.1108	2.1840	0.0791	2.4870	0.3821	8.8	1422	1230
151	560	53.1	0.03		29.7				0.1112	2.1931	0.0795	2.4435	0.3299	8.8	1402	1261
152	560	54.3	0.03		30.4				0.1120	2.2599	0.0918	2.5010	0.3329	8.7	1372	1261
153	560	55.1	0.03		30.9				0.1108	2.1840	0.0944	2.5010	0.4114	8.7	1433	1225
154	560	55.2	0.03		30.9				0.1108	2.1840	0.0851	2.4435	0.3446	8.7	1433	1220
155	560	55.7	0.03		31.2				0.1120	2.2599	0.0904	2.4435	0.2740	8.9	1427	1230
156	560	55.7	0.03		31.2				0.1120	2.2599	0.0851	2.4870	0.3122	9.0	1412	1230
157	560	55.7	0.03		31.2				0.1128	2.3030	0.0904	2.4870	0.2744	8.9	1412	1235
158	560	55.4	0.03		31.0				0.1120	2.2599	0.0870	2.4435	0.2706	8.9	1412	1246
159	560	55.5	0.03		31.1				0.1120	2.2599	0.0870	2.4870	0.3141	9.0	1417	1240
160	560	55.9	0.03		31.3				0.1128	2.3153	0.0810	2.6392	0.4049	8.5	1443	1256
161	560	56.0	0.03		31.4				0.1108	2.2080	0.0845	2.5425	0.4190	9.0	1433	1220
162	560	55.7	0.03		31.2				0.1108	2.2080	0.0815	2.4870	0.3605	8.8	1427	1225
163	560	55.9	0.03		31.3				0.1108	2.2080	0.0784	2.4870	0.3574	9.0	1427	1225
164	560	56.1	0.03		31.4				0.1120	2.2599	0.0740	2.5658	0.3799	9.0	1427	1240
165	560	55.8	0.03		31.2				0.1116	2.2385	0.0750	2.5115	0.3480	9.0	1422	1246
166	560	55.7	0.03		31.2				0.1120	2.1960	0.0758	2.5449	0.4247	9.0	1433	1230
167	560	54.4	0.03		31.0				0.1120	2.1720	0.0616	2.5449	0.4345	8.8	1427	1240
168	560	55.8	0.03		31.2				0.1108	2.2080	0.0811	2.5081	0.3842	8.8	1402	1251
169	560	54.8	0.03		30.7				0.1108	2.1840	0.0704	2.5081	0.3945	8.8	1417	1246
170	560	55.6	0.03		31.1				0.1108	2.1720	0.0635	2.5377	0.4792	8.8	1417	1246
171	560	55.6	0.03		31.1				0.1112	2.2080	0.0653	2.4645	0.3218	8.8	1417	1251
172	560	56.1	0.03		31.4				0.1128	2.3030	0.0811	2.4872	0.2683	8.8	1407	1261
173	560	55.8	0.03		31.2				0.1108	2.2152	0.1056	2.5000	0.2904	8.8	1422	1256
174	560	56.4	0.03		31.6				0.1128	2.3030	0.0111	2.5115	0.2796	8.8	1412	1266
175	560	56.3	0.03		31.5				0.1120	2.2599	0.0741	2.6669	0.4811	8.8	1427	1271
176	560	55.6	0.03		31.1				0.1116	2.2264	0.0853	2.4872	0.3461	8.8	1427	1261
177	560	55.5	0.03		31.1				0.1108	2.1960	0.0734	2.4645	0.3419	8.8	1427	1261
178	560	55.1	0.03		30.9				0.1099	2.1182	0.0711	2.4872	0.4401	8.8	1438	1261
179	560	55.5	0.03		31.1				0.1108	2.2080	0.0654	2.3214	0.1788	8.8	1422	1271
180	560	55.5	0.03		31.1				0.1108	2.2080	0.0870	2.4208	0.2998	8.7	1427	1271
181	560	55.4	0.03		31.0				0.1108	2.2080	0.0730	2.4436	0.3086	8.7	1407	1281
182	560	55.5	0.03		31.1				0.1108	2.2080	0.0654	2.4208	0.2782	8.7	1407	1276
183	560	54.7	0.03		30.6				0.1099	2.1420	0.0678	2.4436	0.3694	8.7	1427	1266
184	560	55.5	0.03		31.1				0.1108	2.1840	0.0737	2.4436	0.3333	8.4	1422	1271
185	560	55.2	0.03		30.9				0.1108	2.1840	0.0682	2.4872	0.3714	8.4	1433	1266
186	560	55.6	0.03		31.1				0.1108	2.1840	0.0578	2.5309	0.4047	8.4	1448	1266
187	560	56.2	0.03		31.5				0.1108	2.1960	0.0664	2.5563	0.4267	8.4	1427	1281
188	560	56.9	0.03		31.9				0.1108	2.2080	0.0696	2.4872	0.3488	8.5	1417	1281
189	560	56.0	0.03		31.4				0.1108	2.1960	0.0729	2.4872	0.3641	8.5	1427	1276
190	560	55.8	0.03		31.2				0.1108	2.1600	0.0664	2.4436	0.3500	8.5	1443	1266
191	560	56.2	0.03		31.5				0.1108	2.1840	0.0761	2.4436	0.3357	8.4	1427	1271

Table D–1 Test data for 500 hour lifetest (continued)

Time (hr)	Current (amps)	Voltage (volts)	m (g/sec)	Thrust (g)	Power (kw)	I_{sp} (sec)	T/P (g/kW)	η (%)	B_z (tesla)	Input magnet power (kW)	Output magnet power (kW) (jacket)	Output magnet power (kW) (coil)	Heat to magnet (kW)	Background pressure (10^{-3} Torr)	Surface temperature Face (°K)	Surface temperature Outer diameter (°K)
192	560	56.1	0.03		31.4				0.1108	2.1840	0.6012	2.4642	0.3414	8.4	1433	1271
193	560	56.7	0.03		31.8				0.1108	2.2080	0.0637	2.4532	0.3089	8.5	1422	1276
194	560	56.2	0.03		31.5				0.1099	2.1420	0.0729	2.3997	0.3306	8.5	1438	1271
195	560	56.9	0.03		31.9				0.11 6	2.2627	0.0679	2.5418	0.3470	8.5	1433	1276
196	560	56.3	0.03	53.5 / 66.2	3.15	1783 / 2207	1.70 / 2.10	145 / 22.3	0.1108	2.2008	0.0711	2.4433	0.3136	8.5	1427	1266
197	560	56.5	0.03		31.6				0.1108	2.1720	0.0646	2.6335	0.5261	8.5	1458	1266
198	560	56.1	0.03		31.4				0.1099	2.1420	0.0644	2.2998	0.2222	8.3	1463	1256
199	560	56.6	0.03		31.7				0.1108	2.1840	0.0633	2.4642	0.3435	8.2	1448	1271
200	560	56.9	0.03		31.9				0.1108	2.2080	0.0679	2.5078	0.3677	8.3	1458	1266
201	560	56.7	0.03		31.8				0.1108	2.1840	0.0501	2.5078	0.3739	8.2	1453	1266
202	560	56.3	0.03		31.5				0.1099	2.1420	0.0781	2.3214	0.2575	8.2	1456	1271
203	560	56.7	0.03		31.8				0.1116	2.2385	0.0617	2.4642	0.2874	8.4	1443	1276
204	560	56.6	0.03		31.7				0.1108	2.2080	0.0711	2.4433	0.3064	8.4	1422	1281
205	560	56.9	0.03		31.9				0.1108	2.2080	0.0644	2.4206	0.2770	8.4	1392	1286
206	560	57.2	0.03		32.0				0.1108	2.2080	0.0724	2.4433	0.3077	8.4	1422	1286
207	560	56.8	0.03		31.8				0.1108	2.2050	0.0679	2.4206	0.2805	8.4	1402	1281
208	560	57.4	0.03		32.1				0.1128	2.2785	0.0599	2.6336	0.4150	8.4	1382	1301
209	550	57.2	0.03		32.0				0.1108	2.2080	0.0761	2.5386	0.4067	8.4	1427	1281
210	560	58.1	0.03		32.5				0.1128	2.2908	0.0842	2.4433	0.2367	8.4	1387	1286
211	560	58.1	0.03		32.2				0.1108	2.1960	0.0760	2.4433	0.3233	8.4	1448	1271
212	560	58.2	0.03		32.6				0.1108	2.2080	0.0857	2.4433	0.3210	8.5	1427	1276
213	565	58.0	0.03		32.5				0.1108	2.1840	0.0791	2.4433	0.3384	8.4	1397	1276
214	560	57.0	0.03		32.0				0.1094	2.1449	0.0760	2.3997	0.3308	8.4	1427	1271
215	560	57.0	0.03		32.0				0.1094	2.1377	0.0829	2.3997	0.3449	8.5	1484	1271
215.5	560	57.9	0.03		32.4				0.1108	2.2200	0.0845	2.5200	0.3845	8.5	1372	1286
216	560	57.9	0.03		32.4				0.1099	2.1539	0.0760	2.4000	0.3221	8.5	1397	1281
217	560	57.2	0.03		32.0				0.1105	2.2080	0.0782	2.4436	0.3138	8.5	1397	1281
218	560	57.1	0.03		32.0				0.1136	2.3465	0.0668	2.5419	0.2622	8.5	1362	1281
219	560	57.6	0.03		32.3				0.1120	2.2842	0.0690	2.5200	0.3028	8.5	1372	1281
220	560	57.2	0.03		32.0				0.1108	2.2080	0.0677	2.4208	0.2805	8.5	1397	1281
221	560	57.8	0.03		32.4				0.1124	2.2936	0.0710	2.4208	0.1982	8.2	1397	1286
222	560	58.2	0.03		32.6				0.1108	2.2320	0.0707	2.4979	0.3366	8.2	1382	1276
223	560	58.7	0.03		32.9				0.1148	2.4000	0.0781	2.4872	0.1653	8.3	1362	1286
224	560	60.5	0.03		33.4				0.1120	2.2842	0.0731	2.4436	0.2325	8.3	1362	1281
225	560	59.6	0.03		33.4				0.1120	2.2842	0.0700	2.4436	0.2244	8.3	1356	1281
226	560	59.2	0.03		33.1				0.1128	2.3153	0.0693	2.4872	0.2412	8.3	1362	1281
227	560	59.4	0.03		33.3				0.1116	2.2506	0.0761	2.4436	0.2691	8.4	1372	1276
228	560	59.5	0.03		33.3				0.1148	2.4000	0.0707	2.5658	0.2365	8.4	1362	1281
229	560	60.5	0.03		33.9				0.1128	2.3275	0.0677	2.5200	0.2602	8.4	1367	1281
230	560	60.2	0.03		33.7				0.1128	2.3153	0.0761	2.5200	0.2808	8.4	1367	1281
231	560	59.7	0.03		33.4				0.1128	2.3030	0.0724	2.6400	0.4099	8.4	1367	1276
232	560	54.7	0.03		33.4				0.1148	2.3750	0.0618	2.5866	0.2734	8.4	1367	1281
233	560	60.1	0.03		33.7				0.1148	2.3875	0.0590	2.6933	0.3648	8.4	1367	1281
234	560	60.8	0.03		34.0				0.1148	2.3750	0.0739	2.5658	0.2647	8.4	1351	1281
235	560	55.8	0.03		31.2				0.1148	2.4125	0.0664	2.5200	0.1734	8.4	1351	1286
236	560	60.2	0.03		33.7				0.1148	2.3750	0.0539	2.5866	0.2655	8.4	1351	1271
237	560	54.0	0.03		33.0				0.1128	2.3030	0.0664	2.5658	0.3292	8.4	1327	1261
238	560	58.6	0.03		32.8				0.1108	2.2200	0.0760	2.4872	0.3432	8.4	1382	1256
239	560	58.3	0.03		32.6											

Table D–1 Test data for 500 hour lifetest (continued)

Time (hr)	Current (amps)	Voltage (volts)	m (g/sec)	Thrust (g)	Power (kw)	I_{sp} (sec)	T/P (g/kW)	η (%)	B_z (tesla)	Input magnet power (kW)	Output magnet power (kW) (jacket)	Output magnet power (kW) (coil)	Heat to magnet (kW)	Background pressure (10^{-3} Torr)	Surface temperature Face (°K)	Surface temperature Outer diameter (°K)
240	560	57.5	0.03		32.2				0.1140	2.2568	0.0664	2.4436	0.2532	8.4	1427	1235
241	560	57.7	0.03	54.5/69.1	32.2	1817/2303	1.63/2.07	142 /22.8	0.1078	2.0737	0.0627	2.2535	0.2425	8.4	1362	1256
242	560	57.8	0.03		32.4				0.1086	2.1150	0.0469	2.4436	0.3755	8.4	1367	1261
243	560	57.9	0.03		32.4				0.1108	2.2206	0.0734	2.4436	0.2970	8.4	1341	1261
244	560	58.4	0.03		32.7				0.1108	2.2200	0.0708	2.4979	0.3487	8.4	1336	1266
245	560	57.9	0.03		32.4				0.1108	2.2200	0.0707	2.4208	0.2715	8.4	1336	1266
246	560	59.4	0.03		33.2				0.1108	2.2200	0.0617	2.4872	0.3289	8.4	1336	1266
247	560	58.8	0.03		32.9				0.1128	2.3153	0.0573	2.5871	0.3291	8.4	1326	1271
248	560	58.5	0.03		32.8				0.1120	2.2842	0.0602	2.4872	0.2632	8.5	1331	1261
249	560	59.2	0.03		33.2				0.1116	2.2506	0.0571	2.4436	0.2501	8.6	1341	1261
250	560	59.4	0.03		33.3				0.1108	2.2080	0.0633	2.4872	0.3425	8.6	1356	1266
251	560	60.2	0.03		33.7				0.1120	2.2599	0.0664	2.4872	0.2937	8.6	1346	1271
252	560	60.4	0.03		33.8				0.1128	2.3030	0.0696	2.4872	0.2538	8.6	1336	1271
253	560	60.5	0.03		33.7				0.1136	2.3589	0.0679	2.4872	0.1962	8.6	1341	1271
254	560	59.7	0.03		33.4				0.1099	2.1539	0.0536	2.3563	0.2560	8.6	1336	1271
255	560	60.4	0.03		33.8				0.1108	2.2080	0.0711	2.4872	0.3503	8.6	1346	1271
256	560	60.7	0.03		33.9				0.1120	2.2721	0.0679	2.5596	0.3554	8.7	1341	1276
257	560	61.0	0.03		33.7				0.1120	2.2721	0.0332	2.5429	0.3540	8.7	1346	1266
258	560	61.3	0.03		34.3				0.1108	2.2080	0.0685	2.4872	0.3477	8.7	1367	1271
259	560	61.2	0.03		34.3				0.1108	2.2320	0.0761	2.4164	0.2605	8.8	1362	1271
260	560	61.6	0.03		34.5				0.1128	2.3030	0.0460	2.3076	0.0506	8.7	1341	1281
261	560	61.4	0.03		34.4				0.1120	2.2842	0.0484	2.6012	0.3659	8.7	1336	1286
262	560	61.3	0.03		34.3				0.1148	2.3875	0.0735	2.6392	0.3252	8.8	1341	1306
263	560	60.8	0.03		34.0				0.1148	2.4075	0.0689	2.6807	0.3421	8.8	1346	1306
264	560	60.6	0.03		33.9				0.1148	2.4000	0.0505	2.7108	0.3613	8.8	1346	1306
265	560	59.8	0.03		33.5				0.1116	2.2821	0.0432	2.6574	0.4185	8.8	1346	1301
266	560	59.6	0.03		33.4				0.1128	2.3153	0.0774	2.5871	0.3492	8.8	1346	1301
267	560	59.2	0.03		33.2				0.1125	2.3036	0.0693	2.5309	0.2972	9.0	1377	1306
268	560	59.2	0.03		33.2				0.1116	2.2603	0.0454	2.6574	0.4425	8.7	1402	1296
269	560	59.4	0.03		33.2				0.1128	2.3030	0.0437	2.5309	0.2766	8.5	1372	1301
270	560	59.3	0.03		33.2				0.1128	2.3030	0.0612	2.5080	0.2662	8.6	1362	1301
271	560	59.6	0.03		33.4				0.1136	2.3292	0.0475	2.5080	0.2263	8.6	1336	1306
272	560	59.5	0.03		33.3				0.1136	2.3292	0.0460	2.5309	0.2477	8.7	1326	1306
273	560	59.7	0.03		33.4				0.1128	2.3030	0.0460	2.4872	0.2302	8.7	1331	1306
274	560	59.0	0.03		33.0				0.1120	2.2721	0.0459	2.5309	0.3047	8.7	1336	1301
275	560	58.8	0.03		32.9				0.1120	2.2599	0.0533	2.4872	0.2906	8.6	1316	1316
276	560	59.5	0.03		33.3				0.1128	2.3030	0.0612	2.4872	0.2454	8.6	1316	1316
277	560	59.5	0.03		33.3				0.1140	2.3560	0.0556	2.6335	0.3341	8.8	1306	1306
278	560	58.9	0.03		33.0				0.1136	2.3342	0.0555	2.4872	0.2085	8.9	1296	1316
279	560	58.4	0.03		32.7				0.1136	2.3342	0.0551	2.5658	0.2867	8.7	1296	1316
280	560	58.0	0.03		32.5				0.1128	2.2785	0.0501	2.5425	0.3141	8.6	1316	1311
281	560	58.1	0.03		32.5				0.1128	2.2785	0.0668	2.6116	0.3999	8.7	1306	1301
282	560	57.5	0.03		32.2				0.1108	2.2080	0.0706	2.5839	0.4465	8.7	1301	1311
283	560	56.5	0.03		31.6				0.1108	2.1960	0.0677	2.5563	0.4260	8.7	1301	1301
284	560	56.7	0.03		31.8				0.1108	2.1960	0.0708	2.4872	0.3620	8.8	1311	1301
285	561	56.1	0.03		31.4				0.1108	2.1720	0.0678	2.3843	0.2851	8.8	1316	1296
286	563	56.3	0.03		31.5				0.1108	2.1840	0.0708	2.3629	0.2497	8.8	1306	1296
287	560	56.0	0.03		31.4				0.1104	2.1558	0.0693	2.3629	0.2764	8.8	1311	1306

Table D–1 Test data for 500 hour lifetest (continued)

Time (hr)	Current (amps)	Voltage (volts)	m (g/sec)	Thrust (g)	Power (kw)	I_{sp} (sec)	T/P (g/kW)	η (%)	B_z (tesla)	Input magnet power (kW)	Output magnet power (kW) (jacket)	Output magnet power (kW) (coil)	Heat to magnet (kW)	Background pressure (10^{-3} Torr)	Surface temperature Face (°K)	Surface temperature Outer diameter (°K)
288	560	54.9	0.03		30.7				0.1056	1.9722	0.0573	2.2383	0.3184	8.5	1326	1286
289	560	55.0	0.03		30.8				0.1051	1.9409	0.0501	2.1992	0.3084	8.5	1336	1281
290	560	57.7	0.03	52.0/62.3	32.3	1733/2077	1.61/1.93	13.42/19.27	0.1108	2.1960	0.0504	2.4452	0.2996	8.7	1326	1306
291	560	58.7	0.03		32.9				0.1116	2.2264	0.0694	2.4268	0.2638	8.8	1372	1246
292	560	60.0	0.03		33.6				0.1136	2.3342	0.0617	2.4645	0.1920	8.8	1382	1291
293	560	59.7	0.03		33.4				0.1120	2.2842	0.0572	2.5419	0.3149	8.8	1356	1301
294	560	57.8	0.03		32.4				0.1142	1.9125	0.0530	2.2385	0.3790	8.8	1407	1286
295	560	59.2	0.03		33.2				0.1104	2.1630	0.0617	2.2998	0.1985	8.8	1372	1301
296	560	59.5	0.03		33.3				0.1116	2.2264	0.0617	2.4436	0.2849	8.8	1351	1311
297	560	59.6	0.03		33.4				0.1108	2.1960	0.0652	2.3629	0.2321	8.8	1346	1316
299	560	60.0	0.03		33.6				0.1108	2.1960	0.0666	2.4872	0.3587	8.8	1341	1316
299	560	60.5	0.03		33.9				0.1120	2.2842	0.0761	2.4872	0.2791	8.8	1331	1361
300	560	61.3	0.03		34.3				0.1128	2.3030	0.0724	2.5200	1.2894	8.8	1306	1306
301	560	62.3	0.03		34.9				0.1148	2.3750	0.0745	2.4436	0.1431	8.9	1326	1326
303	560	61.8	0.03		34.6				0.1108	2.2080	0.0729	2.4645	0.3294	9.0	1321	1316
304	565	62.4	0.03		34.9				0.1128	2.2785	0.0706	2.1992	0.0087	9.0	1321	1316
305	560	62.3	0.03		34.9				0.1108	2.2080	0.0788	2.4266	0.2974	9.0	1306	1301
306	560	62.4	0.03		34.9				0.1128	2.2540	0.0761	2.4266	0.2487	9.0	1311	1316
307	560	61.9	0.03		34.7				0.1108	2.2080	0.0734	2.4533	0.3187	9.0	1316	1311
308	560	61.6	0.03		34.5				0.1128	2.2663	0.0796	2.4436	0.2569	9.0	1311	1316
309	560	60.9	0.03		34.1				0.1108	2.2080	0.0779	2.4000	0.2699	9.0	1306	1311
310	560	60.8	0.03		34.0				0.1128	2.2785	0.0768	2.5200	0.3183	9.0	1306	1311
311	560	60.0	0.03		33.6				0.1108	2.1840	0.0722	2.4087	0.2969	9.0	1291	1301
312	560	54.6	0.03		33.4				0.1108	2.1960	0.0692	2.4000	0.2732	4.0	1286	1301
313	560	59.6	0.03		33.4				0.1090	2.0957	0.0664	2.4000	0.3707	9.0	1292	1301
314	560	59.8	0.03		23.5				0.1108	2.1720	0.0692	2.4000	0.2972	8.9	1291	1301
315	560	61.3	0.03		34.3				0.1116	2.2264	0.0680	2.4666	0.3082	8.9	1296	1301
316	560	61.9	0.03		34.7				0.1112	2.2196	0.0664	2.4266	0.2734	8.9	1301	1301
317	560	62.4	0.03		34.9				0.1104	2.1510	0.0696	2.4979	0.4115	8.9	1306	1306
318	560	62.9	0.03		35.2				0.1108	2.1960	0.0696	2.4533	0.3269	8.9	1306	1296
319	560	62.9	0.03		35.2				0.1128	2.2908	0.0685	2.4881	0.2658	8.7	1301	1306
320	560	63.0	0.03		35.3				0.1116	2.2385	0.0677	2.5200	0.3492	8.8	1301	1301
321	560	62.3	0.03		34.9				0.1108	2.1960	0.0696	2.5200	0.3936	8.7	1301	1296
322	560	62.1	0.03		34.8				0.1108	2.1840	0.0653	2.5200	0.4013	8.7	1301	1296
323	560	62.8	0.03		35.2				0.1116	2.2264	0.0644	2.4533	0.2913	8.7	1306	1301
324	560	63.2	0.03		35.4				0.1120	2.2478	0.0679	2.4980	0.3181	8.9	1316	1301
325	560	63.5	0.03		35.6				0.1120	2.2478	0.0662	2.5200	0.3384	8.9	1306	1296
326	560	63.2	0.03		35.4				0.1120	2.2478	0.0616	2.4522	0.2660	8.9	1306	1296
327	560	62.9	0.03		35.6				0.1120	2.2478	0.0562	2.4522	0.2606	8.9	1306	1296
328	560	62.7	0.03		35.1				0.1128	2.3030	0.0634	2.4980	0.2584	8.9	1301	1296
329	560	62.6	0.03		35.1				0.1108	2.2080	0.0711	2.4436	0.3067	8.9	1316	1306
330	560	62.9	0.03		35.2				0.1128	2.2785	0.0707	2.4000	0.1922	8.9	1306	1296
331	560	63.1	0.03		35.3				0.1128	2.2663	0.0722	2.4000	0.2059	8.9	1316	1306
332	560	63.1	0.03		35.3				0.1120	2.2356	0.0751	2.4208	0.2603	8.9	1316	1306
333	560	63.1	0.03		35.3				0.1128	2.2663	0.0700	2.4208	0.2247	8.9	1301	1291
334	560	62.6	0.03		35.1				0.1128	2.2663	0.0747	2.4000	0.2084	9.0	1301	1296
335	560	62.0	0.03		34.7				0.1104	2.1749	0.0693	2.4319	0.3263	9.0	1296	1291

Table D–1 Test data for 500 hour lifetest (continued)

Time (hr)	Current (amps)	Voltage (volts)	m (g/sec)	Thrust (g)	Power (kw)	I_{sp} (sec)	T/P (g/kW)	η (%)	B_z (tesla)	Input magnet power (kW)	Output magnet power (kW) (jacket)	Output magnet power (kW) (coil)	Heat to magnet (kW)	Background pressure (10^{-3} Torr)	Surface temperature Face (°K)	Surface temperature Outer diameter (°K)
336	560	62.9	0.03		35.2				0.1104	2.1030	0.0776	2.3563	0.2709	9.0	2321	1291
337	560	62.3	0.03		34.9				0.1090	2.1075	0.0761	2.4000	0.3656	8.8	1321	1291
338	560	62.5	0.03		35.0				0.1086	2.0915	0.0776	2.3791	0.3652	8.8	1331	1291
339	560	63.6	0.03		35.6				0.1116	2.2385	0.0843	2.4266	0.2724	8.8	1326	1296
340	560	63.3	0.03		35.4				0.1108	2.1768	0.0761	2.3873	0.2866	8.6	1321	1291
341	560	62.2	0.03		34.8				0.1094	2.1093	0.0791	2.3696	0.3344	8.4	1316	1286
342	560	63.3	0.03		35.4				0.1104	2.1630	0.0766	2.3791	0.2927	8.5	1316	1286
343	560	63.8	0.03		35.7				0.1116	2.2264	0.0826	2.4746	0.3308	8.5	1321	1291
344	560	63.8	0.03		35.7				0.1120	2.2599	0.0795	2.4533	0.2729	8.6	1316	1291
345	560	63.8	0.03		35.7				0.1116	2.2264	0.0759	2.4319	0.2814	8.6	1316	1291
347	560	63.3	0.03		35.4				0.1099	2.1420	0.0711	2.3354	0.2645	8.6	1326	1291
348	560	63.2	0.03		35.4				0.1108	2.1720	0.0711	2.3354	0.2345	8.8	1326	1286
349	560	63.4	0.03		35.5				0.1108	2.1840	0.0711	2.3873	0.2744	8.7	1321	1286
350	560	63.5	0.03		35.6				0.1108	2.1840	0.0781	2.3354	0.2295	8.7	1326	1286
351	560	63.3	0.03		35.6				0.1116	2.2385	0.0826	2.4303	0.2744	8.6	1331	1291
352	560	63.3	0.03		35.9				0.1108	2.2080	0.0813	2.4303	0.3036	8.7	1326	1286
353	560	63.7	0.03		35.7				0.1108	2.2080	0.0751	2.3146	0.1817	8.7	1321	1286
353	560	63.3	0.03		35.4				0.1108	2.2080	0.0827	2.4000	0.2747	8.7	1326	1286
354	560	62.9	0.03		35.2				0.1108	2.1960	0.0874	2.4666	0.3580	8.7	1321	1296
355	560	63.7	0.03		35.7				0.1112	2.2220	0.0866	2.4666	0.3312	8.8	1321	1286
356	560	63.6	0.03		35.6				0.1128	2.2663	0.0873	2.4533	0.2743	8.8	1321	1286
357	560	63.8	0.03		35.7				0.1108	2.2080	0.0857	2.4000	0.2777	8.9	1331	1281
358	560	63.5	0.03		35.6				0.1108	2.2080	0.0813	2.3791	0.2524	8.9	1321	1276
359	560	63.8	0.03		35.7				0.1116	2.2506	0.0852	2.4666	0.3012	8.9	1326	1281
360	560	62.9	0.03		35.2				0.1104	2.1510	0.0770	2.3354	0.2614	8.9	1326	1281
361	560	62.8	0.03		35.2				0.1090	2.1051	0.0594	2.3563	0.3106	8.9	1326	1281
362	560	62.9	0.03		35.2				0.1108	2.1720	0.0620	2.4087	0.2987	8.8	1321	1276
363	560	63.5	0.03		35.6				0.1116	2.2506	0.0780	2.4980	0.3254	8.7	1321	1276
364	560	63.1	0.03		35.3				0.1108	2.1840	0.0804	2.4087	0.3051	8.7	1321	1281
365	560	63.0	0.03		35.3				0.1104	2.1558	0.0780	2.4303	0.3525	8.6	1321	1271
366	560	63.2	0.03		35.3				0.1108	2.1960	0.0745	2.5150	0.3935	8.6	1326	1271
367	560	63.4	0.03		35.5				0.1116	2.2506	0.0752	2.4452	0.2698	8.6	1326	1281
368	560	63.7	0.03		35.7				0.1120	2.2599	0.0815	2.3563	0.1779	8.5	1316	1276
369	560	63.5	0.03		35.6				0.1108	2.2080	0.0761	2.5041	0.3722	8.5	1316	1276
370	560	63.0	0.03		35.4				0.1108	2.1960	0.0761	2.4436	0.3237	8.7	1321	1276
372	560	62.9	0.03		35.2				0.1108	2.2080	0.0761	2.4208	0.2889	8.7	1316	1266
373	560	63.3	0.03		35.4				0.1116	2.2385	0.0833	2.4479	0.3427	8.6	1316	1276
374	560	63.3	0.03		35.5				0.1116	2.2385	0.0854	2.5658	0.4127	8.6	1316	1271
375	560	63.4	0.03		35.7				0.1128	2.3030	0.1053	2.4746	0.2769	8.7	1316	1276
376	560	63.7	0.03		35.7				0.1140	2.3436	0.0980	2.4881	0.2425	8.7	1311	1256
377	560	63.7	0.03		35.7				0.1128	2.2908	0.0956	2.4746	0.2774	8.7	1306	1271
378	560	63.3	0.03		35.4				0.1128	2.2663	0.0826	2.4872	0.3035	8.7	1316	1271
379	560	63.4	0.03		35.5				0.1128	2.2785	0.0835	2.4266	0.2316	8.8	1311	1271
380	560	63.3	0.03		35.6				0.1128	2.2785	0.0810	2.4933	0.2958	8.8	1316	1281
381	560	63.2	0.03		35.4				0.1116	2.2385	0.0669	2.4046	0.2350	8.8	1306	1271
382	560	63.4	0.03		35.5				0.1128	2.2785	0.0918	2.4533	0.2666	8.9	1321	1296
383	560	63.1	0.03		35.3				0.1108	2.1720	0.0798	2.3660	0.2738	8.8	1306	1266

Table D–1 Test data for 500 hour lifetest (continued)

Time (hr)	Current (amps)	Voltage (volts)	m (g/sec)	Thrust (g)	Power (kw)	I_{sp} (sec)	T/P (g/kW)	η (%)	B_z (tesla)	Input magnet power (kW)	Output magnet power (kW) (jacket)	Output magnet power (kW) (coil)	Heat to magnet (kW)	Background pressure (10^{-3} Torr)	Surface temperature Face (°K)	Surface temperature Outer diameter (°K)
384	560	62.5	0.03		35.0				0.1108	2.1840	0.0795	2.4046	0.3001	8.8	1311	1271
385	560	62.8	0.03		35.2				0.1099	2.1420	0.0759	2.3789	0.3128	8.8	1311	1266
386	560	63.0	0.03		35.3				0.1099	2.1420	0.0724	2.3789	0.3093	8.8	1301	1266
387	560	63.0	0.03		35.3				0.1112	2.2172	0.0769	2.4303	0.2900	8.7	1316	1276
388	560	63.1	0.03		35.3				0.1116	2.2264	0.0799	2.4560	0.3095	8.7	1306	1271
389	560	63.1	0.03		35.3				0.1108	2.1720	0.0744	2.4064	0.3088	8.7	1301	1261
390	560	63.7	0.03		35.7				0.1108	2.2080	0.0770	2.3789	0.2479	8.6	1306	1261
391	560	63.8	0.03		35.7				0.1120	2.2769	0.0810	2.4446	0.2987	8.6	1306	1261
392	560	64.1	0.03		35.9				0.1128	2.3030	0.0851	2.5460	0.3281	8.7	1306	1266
393	560	63.6	0.03		35.6				0.1116	2.2385	0.0833	2.4980	0.3428	8.7	1301	1261
394	560	63.6	0.03		35.6				0.1108	2.2080	0.0795	2.3845	0.2560	8.8	1311	1261
395	560	64.3	0.03		36.0				0.1120	2.2721	0.0795	2.5210	0.3284	8.8	1296	1281
396	560	64.1	0.03		35.9				0.1116	2.2506	0.0806	2.5210	0.3510	8.7	1301	1261
397	560	63.9	0.03		35.8				0.1128	2.3030	0.0780	2.4303	0.3053	8.7	1306	1261
398	560	64.1	0.03		35.7				0.1128	2.3030	0.0769	2.4521	0.2260	8.7	1301	1256
399	560	64.1	0.03		35.9				0.1120	2.2599	0.0773	2.3407	0.1585	8.7	1301	1256
400	560	65.0	0.03		36.4				0.1128	2.2785	0.0757	2.4026	0.1998	8.8	1301	1256
401	560	64.2	0.03		36.0				0.1128	2.2785	0.0833	2.5509	0.3557	8.9	1291	1251
402	560	64.2	0.03		36.0				0.1128	2.2785	0.0806	2.5396	0.3417	8.9	1286	1251
403	560	64.3	0.03		36.0				0.1128	2.2785	0.0873	2.5466	0.2554	8.9	1286	1246
404	560	64.5	0.03		36.1				0.1120	2.2478	0.0749	2.6091	0.4362	8.9	1286	1220
405	560	64.2	0.03		36.0				0.1128	2.2785	0.0814	2.6336	0.4365	8.9	1286	1225
406	560	64.5	0.03		36.1				0.1128	2.2785	0.0867	2.4946	0.3028	8.9	1286	1230
407	560	64.3	0.03		36.0				0.1128	2.3030	0.0759	2.4946	0.2675	9.0	1286	1225
408	560	64.2	0.03		36.0				0.1112	2.2413	0.0785	2.5171	0.3543	9.0	1286	1230
409	560	64.1	0.03		35.9				0.1108	2.2032	0.0711	2.4303	0.2982	8.8	1276	1191
410	560	64.2	0.03		36.0				0.1108	2.1960	0.0711	2.5210	0.3961	8.8	1281	1220
411	560	64.3	0.03		36.0				0.1108	2.2080	0.0714	2.4980	0.3614	8.6	1286	1240
412	560	64.4	0.03		36.1				0.1116	2.2385	0.0734	2.4980	0.3329	8.6	1286	1246
413	560	64.1	0.03		35.9				0.1116	2.2506	0.0689	2.4751	0.2934	8.6	1286	1246
414	560	63.6	0.03		35.6				0.1120	2.2599	0.0769	2.4522	0.2692	8.5	1286	1246
415	560	62.9	0.03		35.2				0.1099	2.1368	0.0761	2.3563	0.2856	8.5	1281	1235
416	560	63.5	0.03		35.6				0.1108	2.1840	0.0845	2.4000	0.3005	8.5	1281	1235
417	560	63.6	0.03		35.6				0.1108	2.1720	0.0795	2.4087	0.3162	8.6	1276	1235
418	560	62.4	0.03		34.9				0.1099	2.1420	0.0729	2.3563	0.2872	8.6	1276	1235
419	560	63.5	0.03		35.6				0.1116	2.2385	0.0759	2.4741	0.3115	8.6	1281	1235
420	560	63.8	0.03		35.7				0.1116	2.2385	0.0731	2.4741	0.3087	8.6	1281	1240
421	560	63.7	0.03		35.7				0.1128	2.2408	0.0693	2.4741	0.2526	8.7	1281	1235
422	560	63.6	0.03		35.6				0.1116	2.2385	0.0759	2.3873	0.2247	8.8	1276	1230
423	560	63.8	0.03		35.7				0.1108	2.2080	0.0759	2.4741	0.3420	8.7	1276	1215
424	560	63.5	0.03		35.6				0.1116	2.2264	0.0757	2.3039	0.1532	8.7	1276	1230
425	560	63.6	0.03		35.6				0.1108	2.2080	0.0758	3.3733	0.2411	8.6	1281	1220
426	560	62.8	0.03		35.3				0.1108	2.2080	0.0777	2.3563	0.2260	8.6	1276	1230
427	560	63.1	0.03		35.2				0.1112	2.2172	0.0833	2.2825	0.2486	8.6	1281	1230
428	560	63.5	0.03		35.6				0.1108	2.2080	0.0784	2.3825	0.2529	8.6	1281	1235
429	560	59.2	0.03		33.2				0.1128	2.2785	0.0815	2.3791	0.1821	8.6	1266	1276
430	560	61.2	0.03		34.2				0.1116	2.2264	0.0777	2.3791	0.2304	8.8	1286	1281
431	560	61.5	0.03		34.4				0.1128	2.3030	0.0697	2.4741	0.2408	8.8	1286	1271

Table D–1 Test data for 500 hour lifetest (continued)

Time (hr)	Current (amps)	Voltage (volts)	m (g/sec)	Thrust (g)	Power (kw)	I_{sp} (sec)	T/P (g/kW)	η (%)	B_z (tesla)	Input magnet power (kW)	Output magnet power (kW) (jacket)	Output magnet power (kW) (coil)	Heat to magnet (kW)	Background pressure (10^{-3} Torr)	Surface temperature Face (°K)	Surface temperature Outer diameter (°K)
432	560	61.2	0.03		34.3				0.1112	2.2172	0.0724	2.3354	0.1906	8.8	1271	1261
433	560	61.2	0.03		34.3				0.1116	2.2385	0.0759	2.3563	0.1937	8.7	1276	1256
434	560	61.0	0.03		34.2				0.1108	2.2080	0.0688	2.3563	0.2171	8.7	1271	1251
435	560	61.1	0.03		34.2				0.1108	2.2152	0.0795	2.4241	0.3384	8.7	1266	1246
436	560	60.0	0.03		33.8				0.1108	2.2080	0.0773	2.3563	0.2256	8.6	1266	1246
437	560	61.2	0.03		34.3				0.1116	2.2506	0.0704	2.4533	0.2731	8.6	1266	1246
438	560	61.0	0.03		34.1				0.1116	2.2458	0.0689	2.3791	0.2072	8.6	1266	1246
439	560	61.0	0.03		34.1				0.1108	2.2030	0.0754	2.3466	0.2145	8.5	1266	1246
440	560	60.9	0.03		34.1				0.1116	2.2385	0.0738	2.3791	0.2144	8.6	1266	1240
441	560	60.3	0.03		33.8				0.1099	2.1539	0.0645	2.2909	0.2015	8.6	1261	1230
442	560	60.2	0.03		32.7				0.1099	2.1420	0.0616	2.2503	0.1699	8.8	1256	1225
443	560	60.5	0.03		33.9				0.1099	2.1539	0.0711	2.2706	0.1878	8.8	1261	1235
444	560	60.5	0.03		33.9				0.1108	2.1840	0.0741	2.3563	0.2464	8.8	1261	1235
445	560	60.4	0.03		33.8				0.1108	2.1960	0.0711	2.2601	0.1352	8.8	1256	1230
446	560	61.0	0.03		34.2				0.1128	2.2785	0.0723	2.3845	0.1783	8.8	1261	1230
447	560	61.1	0.03		34.2				0.1128	2.2408	0.0781	2.5200	0.3073	8.9	1256	1230
448	560	60.6	0.03		33.9				0.1108	2.2080	0.0862	2.3146	0.1928	8.9	1251	1220
449	560	60.3	0.03		33.8				0.1108	2.1840	0.0781	2.3095	0.2036	8.9	1251	1215
450	560	60.2	0.03		33.7				0.1099	2.1420	0.0793	2.2123	0.1496	9.0	1251	1210
451	560	60.2	0.03		33.7				0.1099	2.1539	0.0791	2.3130	0.2382	9.0	1251	1220
452	560	60.2	0.03		33.7				0.1099	2.1420	0.0696	2.2647	0.1923	8.9	1251	1201
453	560	60.6	0.03		33.9				0.1099	2.1539	0.0740	2.3146	0.2347	8.9	1251	1201
454	560	60.0	0.03		33.6				0.1086	2.1033	0.0729	2.2337	0.2033	8.9	1240	1177
455	560	60.1	0.03		33.7				0.1099	1.9992	0.0661	2.3000	0.3669	8.7	1256	1196
456	560	60.2	0.03		33.7				0.1086	2.1150	0.0693	2.2918	0.2461	8.8	1240	1167
457	560	59.9	0.03		33.5				0.1065	2.0240	0.0598	2.1673	0.2031	8.7	1210	1142
458	560	59.9	0.03		33.5				0.1073	2.0764	0.0569	2.2709	0.2514	8.7	1230	1157
459	560	60.2	0.03		33.7				0.1108	2.1720	0.0584	2.2918	0.1782	8.6	1240	1171
460	560	60.3	0.03		33.8				0.1099	2.1658	0.0514	2.1574	0.0430	8.4	1230	1162
461	560	60.0	0.03		33.6				0.1104	2.1869	0.0405	2.3340	0.1876	8.4	1240	1162
462	560	60.4	0.03		33.8				0.1108	2.2080	0.0281	2.3427	0.1628	8.3	1230	1142
463	560	60.2	0.03		33.7				0.1094	2.1567	0.0384	2.3845	0.2662	8.4	1240	1152
464	560	61.0	0.03		34.2				0.1108	2.2080	0.2550	2.1136	0.3444	8.4	1246	1177
465	560	60.7	0.03		34.0				0.1108	2.2200	0.2518	2.1115	0.3603	8.4	1246	1152
466	560	59.8	0.03		33.5				0.1086	2.1150	0.2486	1.9917	0.3719	8.4	1220	1068
467	560	59.7	0.03		33.4				0.1099	2.1658	0.2580	2.0129	0.4109	8.5	1206	979
468	560	59.9	0.03		33.6				0.1099	2.1658	0.2185	1.9693	0.4150	8.5	1220	1098
469	560	–	0.03		–				0.1116	2.2506	0.2185	2.0897	0.3794	8.6	1225	1049
470	560	59.4	0.03		33.3				0.1108	2.2080	0.2076	2.1433	0.2723	8.5	1206	1000
471	560	59.7	0.03		33.4				0.1120	2.2842	0.1730	2.1662	0.2910	8.6	1210	891
472	560	59.3	0.03		33.2				0.1116	2.2506	0.1963	2.3631	0.0838	8.5	1220	995
473	560	59.2	0.03		33.2				0.1108	2.2320	0.1752	2.0897	0.3175	8.6	1206	995
474	560	59.4	0.03		33.3				0.1108	2.2320	0.1831	2.1695	0.2456	8.6	1191	891
475	560	59.3	0.03		33.2				0.1108	2.2320	0.1617	2.2051	0.1886	8.5	1196	842
476	560	58.5	0.03		32.8				0.1099	2.1539	0.1850	2.0903	0.2486	8.5	1152	667
477	560	59.2	0.03		33.2				0.1108	2.2080	0.1683	2.1449	0.2314	8.6	1196	868
478	560	59.4	0.03		33.3				0.1099	2.1539	0.1865	2.0912	0.2492	8.6	1181	902
479	560	59.1	0.03		33.1				0.1086	2.1150	0.1751	2.1115	0.1786	8.6	1142	713

Table D–1 Test data for 500 hour lifetest (continued)

Time (hr)	Current (amps)	Voltage (volts)	m (g/sec)	Thrust (g)	Power (kw)	I_{sp} (sec)	T/P (g/kW)	η (%)	B_z (tesla)	Input magnet power (kW)	Output magnet power (kW) (jacket)	Output magnet power (kW) (coil)	Heat to magnet (kW)	Background pressure (10^{-3} Torr)	Surface temperature Face (°K)	Surface temperature Outer diameter (°K)
480	560	58.7	0.03		32.9				0.1065	2.0355		2.3052	0.3297	8.8	1132	
481	560	54.2	0.03		33.2				0.1073	2.0648		2.4621	0.3973	8.6	1177	
482	560	59.6	0.03		33.4				0.1078	2.0784		2.4405	0.3621	8.6	1181	
483	560	60.7	0.03		34.0				0.1094	2.1496		2.5024	0.3508	8.5	1230	
484	560	60.3	0.03		33.8				0.1086	2.1197		2.4498	0.3301	8.3	1196	
485	560	60.8	0.03		34.0				0.1099	2.1848		2.4163	0.2315	8.3	1240	
486	560	61.0	0.03		34.2				0.1099	2.1848		2.5366	0.3518	8.3	1230	
487	560	61.2	0.03		34.3				0.1108	2.2080		2.5366	0.3286	8.3	1225	
488	560	61.1	0.03		34.2				0.1099	2.1658		2.5323	0.3665	8.3	1220	
489	560	61.1	0.03		34.2				0.1090	2.1240		2.6479	0.5239	8.3	1225	
490	560	61.8	0.03		34.6				0.1094	2.1150		2.4162	0.3012	8.4	1210	
491	560	61.0	0.03		34.2				0.1099	2.1777		2.5275	0.3498	8.4	1230	
492	560	61.2	0.03		34.3				0.1099	2.1658		2.4092	0.2434	8.4	1220	
493	560	61.6	0.03		34.5				0.1108	2.2080		2.4578	0.2498	8.4	1251	
494	560	62.2	0.03		34.8				0.1116	2.2748		2.5875	0.3127	8.4	1261	
495	560	61.8	0.03		34.6				0.1108	2.2320		2.5200	0.2889	8.4	1246	
496	560	62.2	0.03		34.8				0.1108	2.2320		2.4550	0.7230	8.5	1251	
497	560	61.6	0.03		34.5				0.1099	2.1896		2.5772	0.3876	8.7	1246	
498	560	61.8	0.03		34.6				0.1108	2.2200		2.4864	0.2664	8.9	1230	
499	560	61.3	0.03		34.3				0.1108	2.2080		2.5122	0.3042	8.6	1220	
500	560	61.4	0.03		34.4				0.1108	2.2080		2.5126	0.3046	8.5	1235	
501	560	61.6	0.03		34.5				0.1108	2.2320		2.6250	0.3930	8.6	1230	
502	560	61.0	0.03		34.2				0.1108	2.2080		2.4834	0.2754	8.6	1230	
503	560	59.9	0.03		33.5				0.1086	2.1033		2.3963	0.2930	8.6	1196	
504	560	59.4	0.03	57.0	33.3	1900	1.71	15.63	0.1090	2.0674		2.3443	0.2764	8.6	1107	
505	560	51.6	0.03		28.9				0.1065	2.0470		2.3975	0.3505	8.5	1147	
506	560	51.5	0.03		28.8				0.1051	1.9976		2.2704	0.2728	8.5	1191	
507	560	52.0	0.03		29.1				0.1094	2.1686		2.6207	0.4521	8.3	1220	
508	560	51.6	0.03		28.9				0.1086	2.1268		2.6513	0.5245	8.3	1220	
508.5	560	51.2	0.03		28.8				0.1086	2.1150		2.2904	0.1754	8.3	1220	
508.6	Shut	Down														

APPENDICES

7 References

1. Bennett, S., Enos, G., John, R., and Powers, W., "Magnetoplasmadynamic Thruster Research," NASA CR–72345, 21 May 1967.

2. Nelson, S.T., et al, "Magnetoplasmadynamic Thruster Research," Report No. EOS 7223–IR–2, Electro-Optical Systems, Inc., May 1968.

3. Ducati, A.C., Gianaini, G.M., Muehlberger, "Recent Progress in High Specific Impulse Thermoionic Acceleration," AIAA Paper 65–96, January 1965.

4. Patrick, R.M., and Schneiderman, A.M., "Performance Characteristics of a Magnetic Annular Arc," AIAA J. 4, 283, (1966).

5. Burlock, J., Brockman, P., Hess, R.V., and Brooks, D.R., "Measurement of Velocities and Acceleration Mechanism for Coaxial Hall Accelerators," AIAA J. 5, 558 (1967).

6. Connolly, D.J., Sovie, R.J., and Mickels, C.J., "Low Environmental Pressure MPD Arc Tests," AIAA Paper 67–685, September 1967.

7. Jakob, M., "Heat Transfer," Vol. I, John Wiley and Sons, Inc., October 1959.

8. Johansen, A.E., and Palmer, R.W., "Lightweight Magnets for MPD Arcs," AIAA Paper 67–686, September 1967.

9. Evershed, S., "Permanent Magnets in Theory and Practice," Journal Inst. Elec. Eng., 58, 780–837, (1920).

10. Connolly, D.J., and Sovie, R.J., "The Effect of Background Pressure and Magnetic Field Shape on MPD Thruster Performance," AIAA Paper 69–243, March 1969.

11. John, R.J., et al, "Magnetoplasmadynamic Arc-Jet Thruster," Report No. AVSSD–0161–67, Avco Corp., March 1967.

12. Jones, R.E., and Walker, E.L., "Status of Large Vacuum Facility Tests of MPD Arc Thrusters," NASA TMX–52155, January 1966.

13. Larson, A., "Experiments on Current Rotations in an MPD Engine," AIAA Paper, 67–687, September 1967

14. Ekdahl, C., Kribal, R., and Lovberg, R., "Internal Measurements of Plasma Rotation in an MPD Arc," AIAA Paper, 67–655, September 1967

15. Malliaris, A.C., "Oscillations in an MPD Accelerator," AIAA J,. 6 No. 8, 1575–1577, 1968

8 Distribution list

NASA Lewis Research Center (1)
21000 Brookpark Road
Cleveland, Ohio 44135
Attention: Research Support
Procurement Section
(M.S. 500–312)

NASA Lewis Research Center (1)
21000 Brookpark Road
Cleveland, Ohio 44135
Attention: Technology Utilization Office
(M.S. 3–19)

NASA Lewis Research Center (1)
21000 Brookpark Road
Cleveland, Ohio 44135
Attention: Technical Information Division
(M.S. 5–5)

NASA Lewis Research Center (2)
21000 Brookpark Road
Cleveland, Ohio 44135
Attention: Library (M.S. 60–3)

NASA Lewis Research Center (1)
21000 Brookpark Road
Cleveland, Ohio 44135
Attention: Report Control Office
(M.S. 5–5)

NASA Lewis Research Center (1)
Spacecraft Technology Section
21000 Brookpark Road
Cleveland, Ohio 44135
Attention: C.C. Conger
(M.S. 54–1)

NASA Lewis Research Center (1)
Spacecraft Technology Section
21000 Brookpark Road
Cleveland, Ohio 44135
Attention: H. Hunczak (M.S. 54–3)

NASA Lewis Research Center (1)
Spacecraft Technology Section
21000 Brookpark Road
Cleveland, Ohio 44135
Attention: S. Domitz (M.S. 54–3)

NASA Lewis Research Center (1)
Spacecraft Technology Section
21000 Brookpark Road
Cleveland, Ohio 44135
Attention: E.W. Otto (M.S. 54–1)

NASA Lewis Research Center (1)
Electromagnetic Propulsion Division
21000 Brookpark Road
Cleveland, Ohio 44135
Attention: W. Moeckel (M.S. 301–1)

DISTRIBUTION LIST

NASA Lewis Research Center (1)
Electromagnetic Propulsion Division
21000 Brookpark Road
Cleveland, Ohio 44135
Attention: G. Seikel (M.S. 301–1)

NASA Lewis Research Center (84)
Electromagnetic Propulsion Division
21000 Brookpark Road
Cleveland, Ohio 44135
Attention: D. Connolly (M.S. 301–1)

National Aeronautics and Space Administration (1)
Washington, D.C. 20546
Attention: RNT/James Lazar

National Aeronautics and Space Administration (1)
Washington D.C. 20546
Attention: RRP/Dr. K.H. Thom

National Aeronautics and Space Administration (1)
Washington, D.C. 20546
Attention: RNT/J. Mullin

NASA Scientific and Technical Information Facility (6)
P.O. Box 33
College Park, Maryland 20740
Attention: NASA Representative RQT–2448

NASA Marshall Space Flight Center (1)
Huntsville, Alabama 35812
Attention: Ernest Stuhlinger (M–RP–DIR)

NASA Langley Research Center (1)
Langley Field Station
Hampton, Virginia 23365
Attention: M. Ellis

NASA Ames Research Center (1)
Moffett Field, California 94035
Attention: H. Stine

Research and Technology Division (1)
Wright-Patterson AFB, Ohio 45433
Attention: AFAPL (APIE–1)/ David Fritts

United States Air Force (1)
Office of Scientific Research
Washington, D.C. 20025
Attention: M.Slawsky

Case Institute of Technology (1)
10900 Euclid Avenue
Cleveland, Ohio 44106
Attention: Dr. Eli Reshotko

Princeton University (1)
Forrestal Research Center
Princeton, New Jersey 08540
Attention: Dr. R. G. Jahn

Aerospace Corporation (1)
P.O. Box 95085
Los Angeles, California 90045
Attention: Library/Technical Documents Group

Electro-Optical Systems, Inc. (1)
300 North Halstead Street
Pasadena, California 91107
Attention: G.L. Cann

General Dynamics/Convair (1)
P.O. Box 1128
San Diego, California 92112
Attention: Dr. A.V. Larson

Giannini Scientific Corporation (1)
3839 South Main Street
Santa Ana, California 92702
Attention: Adriano Ducati

NASA Marshall Space Flight Center (1)
Huntsville, Alabama 35812
Attention: G. Heller

NASA Langley Research Center (1)
Langley Field Station
Hampton, Virginia 23365
Attention: R. Hess

Air Force Weapons Laboratory
Kirtland AFB, New Mexico 87417
Attention: WLPC/Capt. C.F. Ellis

Thermal Mechanical Research Laboratory (1)
OAR USAF
Wright-Patterson Air Force Base, Ohio 45433
Attention: Eric Soehngen

Case Institute of Technology (1)
10900 Euclid Avenue
Cleveland, Ohio 44106
Attention: Professor O.K. Mawardi

Catholic University of America (1)
Department of Space Sciences and Applied Physics
Washington, D.C. 20017
Attention: Professor C.C. Chang

University of Minnesota (1)
Department of Mechanical Engineering
Heat Transfer Laboratory
Minneapolis, Minnesota 55435
Attention: Dr. E. Pfender

Avco Everett Research Laboratory (1)
A Division of Avco Corporation
2385 Revere Beach Parkway
Attention: Dr. R.M. Patrick

General Electric Company (1)
Missile and Space Division
Space Sciences Laboratory
P.O. Box 8555
Philadelphia, Pennsylvania 19101
Attention: P. Gloersen

Jet Propulsion Laboratory (1)
4800 Oak Grove Drive
Pasadena, California 91103
Attention: N.M. Nerheim

Los Alamos Scientific Laboratories (1)
P.O. Box 1663
Los Alamos, New Mexico 87544
Attention: Dr. Stratton

Westinghouse Astronuclear Laboratories (1)
Electric Propulsion Laboratories
Pittsburgh, Pennsylvania 15234

Avco Corporation (1)
Research and Advanced Development Division
201 Lowell Street
Wilmington, Massachusetts 01887
Attention: R.R. John

Avco Corporation (1)
Research and Advanced Development Division
201 Lowell Street
Wilmington, Massachusetts 01887
Attention: S. Bennett

Avco Corporation (1)
Research and Advanced Development Division
Wilmington, Massachusetts 01887
Attention: A.C. Malliaris

University of California, San Diego (1)
La Jolla, California 92037
Attention: Professor R. Lovberg

Colorado State University (1)
Fort Collins, Colorado 80521
Attention: Professor W. Mickelsen

TRW Systems Incorporated (1)
One Space Park
Redondo Beach, California 90278
Attention: Dr. J.M. Sellen

DISTRIBUTION LIST

Plasma Physics Engineering Laboratory (1)
State University of New York at Buffalo
Buffalo, New York
Attention: Dr. D.M. Benenson

Ion Physics Department (1)
Hughes Research Laboratories
301 Malibu Canyon Road
Malibu, California
Attention: Jerome H. Molitar

Department of Mechanical and Aerospace Engineering(1)
North Carolina State University
Raleigh, North Carolina, 27607
Attention: Professor H.A. Hassan

Institut fur Plasmadynamic, (1)
Deutsche Versuchsanstalt fur
Luft-und Raumfahrt e.v.
West Germany
Attention: Dr. W.L. Bohn

Comsat Laboratories (1)
Positioning and Orientation Branch
Washington, D.C.
Attention: Bernard Free

NASA Mission Analysis Division OART (1)
Moffett Field, California 94035
Attention: Dr. Frederico G. Cassal

NASA Goddard Space Flight Center (1)
Systems Analysis and Electric Propulsion Section
Greenbelt, Maryland 20771
Attention: Mr. William C. Isley

Jet Propulsion Laboratory
4800 Oak Grove Drive
Pasadena, California 91109
Attention: Mr. Daniel J. Kerrisk

NASA Marshall Space Flight Center (1)
Nuclear and Plasma Physics Branch
Huntsville, Alabama 35812
Attention: Mr. Russell D. Shelton

Princeton University (1)
Guggenheim Laboratories
James Forrestal Campus
Princeton, New Jersey
Attention: Woldemar F. von Jaskowsky

TRW Systems Incorporated (1)
One Space Park
Redondo Beach, California 90278
Attention: Dr. C.L. Dailey

Institut fuer Plasma-dynamik (1)
Deutsche Versuchsanstalt fuer Luft-
und Raumfahrt, Stuttgart
German Federal Republic
West Germany
Attention: G. Kruelle

Institute for Jet Propulsion (1)
Deutsche Farschungsanstalt fur
Luft-und Raumfahrt
DFL, Braunschwieg
West Germany
Attention: Gunther F. Au
Head, Electric Propulsion Section

Electro-Optical Systems Incorporated (1)
Electric Propulsion Applications Office
306 North Halsted Street
Pasadena, California 91109
Attention: Mr. Ronald S.H. Toms

Republic Aviation (1)
Farmingdale, Long Island, New York 11735
Attention: Mr. William J. Guman
Head, Electric Propulsion Power
Conversion Division

MCDONNELL RESEARCH LABORATORIES

Saint Louis, Missouri 63166

MCDONNELL DOUGLAS CORPORATION